BIOCHEMISTRY

Methane oxidation in African and European rivers depends on stream size and wetland connectivity

Alberto V. Borges[1]*, Cédric Morana[1,2], Fleur A. E. Roland[1], William Okello[3,4], Mwapu Isumbisho[5], Jean-Jacques Bowanga[5], Likoko Kashala[5], Patrick Omeja[6], Willy Champenois[1], Steven Bouillon[2]

Rivers are large natural sources of methane (CH_4) resulting from the net balance of inputs from methanogenesis and removal by methane oxidation (MOX). Here, we use an extensive dataset collected from African and European rivers to investigate spatial patterns and causes of variability of MOX. The MOX rates were highest in African streams draining flooded forests and increased with river catchment size. In large rivers, MOX represented the more important pathway of dissolved in-stream CH_4 removal compared to diffusive degassing to the atmosphere; but this relative share was minimal in small rivers and was, on average, higher in African streams (37%) than European streams (9%). The relationships between MOX rates and potential drivers such as total suspended matter, pH, or dissolved nutrient concentrations did not follow the patterns expected from controlled experiments reported in the literature and reflected the broad spatial patterns across and within the studied river networks driven by stream size and wetland connectivity.

INTRODUCTION

Emissions of CH_4 from rivers to the atmosphere are quantitatively important in the global CH_4 budget (*1*). Current estimates of global riverine CH_4 emissions [~28 $TgCH_4$ $year^{-1}$; (*2*)] correspond to ~18% of the freshwater wetland emission (~157 $TgCH_4$ $year^{-1}$), which represents the largest natural source of CH_4 (*1*) and are comparable to recent estimates of global lake CH_4 emissions [~42 $TgCH_4$ $year^{-1}$; (*3*)]. Diffusive fluxes account for about half of riverine CH_4 emissions, with the remainder attributed to ebullition, although estimates of ebullitive fluxes are more uncertain due to limited data availability and their highly stochastic nature (*2*, *4*). Diffusive riverine CH_4 emissions reflect the balance between CH_4 production via streambed methanogenesis (*5*, *6*) and CH_4 removal through microbial methane oxidation (MOX) occurring in both sediments (*7*–*9*) and the water column (*10*–*13*). Ebullition of CH_4 enables a variable fraction of the CH_4 produced by methanogenesis to be directly emitted to the atmosphere, thereby bypassing removal by MOX. Lateral inputs of dissolved CH_4 from upland and wetland soils also play an important role in sustaining diffusive CH_4 emissions from streams in both tropical (*14*, *15*) and higher-latitude systems (*16*).

The relative importance of MOX compared to diffusive emissions in the total removal of dissolved CH_4 or compared to methanogenesis seems variable but has rarely been quantified in streams and rivers (*10*–*13*). Moreover, large-scale variations in MOX across river networks and the drivers underlying this variability remain poorly constrained, in contrast to streambed methanogenesis, which is known to depend on sediment characteristics and temperature (*5*, *6*). This knowledge gap limits our capacity to predict how riverine MOX may respond to changes in temperature associated with global warming and to nutrient enrichment resulting from eutrophication (*17*), and, consequently, to assess future trajectories of riverine CH_4 emissions (*18*) and potential feedback on rising atmospheric CH_4 concentrations.

MOX occurs under aerobic conditions using O_2 as an electron acceptor, as well as under anaerobic conditions using alternative electron acceptors such as NO_3^-, Mn/Fe oxides, or SO_4^{2-}. Aerobic MOX predominates in stream surface waters, which are almost always oxic, as strictly anoxic conditions are extremely rare (*19*), although O_2 levels in rivers worldwide have declined and are projected to continue decreasing (*20*). Field observations in lakes and soils, together with controlled laboratory and mesocosm experiments, indicate that MOX generally increases with higher dissolved CH_4 (*21*), water temperature (*21*), dissolved PO_4^{3-} (*22*), dissolved inorganic nitrogen (DIN) (*17*), and total suspended matter (TSM) (*23*, *24*); and is inhibited by light (*25*), elevated dissolved NH_4^+ and NO_2^- (*26*), and low pH (*27*). Aerobic MOX is optimal at O_2 concentrations between 5 and 30 μM and is partially inhibited at concentrations below or above this range (*21*, *28*). Variations in these drivers can influence MOX rates at the cellular level or by changing the composition of the communities of aerobic methane-oxidizing bacteria (MOB). Aerobic MOB are commonly classified into two major groups: type I (Gammaproteobacteria) and type II (Alphaproteobacteria), which exhibit distinct life strategies, enabling them to occupy different ecological niches under contrasting environmental conditions (*29*). The relative abundance of type I and type II MOB varies within stream networks, although the drivers of this variability remain poorly understood (*30*, *31*).

Here, we characterize spatial variations in MOX rates across rivers and streams in Africa and Europe (Fig. 1). We test the influence of several biogeochemical variables—including dissolved O_2, CH_4, TSM, nutrients (NH_4^+, NO_2^-, DIN, and PO_4^{3-}), pH, and temperature—on MOX rates to identify potential drivers. We test whether connectivity with extensive flooded forests in Africa affects MOX rates and whether MOX rates vary systematically with stream size within river networks. Last, we quantify the relative contribution of MOX to total dissolved CH_4 removal in the water column (via MOX and diffusive degassing to the atmosphere) and assess how this contribution changes with stream size and among continents.

RESULTS AND DISCUSSION

MOX rates increase with river size and connectivity with flooded forest

We conducted 262 measurements of MOX rates across African and European river systems (Fig. 1), encompassing a broad range of stream

[1]University of Liège, Liège, Belgium. [2]KU Leuven, Leuven, Belgium. [3]National Fisheries Resources Research Institute, Jinja, Uganda. [4]Soroti University, Soroti, Uganda. [5]Institut Supérieur Pédagogique de la Gombe, Kinshasa, Democratic Republic of Congo. [6]Makerere University, Kampala, Uganda.
*Corresponding author. Email: alberto.borges@uliege.be

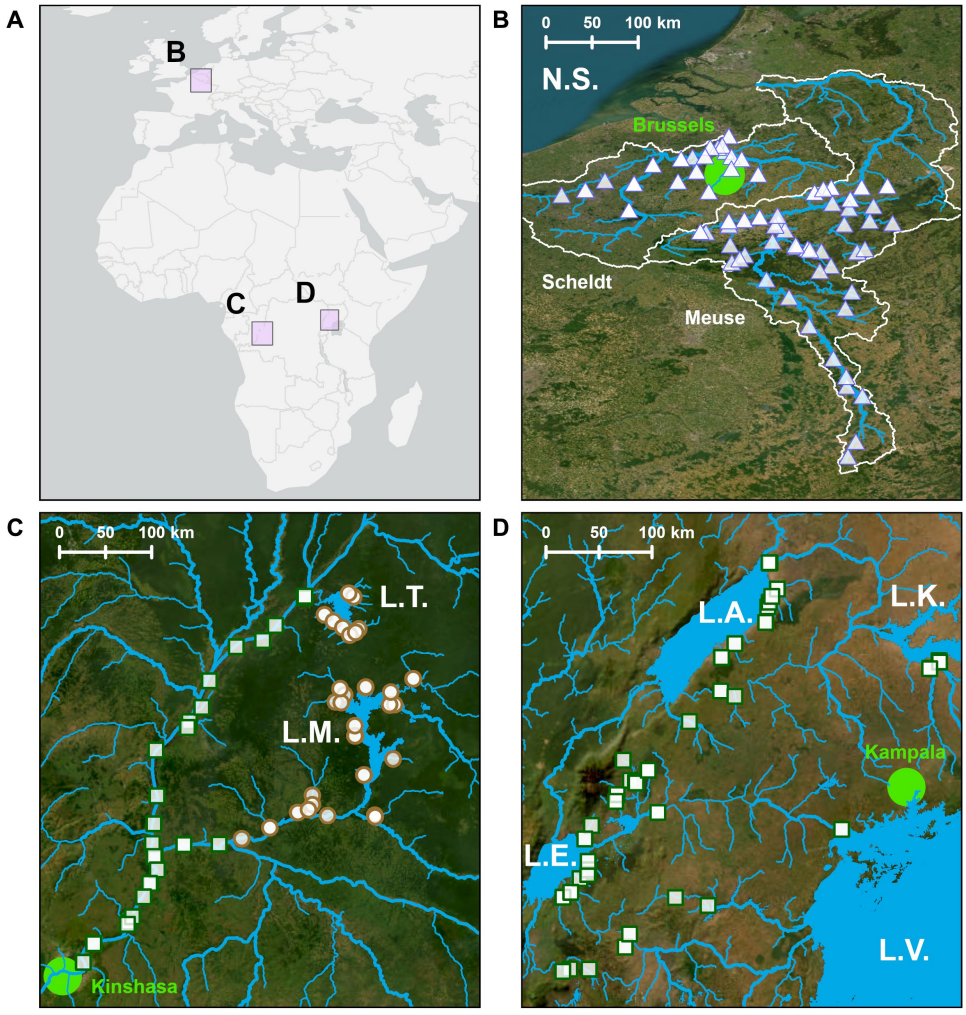

Fig. 1. Study extends over Europe and Africa covering a range of land cover and stream size. (**A** to **D**) Map of streams and rivers where MOX was measured in Europe (Meuse and Scheldt river basins; A and B), West Africa (Congo River basin; A and C), and East Africa [catchments of Lakes Victoria (L.V.), Kyoga (L.K.), Edward (L.E.), and Albert (L.A.); A and D]. N.S., North Sea; L.T., Lake Tumba; L.M., Lake MaiNdombe.

sizes (catchment areas from 9 to 3,626,000 km^2) and land-cover types, including intensive agricultural landscapes, temperate forests, tropical flooded forests, tropical rainforests, and savannas (table S1). African rivers were divided into two groups: those draining the Cuvette Centrale Congolaise (CCC)—an extensive flooded forest region in the Congo River basin (total area: ~1,760,000 km^2; flooded area: ~360,000 km^2)—and all other African systems. Previous works have shown that the CCC strongly influences riverine carbon biogeochemistry, including dissolved CH_4 concentrations and diffusive emissions (*14*, *15*).

Streams and rivers draining the CCC exhibited lower pH, nutrient concentrations (NH_4^+, NO_2^-, DIN, and PO_4^{3-}), TSM, and dissolved O_2 concentrations compared to other African and European systems (fig. S1). Forests covered, on average, 92% of the catchment area of CCC-draining streams and 58% of non-CCC African streams (table S1). Savanna and cropland accounted for 12 and 26%, respectively, of non-CCC African catchments (table S1). Rivers draining the CCC were also characterized by greater inundation extent than non-CCC African rivers (fig. S2). European streams exhibited higher nutrient concentrations (fig. S1) than the African rivers, reflecting eutrophication associated with intensive agriculture. Croplands and pastures covered, on average, 76% of European catchments compared to 18% in Africa (table S1).

Dissolved CH_4 concentrations ranged from 16 to 97,345 nM and were highest in the rivers draining the CCC (Fig. 2). Mean dissolved CH_4 concentrations did not differ significantly between European rivers and African rivers outside the CCC (Fig. 2). Dissolved CH_4 concentrations decreased with increasing catchment area and tended to be higher in lower stream orders (Fig. 3 and fig. S3), consistent with patterns reported at basin (*15*), regional (*4*), and global scales (*32*).

MOX rates ranged from 0.3 to 126,973 nM day^{-1} and were highest in the rivers draining the CCC (Figs. 2 and 3). In non-CCC African and European streams, MOX rates showed no consistent relationship with catchment size and across stream orders (fig. S4). In CCC African rivers, MOX rates decreased with increasing catchment size and stream order (fig. S4). Vertically integrated MOX rates in streambed sediments compiled from the literature (fig. S5 and table S2) ranged between 0 and 441,750,000 nmol m^{-2} day^{-1} (median = 634,963;

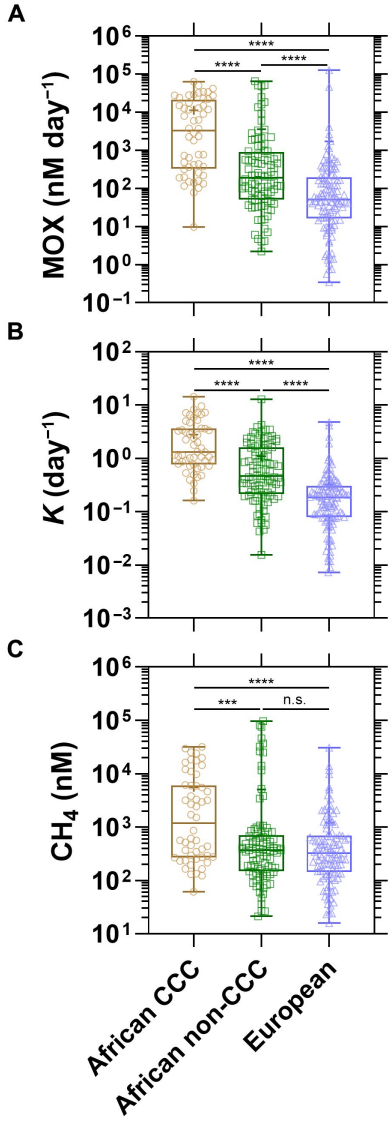

Fig. 2. MOX follows broad geographical gradients. MOX rate (nM day^{-1}) (**A**), MOX apparent rate constant (*K* in day^{-1}) (**B**), and dissolved CH_4 concentration (nM) (**C**) in African streams draining the flooded forest of the CCC, other African streams, and European streams (Fig. 1). The box represents the first and third quartile, the horizontal line corresponds to the median, the cross corresponds to the mean, error bars correspond to the maximum and minimum, and symbols show all data points. Plot with *K* values normalized to a temperature of 25°C is shown in fig. S7. Results of the statistical comparison of means are summarized on top of the figures and detailed in table S3. n.s., not significant; ***$P \leq 0.001$; ****$P \leq 0.0001$.

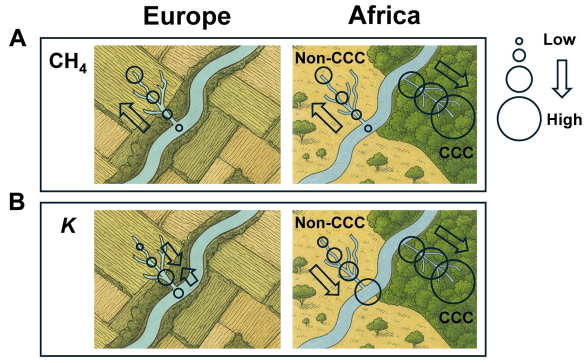

Fig. 3. Schematic representation of the dependency of MOX on stream size and wetland connectivity. General patterns of the variability of dissolved CH_4 concentration (**A**) and MOX apparent rate constant (*K*) (**B**) in Europe and Africa located within (CCC) or outside (non-CCC) the CCC.

mean = 10,765,851 nmol m^{-2} day^{-1}) encompassing values measured in the water column of African and European rivers (range 103 to 62,484,419; median = 222,284; mean = 4,157,269 nmol m^{-2} day^{-1}). In headwaters (stream order ≤3), vertically integrated MOX rates in the water column were significantly higher than in sediments for both African and European systems (fig. S5 and table S3). In larger systems (stream order ≥4), the vertically integrated MOX values in the water column did not differ significantly from sediments in African rivers but were significantly lower in European rivers (fig. S5 and table S3). Although these sediment and water column MOX rates were not collected concurrently nor at the same sites, this comparison demonstrates that MOX in rivers is not restricted to sediments, as previously suggested (*33*). Rather, MOX rates in the water column are comparable to those in sediments in large systems and may even exceed them in headwaters. The lower sediment MOX reported in headwaters compared to lowland rivers likely reflects reduced deposition of fine particles (*34*), which have been shown to enhance sedimentary MOX (*9*).

MOX rates were positively related to dissolved CH_4 concentrations (Fig. 4), consistent with previous studies identifying CH_4 availability as a key driver of MOX in streams (*5*, *10*–*13*). The slopes of the log-log relationships between MOX rates and dissolved CH_4 concentrations exceeded 1 in African and European rivers, indicating nonlinear relationships. This implies that apparent MOX rate constants (*K*; Eqs. 1 and 2) varied along CH_4 gradients, with a tendency for apparent *K* to increase with dissolved CH_4 concentrations in African and European rivers. Variability in *K* is further explored by examining relationships between empirically derived apparent *K* (Eq. 1) and potential environmental drivers. An increase in the apparent *K* value reflects higher abundance and/or activity of MOB under favorable environmental conditions other than dissolved CH_4 concentration.

The apparent *K* values were higher in the rivers draining the CCC than the other African and European rivers (Figs. 2 and 3). The higher apparent *K* values in the streams draining the CCC characterized by a higher inundation extent (fig. S2) is likely attributable to stronger inoculation of MOB from flooded forest soils compared to upland soils in non-CCC African and European catchments. This explanation is consistent with the positive relationship between apparent *K* and inundation extent (wetland cover) observed in African streams (fig. S6). Flooding enhances microbial transfer from soils to streams (*35*). Soils exposed to regular flooding, such as the Amazon floodplains, have higher MOX rates and MOB abundances than upland soils (*36*). The combination of a higher abundance of MOB in wetland soils and an enhanced hydrological transfer from wetland soils to streams could explain the higher apparent *K* in the streams draining the flooded forest (CCC) (Figs. 2 and 3). This could also explain that apparent *K* decreased with catchment area and stream order in streams draining the flooded forest (CCC), testifying enhanced transfer of MOB from flooded forest soils into small streams (small catchments) and a dilution effect as catchment size increased

(Figs. 3 and 5). The mean apparent *K* value in stream orders 1 to 4 was higher than stream orders 5 to 8 in African CCC streams [3.3 ± 2.8 versus 2.1 ± 3.0 day^{-1}, mean ± SD, *t* test (log transformed) $P = 0.0368$, df = 50]. Notably, environmental variables previously proposed to enhance MOX rates and *K* such as TSM (*23*, *24*), PO_4^{3-} (*22*), and DIN (*17*) were lower (more unfavorable) in CCC streams than in other African and the European systems (fig. S1). Hence, in the overall dataset presented here, their influence, if any, was outweighed by the stream-wetland connectivity.

Some particulate organic carbon (POC) samples from CCC streams were extremely depleted in ^{13}C, with $^{13}C/^{12}C$ ratios (δ^{13}C-POC) as low −43 per mil (‰) (fig. S7). This suggests substantial incorporation of ^{13}C-depleted CH_4 into MOB biomass in these streams poor in suspended particulate matter (TSM = 2.8 ± 4.3 mg $liter^{-1}$, $n = 52$) but with high CH_4 concentrations (Fig. 2). This interpretation is supported by negative relationships between δ^{13}C-POC and dissolved CH_4 concentration, MOX rates, and apparent *K* (fig. S7). The low POC to particulate nitrogen (PN) ratios (POC:PN) (down to ~6:1), associated with low δ^{13}C-POC values (fig. S7), were below typical values for vascular plants (20:1 to 50:1) and tropical forest soils (9:1 to 15:1). The low POC:PN values were consistent with bacteria biomass (*37*), further supporting a strong MOB contribution to the POC pool.

The lower apparent *K* values observed in European streams relative to African systems are more difficult to attribute unambiguously (Fig. 2). Although methanotrophs may be more abundant in high-latitude forest soils than tropical forest and savanna soils (*38*), European catchments such as the Scheldt and Meuse are dominated by croplands and pastures, where methanotroph abundance is generally lower (*38*). Furthermore, river embankment in Europe is likely to reduce the transfer of microorganisms from soils to streams.

In the European and non-CCC African streams, apparent *K* values increased with stream size, as indicated by the positive linear relation to catchment area (Figs. 3 and 5). The mean apparent *K* value in stream orders 1 to 3 was lower than stream orders 7 to 9 in African non-CCC stream (0.6 ± 0.6 versus 1.7 ± 1.1 day^{-1}, $P < 0.0001$, df = 77) and stream orders 4 to 6 in European streams (0.3 ± 0.7 versus 0.4 ± 0.6 day^{-1}, $P = 0.0422$, df = 106). The pattern of downstream increase in apparent *K* likely reflects the increase in the absolute abundance of better adapted and more competitive MOB with downstream transport along the river network (*29*). Earlier works showed that river microbial communities are inoculated from soils (*39*), although these are often poorly adapted to aquatic environments leading to downstream changes in the composition due to species sorting (*40*–*42*). Nevertheless, microbial abundance increases through growth and accumulation with the downstream transport (*40*–*42*).

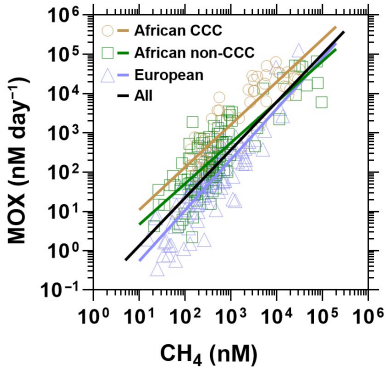

Fig. 4. MOX is mainly driven by dissolved CH_4 content in streams. MOX rate (nM day^{-1}) versus dissolved CH_4 concentration (nM) in African streams draining the flooded forest of the CCC, other African streams, and European streams (Fig. 1). Lines show the quantile linear regressions (table S4).

Variations of the MOX apparent rate constant do not follow patterns from controlled experiments and reflect broad spatial variations at the network scale

Apparent *K* values were positively related to water temperature (Fig. 6), potentially indicating a temperature-dependent enhancement of MOX

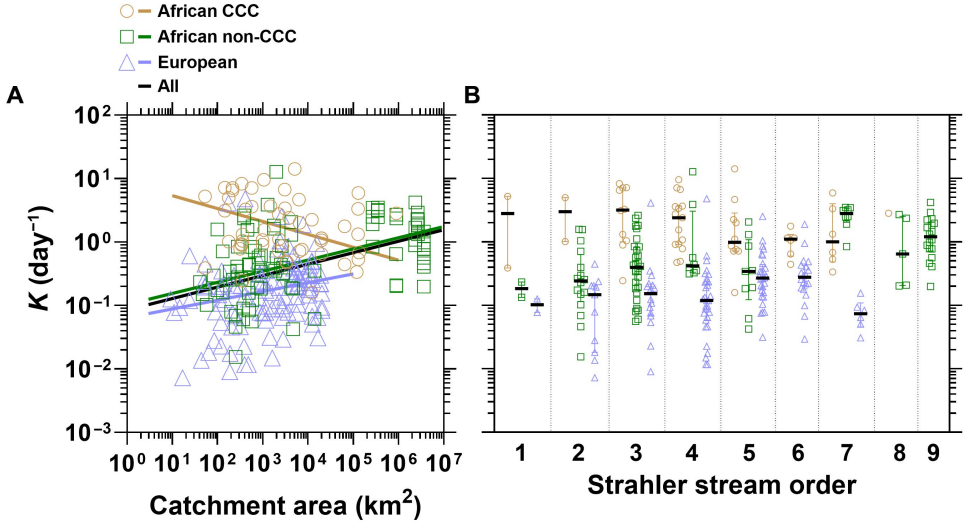

Fig. 5. MOX apparent rate constant (*K*) increases with stream size. *K* (day^{-1}) in African streams draining the flooded forest of the CCC, other African streams, and European streams (Fig. 1) versus catchment area (km^2) (**A**) and stream order (**B**). The horizontal black line corresponds to the median, error bars correspond to the first and third quartile, and symbols show all data points. Other lines show the quantile linear regressions (table S4). Plots with *K* values normalized to a temperature of 25°C are shown in fig. S16.

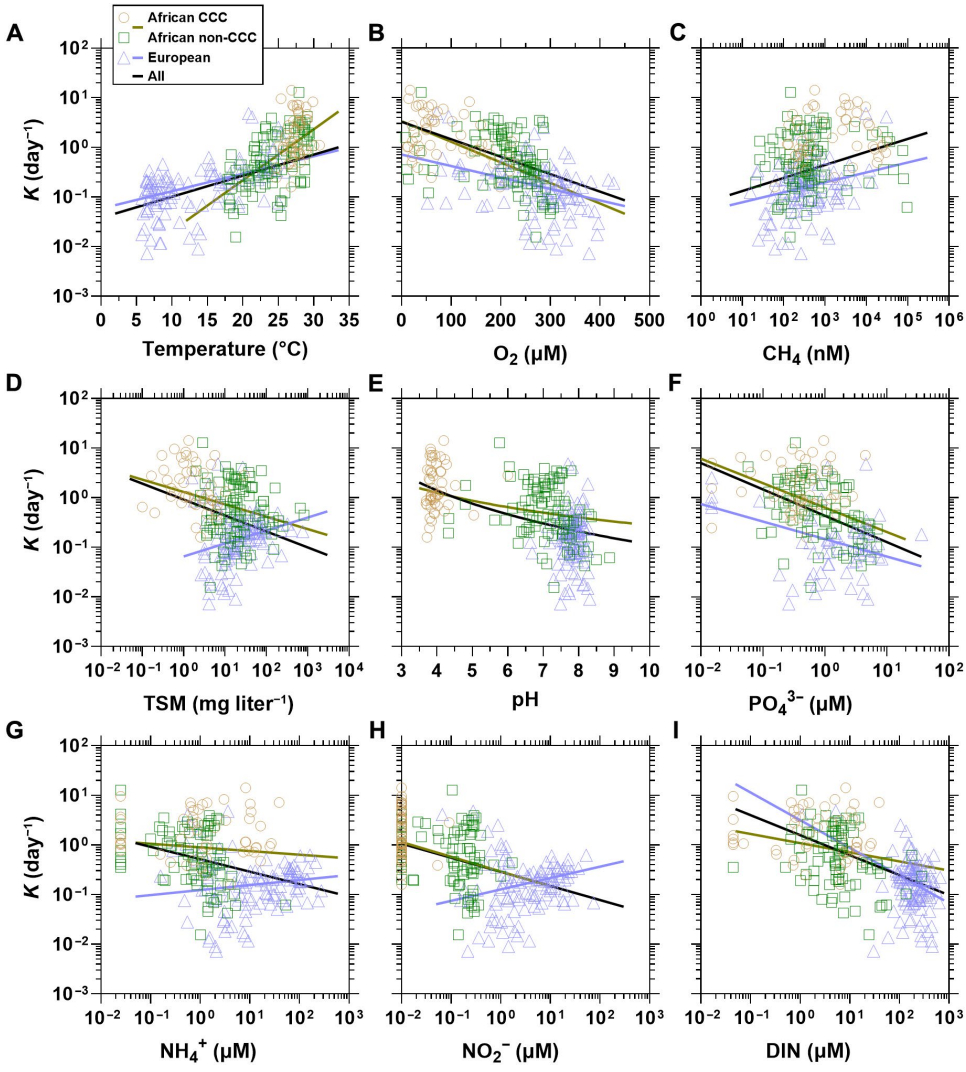

Fig. 6. MOX apparent rate constant (*K*) dependency on several biogeochemical variables. *K* (day^{-1}) versus water temperature (°C) (**A**), dissolved O_2 (μM) (**B**), dissolved CH_4 (nM) (**C**), TSM (in mg $liter^{-1}$) (**D**), pH (**E**), PO_4^{3-} (μM) (**F**), NH_4^+ (μM) (**G**), NO_2^- (μM) (**H**), and DIN (in μM) (**I**), in African streams draining the flooded forest of the CCC, other African streams, and European streams (Fig. 1). Lines show the quantile linear regressions (table S4). Plots with *K* values normalized to a temperature of 25°C are shown in fig. S9.

rates. When apparent *K* values were normalized to 25°C ($K_{25°C}$) using a temperature dependence reported in the literature (Q_{10} ~ 2.3), they exhibited patterns similar to apparent *K* values with respect to differences among the three groups of streams (Fig. 2 and fig. S8). Patterns of *K* and $K_{25°C}$ as a function of other variables were similar (figures hereafter). Notably, the positive relationship between apparent $K_{25°C}$ and temperature across the full dataset (fig. S9) was likely indirect and reflected other broader differences between continents rather than a direct temperature effect. If temperature were a dominant driver of *K*, the normalization to 25°C would remove this relationship. This suggests that temperature differences did not drive the main patterns of apparent *K* variability across the entire dataset, consistent with the broad thermal tolerance of methanotrophs. Type II methanotrophs have optimal growth between 23° and 34°C (*43*), whereas type I methanotrophs have lower optima (8° to 15°C) (*44*), due to physiological adaptations to low temperature (*45*, *46*). Together, type I and II methanotrophs span a wide optimal temperature range (8° to 34°C). This aligns with studies indicating that temperature is not a primary control on MOX in lake water column (*21*) and sediment (*47*). In soils, methanotroph responses to temperature vary widely and depend on microbial community composition and environmental conditions (*48*).

Across the dataset, apparent *K* values were negatively related to O_2, nutrients (PO_4^{3-}, NH_4^+, NO_2^-, and DIN), pH, and TSM (Fig. 6). The negative relationship between apparent *K* and dissolved O_2 concentrations (Fig. 6) likely reflected inhibition of MOX at O_2 concentrations above the optimal range (5 to 30 μM) (*21*, *28*). Dissolved O_2 were negatively related to dissolved CH_4 concentrations (fig. S10), showing that inhibition at high O_2 concentrations may contribute to the observed positive relationship between apparent *K* and CH_4 (Fig. 6). A similar positive relationship between apparent *K* and dissolved CH_4 concentration was reported in marine systems (*49*), where it was attributed to covarying factors enhancing MOX such as particle resuspension or increased nutrient availability in bottom waters with

high CH_4 concentrations (*50*). Note that the higher O_2 concentrations in European rivers (fig. S1) might also contribute to explain lower apparent *K* values than in African rivers (Fig. 2).

The negative relationships between apparent *K* and PO_4^{3-} or DIN (Fig. 6) contrasted with the hypothesis of nutrient limitation of methanotrophy (*17*,*22*). Similarly, the negative relationship between apparent *K* and pH (Fig. 6) contradicted the assumption of optimal methanotroph growth under circumneutral pH (*27*), although some methanotrophs are adapted to acidic environments such as peat bogs (*51*). Negative relationships between apparent *K* and NH_4^+ and NO_2^- across the full dataset were consistent with NH_4^+ and NO_2^- inhibition of methanotrophy (*26*). However, in the European streams, where the highest NH_4^+ and NO_2^- concentrations were observed, apparent *K* was positively related to NH_4^+ and NO_2^- (Fig. 6), which is inconsistent with inhibition of methanotrophy. Although NH_4^+ has been shown to inhibit methane monooxygenase activity, other studies have reported stimulation or no effect, suggesting that responses depend on MOB community composition or NH_4^+ load (*25*). The positive relationships between apparent *K* and NH_4^+ and NO_2^- in European streams likely reflect variations in soil-river inputs of both nutrients and MOB.

The negative relationship between apparent *K* and TSM across the entire dataset (Fig. 6) was contrary to expectations of enhanced MOX rates associated with particle-attached methanotrophs (*23*, *24*). However, in the Meuse, Scheldt, and tidal Scheldt, the contribution of particle-attached MOB (>5 μm) to MOX rates (%$MOX_{>5\mu m}$) averaged 54 to 96% and increased in streams with higher TSM (fig. S11). The Meuse exhibited the lowest average TSM due to filtration by the invasive clam *Corbicula* spp. (*52*), whereas the tidal Scheldt exhibited the highest TSM due to sediment resuspension driven by tidal currents (*53*). The pattern of %$MOX_{>5\mu m}$ among these three systems was consistent with an enhancement of MOX rates with turbidity, as well as the positive relationship between apparent *K* and TSM in the European streams, although this was not the case for the entire dataset for which apparent *K* was negatively related to TSM (Fig. 6). Apparent *K* increased with POC (fig. S12), consistent with its relationship with TSM (Fig. 6), as POC and TSM were positively related (fig. S12), in agreement with observations across river basins (*54*).

In northern lakes, dissolved organic carbon (DOC) has been shown to influence the ratio of methanotrophy to total heterotrophy by modulating microbial competition (*55*). Yet, the positive relationship between apparent *K* and DOC or colored dissolved organic matter absorbance at 350 nm (a_{350}) (fig. S13) likely reflected enhanced methanotroph abundance due to connectivity with flooded forest soils, which also increased DOC and a_{350}. The connectivity with flooded forest soils also explained observed relationships between apparent *K* and potential explanatory variables across African and European streams as the rivers draining the flooded forest were characterized by lower pH, nutrients (NH_4^+, NO_2^-, DIN, and PO_4^{3-}), TSM, and O_2 concentrations but higher dissolved CH_4 concentrations (fig. S1).

The discrepancy between the observed relationships between apparent *K* and environmental gradients of nutrients (PO_4^{3-}, NH_4^+, NO_2^-, and DIN), TSM, pH, and DOC and those inferred from controlled experiments (micro- or mesocosms) highlights the challenges of extrapolating information on microbial functioning from controlled experiments to the community or ecosystem scale (*56*, *57*). These challenges arise from the complexity resulting from interactions within the whole microbial community and interactions with other organisms (autotrophs and grazers) and the historical lack of conceptual frameworks for microbial dynamics in lotic systems. Recent studies (*40*–*42*) have described variations in bacterial abundance and diversity at the river network scale within the frame of the river continuum concept (*58*), characterized by increasing abundance but decreasing diversity downstream. The observed increase in apparent *K* with river catchment and stream order (Figs. 3 and 5) is consistent with this framework. However, the patterns of apparent *K* (Fig. 6) suggest that the spatial variations of methanotroph abundance in African CCC streams also depended in part on the connectivity with flooded forests and therefore should also be framed by the flood pulse concept (*59*). Paired measured dissolved CH_4 concentrations and MOX rates in the streams draining the CCC were significantly higher during the high-water than the low-water period in agreement with the flood pulse concept (fig. S14). However, the apparent *K* values were not significantly different during high-water and low-water periods (fig. S14), indicating seasonal stability of apparent *K* despite spatial dependence of apparent *K* on connectivity with flooded forests (Figs. 3 and 6).

Contribution of MOX to total dissolved CH_4 removal increases with river size

The contribution of MOX to total dissolved CH_4 removal in the water column ($MOX_{removal}$) reflects the relative importance of water-column oxidation versus diffusive emissions, excluding, by definition, sedimentary MOX, which may also be substantial (*5*–*8*). Across the dataset, $MOX_{removal}$ ranged from 0.01 to 91.6% (Fig. 7). In African rivers, $MOX_{removal}$ was low in stream orders 1 to 3 (median: 0.8 to 2.4%), increased to stream order 7 (median: 75.9%), and stabilized in stream orders 8 and 9 (median: 78.8 to 84.9%). $MOX_{removal}$ was higher in CCC (median: 17.9%) than non-CCC (median: 0.7%) headwaters (stream order ≤3), reflecting higher apparent *K* values (Fig. 5), but lower than in respective higher stream orders (≥4, median: 44.1% in CCC streams and median: 72.4% in non-CCC streams) (fig. S15 and table S5). When weighted by stream-order areal coverage in the Congo basin (*15*), the central value of $MOX_{removal}$ was 36.6% for African streams (58% of the data on MOX in African streams were acquired in the Congo basin). In European streams, $MOX_{removal}$ was similarly low in stream orders 1 to 4 (median: 0.2 to 4.5%) and increased in stream orders 5 and 6 (median: 24.0 to 26.4%) but declined in stream order 7 (median: 6.7%), corresponding to the Meuse main stem. The decline of $MOX_{removal}$ in stream order 7 likely reflects strong anthropogenic alteration of the Meuse river—reduced soil-river connectivity due to embankment and filtration by *Corbicula* spp. (*52*). The area-weighted central value for the Meuse and Scheldt networks was 8.9% based on stream-order areal coverage (*60*), substantially lower than in African rivers (36.6%). This reflects the lower coverage of larger rivers in the sampled European streams (maximum stream order 7 versus 9 in Africa) and lower apparent *K* values at equivalent stream orders (Figs. 3 and 5).

In seven large rivers (stream orders 8 to 10) of the Amazon basin, $MOX_{removal}$ ranged from 59 to 96% (*12*), comparable to African rivers of similar size. These Amazon estimates were derived using a Rayleigh isotopic fractionation model for closed systems based on the $^{13}C/^{12}C$ ratio of dissolved CH_4 ($\delta^{13}C\text{-}CH_4$) (*12*). MOX rates derived from an isotopic fractionation model (MOX_{iso}) were compared to paired rates derived from incubations (MOX_{inc}) in 171 African and European sites (fig. S16). Both approaches were linearly related but the median of MOX_{iso} was between 9.7 and 40.6 times higher

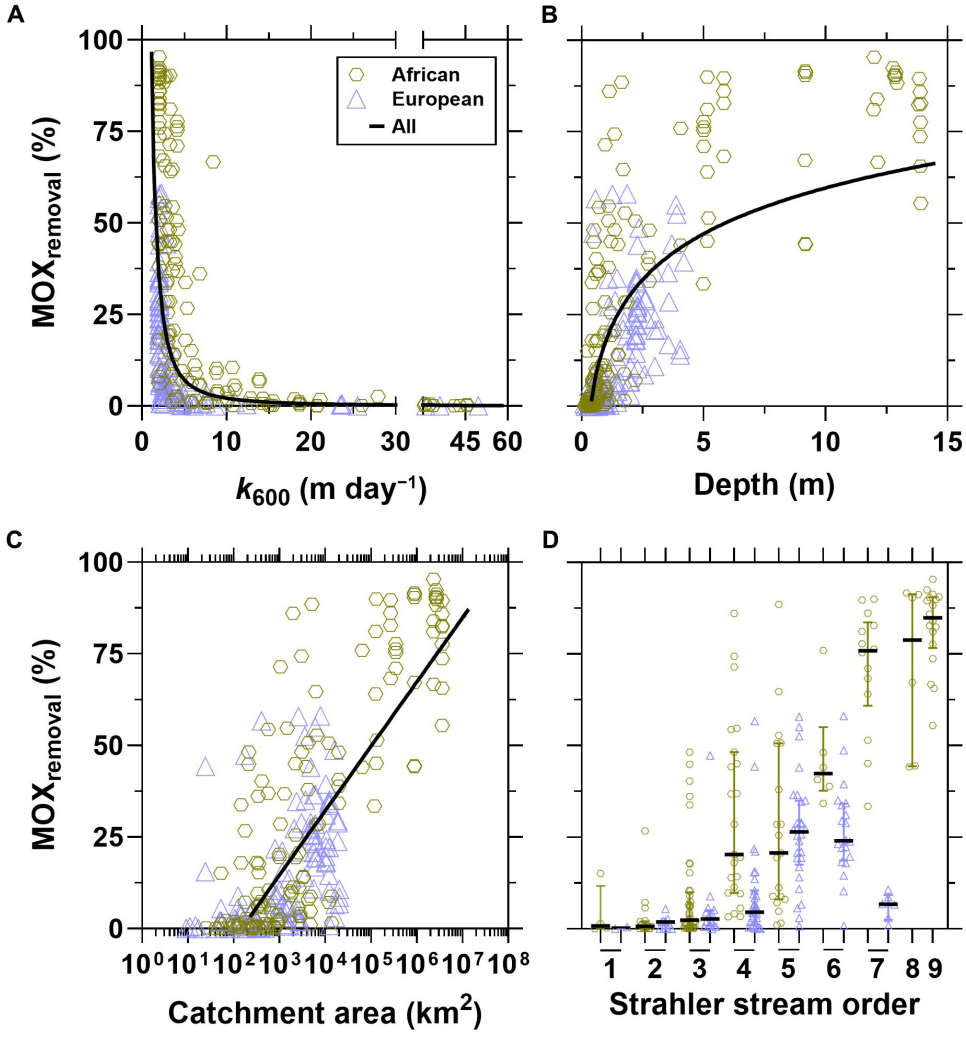

Fig. 7. Contribution of MOX to total dissolved CH_4 removal including degassing to the atmosphere ($MOX_{removal}$) increases with stream size. $MOX_{removal}$ (%) versus gas transfer velocity (k_{600} in m day^{-1}) (**A**), stream depth (**B**), catchment area (km^2) (**C**), and stream order (**D**) in African and European streams (Fig. 1). In plot (D), the horizontal black line corresponds to the median, error bars correspond to the first and third quartile, and symbols show all data points. In plots (A), (B), and (C), lines show the quantile linear regressions (table S4). $MOX_{removal}$ per stream order with African rivers separated into CCC and non-CCC groups is shown in fig. S15.

than the median of paired MOX_{inc}, depending on the choice of the initial value of $\delta^{13}C$-CH_4 used in the isotopic fractionation model (−60 or −80‰, respectively) (fig. S16). The higher values of MOX_{iso} than MOX_{inc} reflect the isotopic fractionation model providing an estimate of MOX rates integrated over a long timescale, accounting for the fractionation since the formation of CH_4 by methanogenesis, including in sediments that are potentially important sinks of CH_4 (*5*–*8*). Incubations provide an estimate of MOX rates that is directly related to the CH_4 concentration at the start of the incubation.

$MOX_{removal}$ increased with stream depth and catchment area and decreased with k_{600} (Fig. 7). Stream depth increases and k_{600} decreases with stream size/order (*61*), possibly explaining the increase in $MOX_{removal}$ with catchment area and stream order (Fig. 7). Sensitivity analyses (fig. S17) using constant (median) values of either k_{600}, depth, or K showed that increasing depth and apparent K in the higher stream orders were equally important, explaining the increase in $MOX_{removal}$ in the largest systems with little contribution from the changes of k_{600}.

Our analysis focused on the spatial variations of MOX rates and apparent K in streams, and we only have information on their seasonal variations from time series of dissolved CH_4 concentration in two African (Congo and Kasai) and two European (Meuse and Ourthe) rivers (figs. S18 and S19). Dissolved CH_4 concentrations (hence MOX) and k_{600} vary seasonally with freshwater discharge (*15*, *62*), potentially propagating to seasonal variations of $MOX_{removal}$. In these four rivers, $MOX_{removal}$ showed modest seasonal variability and correlated with dissolved CH_4 concentration (figs. S18 and S19). The seasonal variability of $MOX_{removal}$ was smaller than differences in $MOX_{removal}$ between the two rivers in each continent, as given by the comparison of the variance between- and within-groups (t-statistic = 38.4, df = 53, $P < 0.0001$ for Africa; t-statistic = 32.3, df = 223, $P < 0.0001$ for Europe) and among all four rivers [analysis of variance (ANOVA) F-statistic = 69165, df = 279, $P < 0.0001$].

Low-order streams account for most (≥75%) of diffusive riverine CH_4 emissions (*4*, *15*, *32*, *63*, *64*) yet exhibit low $MOX_{removal}$ values (<5%; Fig. 7). This suggests that changes in MOX driven by warming

or eutrophication (*17*) are likely to have limited impact on total diffusive CH_4 emissions from rivers.

We presented an extensive dataset of MOX rate measurements ($n = 262$) from rivers and streams in Europe and Africa, including systems within and outside the CCC—a large flooded forest region—and spanning a wide range of stream sizes and land-cover types. MOX rates, dissolved CH_4 concentrations, and apparent K were highest in streams draining the CCC, likely reflecting inputs of CH_4 and methanotrophs from flooded forest soils. This highlights the importance of wetland-river connectivity in driving stream CH_4 dynamics, consistent with the flood pulse concept.

MOX and apparent K were higher in non-CCC African rivers than in European rivers, although dissolved CH_4 concentrations did not differ significantly. Lower apparent K values in European rivers were likely attributable to anthropogenic impacts, such as filtration by invasive clams, disruption of soil-river connectivity (e.g., embankment), or dominance of agricultural soils with lower methanotroph abundance compared to forests.

Production of CH_4 in stream sediments is expected to increase under eutrophication and warming. The extent to which this translates into increased diffusive CH_4 emissions will depend partly on the response of MOX in both sediments and the water column. Our results indicate that water column MOX rates are comparable to sediment rates in lowland systems and may exceed them in headwaters, although this conclusion is based on limited sediment data compiled from the literature and warrants further investigation.

Temperature did not seem to explain differences in apparent K between African and European systems, consistent with the broad thermal tolerance of methanotrophs. Consequently, future warming is likely to result in only minor or undetectable increases in MOX. In contrast, warming is expected to enhance ebullition, allowing a greater fraction of CH_4 produced in sediments to bypass MOX in the water column. The negative relationships between apparent K and nutrients (PO_4^{3-} and DIN) suggest that increased nutrient availability from eutrophication may not enhance MOX in these already nutrient-rich systems. Conversely, decreasing O_2 concentrations under warming and eutrophication may stimulate MOX by bringing conditions closer to the optimal O_2 range, consistent with inhibition of MOX at high O_2 concentrations shown by the negative relationship between apparent K and O_2 across the full dataset. In addition, increased phytoplankton biomass resulting from eutrophication may enhance MOX by promoting particle-attached methanotrophs, consistent with the observed positive relationship between apparent K and TSM in European rivers and most MOX being attributed to particle-attached MOB (>5 μm) to MOX rates ($\%MOX_{>5\mu m}$) in the Meuse and Scheldt rivers. Overall, these findings indicate a complex and potentially mixed response of MOX to eutrophication and warming, driven by interacting factors leading to an increase (lower O_2 and higher TSM) or small/no changes (higher temperature and nutrients).

In non-CCC African and European rivers, apparent K increased with stream size (catchment area and stream order), reflecting increasing methanotroph abundance downstream, consistent with the river continuum concept. This resulted in increasing $MOX_{removal}$ with stream size. $MOX_{removal}$ was lower in European streams (9%), which are more heavily affected by human activities, than in African streams (37%). Given that low-order streams dominate diffusive CH_4 emissions (≥75%) but exhibit low $MOX_{removal}$ (<5%), changes in MOX due to warming or eutrophication are unlikely to substantially alter total riverine CH_4 diffusive emissions.

MATERIALS AND METHODS

Sampling and laboratory analysis

Samples were collected multiple times within each river network. Consequently, the dataset captures seasonal variability in dissolved CH_4 concentrations, which is primarily driven by changes in freshwater discharge between dry and wet seasons in Africa (*15*) and between winter and summer in Europe (*62*). Sampling was carried out during daytime (early morning to late afternoon) and designed to encompass the widest possible spatial gradients within river networks, including variations in stream size and catchment land cover.

Water temperature, specific conductivity, pH, and dissolved oxygen concentration were measured in surface waters with YSI EXO-II or YSI Pro Plus multiparameter probes. Sensors were calibrated according to manufacturer's specifications: O_2 in air, pH with commercial buffers (4.00, 7.00, and 10.00), and conductivity with a standard of 1000 μS cm^{-1}. Samples for CH_4 analysis (MOX and $\delta^{13}C\text{-}CH_4$) were collected from surface waters with a Niskin bottle and transferred via silicone tubing into six 60-ml borosilicate serum bottles (Wheaton). Bottles were immediately sealed with butyl stoppers and crimped with aluminum caps. Samples for $\delta^{13}C\text{-}CH_4$ and the initial MOX incubation time point (T_0) were immediately poisoned after collection with 200 μl of a saturated $HgCl_2$ solution injected through the butyl stopper using a 1-ml syringe fitted with a stainless steel needle, allowing water displacement during injection with a second needle. The remaining four bottles (T_1 to T_4) were incubated in the dark in a cool box filled at the start of the incubation with in situ water and sequentially poisoned with 200 μl of a saturated $HgCl_2$ solution approximately every 12 hours over a total incubation period of ~48 hours. The exact poisoning times were recorded. Water temperature in the cool box was not systematically monitored; however, preliminary tests indicated minimal temperature variation over 48 hours.

Dissolved CH_4 concentrations were measured using the headspace technique and a gas chromatograph with a flame ionization detector. A 20-ml headspace of ultrapure N_2 (Air Liquide, Belgium) was introduced into each serum bottles and allowed to equilibrate overnight at room temperature. A 12-ml subsample of headspace gas was injected into the gas chromatograph (SRI 8610C) calibrated with certified CH_4:N_2 gas mixtures [1, 10, 30, 509, and 2011 parts per million (ppm); ±2%; Air Liquide, Belgium]. Measurement precision was ±3%, and the detection limit was 0.5 nM.

The $\delta^{13}C\text{-}CH_4$ was measured in the headspace gas (20 ml of synthetic air, Air Liquide, Belgium) equilibrated overnight at room temperature with 40 ml of the water sample. When the headspace partial pressure of CH_4 (PCH_4) exceeded 10 ppm, gas samples were diluted to ~6 ppm to fall within the manufacturer's recommended instrumental operational range (2 to 10 ppm). The (un)diluted gas samples were analyzed with a cavity ring-down spectrometer (Picarro G2201-*i*) equipped with a Small Sample Introduction Module 2 (Picarro). Data were corrected using calibration curves relating $\delta^{13}C\text{-}CH_4$ to PCH_4, prepared from dilutions of two certified standards (−23.9 ± 0.3 and −69.0 ± 0.3‰ Airgas Specialty Gases) referenced to Vienna Pee Dee belemnite. Analytical precision based on repeated analysis of the two standards was better than ±1.0‰.

In the Meuse and Scheldt catchments, incubations were conducted to determine $\%MOX_{>5\mu m}$ in surface waters. At each site, two 60-ml borosilicate serum bottles were filled with filtered (5.0-μm pore size polycarbonate filters, Millipore; "F" treatment) and two bottles with unfiltered water ("UF" treatment). All bottles were amended

with 100 µl of a solution of dissolved $^{13}CH_4$ (50 µM final concentration, 99% enrichment). One bottle per treatment was immediately poisoned with pH-neutral formaldehyde (0.5% final concentration) and served as a killed control. Bottles were sealed with a butyl stopper and crimped with an aluminum cap and incubated in the dark for 72 hours at in situ temperature. At the end of the incubation, a 12-ml subsample was transferred into Exetainer vials (Labco) and preserved with 50 µl of saturated $HgCl_2$ for analysis of the $^{13}C/^{12}C$ ratio of dissolved inorganic carbon (δ^{13}C-DIC). The remaining sample (~50 ml) was filtered onto precombusted GF/F filters (25 mm in diameter) for δ^{13}C-POC analysis and stored frozen.

For ancillary measurements, 2 liters of surface water was collected and filtered through precombusted Whatman GF/F filters (450°C, >4 hours) for δ^{13}C-POC analysis (25 mm) and TSM (47 mm) determination, stored dry at room temperature. POC filters were decarbonated with HCl fumes for 4 hours, dried, and encapsulated in silver cups. POC concentration and δ^{13}C were measured using an elemental analyzer–isotope ratio mass spectrometer (EA-IRMS; Thermo Fisher Scientific Flash HT with Delta V Advantage) with reproducibility better than ±5%, calibrated against certified (IAEA-600 caffeine) and in-house standards (leucine and muscle tissue of Pacific tuna) that were previously calibrated versus certified standards. δ^{13}C-DIC was determined following equilibration with a 2-ml helium headspace after acidification with 99% H_3PO_4, with CO_2 analyzed by EA-IRMS. TSM filters were dried at 50°C for 12 hours and weighed before and after filtration using an analytical microbalance (±0.1 mg), yielding a final precision of ±10%.

Filtrate from GF/F filters was further passed through 0.2-µm polyethersulfone syringe filters for analysis of DOC, a_{350}, and nutrients (NO_3^-, NO_2^-, NH_4^+, and PO_4^{3-}). DOC samples were stored in 40-ml brown borosilicate vials with polytetrafluoroethylene (PTFE)–coated septa, poisoned with 50 µl of H_3PO_4 (85%) at ambient temperature and in the dark. DOC was measured using a wet oxidation TOC analyzer (IO Analytical Aurora 1030W; reproducibility: ±5%). Samples for a_{350} analysis were stored in 15-ml brown borosilicate vials with PTFE-coated septa at 4°C and in the dark. Absorbance spectra (190 to 900 nm) were measured using a PerkinElmer UV/Vis 650S spectrophotometer, with a 1-cm quartz cuvette, using ultrapure water as a blank. Nutrients were stored frozen (−20°C) in 50-ml polypropylene vials. NO_3^- and NO_2^- were determined with the sulfanilamide cadmium reduction colorimetric method (*65*), NH_4^+ were determined with the dichloroisocyanurate-salicylate-nitroprussiate colorimetric method (*66*), and PO_4^{3-} were determined with the ammonium molybdate, ascorbic acid, and potassium antimony tartrate colorimetric method (*67*). Precisions were ±0.05, ±0.02, ±0.02, and ±0.02 µM for PO_4^{3-}, NH_4^+, NO_2^-, and NO_3^-, respectively. Detection limits were 0.03, 0.05, 0.02, and 0.02 µM for PO_4^{3-}, NH_4^+, NO_2^-, and NO_3^-, respectively.

Computations

The CH_4 concentration at each time step ($CH_{4(t)}$ nM) was fitted as a function of time (t in days) through the five data points (T_0 to T_4) (*22*)

$$CH_{4(t)} = CH_{4(T0)}e^{-Kt} \quad (1)$$

where $CH_{4(T0)}$ is the initial CH_4 at T_0, and K (day^{-1}) is the fitted coefficient corresponding to the MOXS apparent rate constant, allowing to compute MOX (nM day^{-1})

$$MOX = K \times CH_{4(T0)} \quad (2)$$

K values were normalized to 25°C ($K_{25°C}$) using a Q_{10} of 2.3, based on a value of 2.2 computed from the incubation experiments in Lake Suwa (Japan) (*68*) and the value of 2.4 derived from the statistical analysis of in situ MOX rate measurements in six Canadian lakes (*21*). These Q_{10} values are consistent with the value of 2.0 reported for methanotrophs in wetland (*69*) and forest (*48*) soils.

Air-water diffuse CH_4 flux (F_{CH4}) was calculated as

$$F_{CH4} = kt \cdot \Delta CH_4 \quad (3)$$

where ΔCH_4 is the air-water CH_4 concentration gradient derived from measured dissolved CH_4 concentration, the atmospheric PCH_4 of 1.9 ppm, and the Henry constant of CH_4 (*70*), and k_t is the gas transfer velocity (m day^{-1}) derived with the Schmidt number of CH_4 for fresh water (*71*) and k_{600} (m day^{-1}) computed following (*62*)

$$k_{600} = 2.02 + 2841 \times VS \quad (4)$$

where V is the stream velocity (m s^{-1}), and S is the stream slope (unitless).

V was estimated from freshwater discharge (Q in m^3 s^{-1}) divided by the cross-sectional area (m^2) computed as the product of stream width and depth. Stream width, depth, and S were derived from RiverATLAS (*60*) for all rivers. Q was derived from RiverATLAS (*60*) for the African rivers and from gauged measurements in European rivers from various public databases (Service Public de Wallonie, Flanders Environment Agency).

The fraction of oxidized CH_4 (FOX) was calculated with a closed-system Rayleigh fractionation model (*72*)

$$\ln(1-FOX) = \left[\ln\left(\delta^{13}C-CH_{4\_initial}+1000\right)-\ln\left(\delta^{13}C-CH_4+1000\right)\right]/[\alpha-1] \quad (5)$$

where δ^{13}C-$CH_{4\_initial}$ is the signature of dissolved CH_4 as produced by methanogenesis in sediments, δ^{13}C-CH_4 is the signature of dissolved CH_4 measured in situ, and α is the fractionation factor.

We used α = 1.016 based on field measurements in a tropical lake (*73*). For δ^{13}C-$CH_{4\_initial}$, we used two values (−60 and −80‰) that correspond to the upper and lower bounds of the range of values of δ^{13}C-CH_4 typically encountered in stream sediment pore waters and riparian soils (*74*).

MOX_{iso} was calculated as (*75*)

$$MOX_{iso} = F_{CH_4} \times \frac{FOX}{1-FOX} \quad (6)$$

Methanotrophic bacterial production (MBP), defined as the CH_4-derived ^{13}C incorporation rates into the POC pool, was calculated as (*25*)

$$MBP = \frac{POC_t \times \left(\%^{13}C-POC_t/\%^{13}C-POC_i\right)}{t \times \left(\%^{13}C-CH_4/\%^{13}C-POC_i\right)} \quad (7)$$

where POC_t is the concentration of POC at the end of the incubation, $\%^{13}$C-POC_t and $\%^{13}$C-POC_i are the final and initial percentage of ^{13}C in the POC, t is the incubation time, and $\%^{13}$C-CH_4 is the percentage of ^{13}C in CH_4 after tracer inoculation.

The methanotrophic bacterial respiration (MBR) rates, defined as the CH_4-derived ^{13}C incorporation rates into the DIC pool, were calculated as (*25*)

$$\mathrm{MBR} = \frac{\mathrm{DIC_t} \times \left(\%^{13}\mathrm{C} - \mathrm{DIC_t} / \%^{13}\mathrm{C} - \mathrm{DIC_i}\right)}{t \times \left(\%^{13}\mathrm{C} - \mathrm{CH_4} / \%^{13}\mathrm{C} - \mathrm{DIC_i}\right)} \quad (8)$$

where $\mathrm{DIC_t}$ is the concentration of DIC at the end of the incubation, $\%^{13}\mathrm{C\text{-}DIC_t}$ and $\%^{13}\mathrm{C\text{-}DIC_i}$ are the final and initial percentage of $^{13}\mathrm{C}$ in DIC, and $\%^{13}\mathrm{C\text{-}CH_4}$ is the percentage of $^{13}\mathrm{C}$ in $\mathrm{CH_4}$ after tracer inoculation.

$\%\,\mathrm{MOX}_{>5\mu m}$ was calculated as

$$\%\,\mathrm{MOX}_{>5\mu m} = \frac{\left(\mathrm{MBP_{UF}} + \mathrm{MBR_{UF}}\right) - \left(\mathrm{MBP_F} + \mathrm{MBR_F}\right)}{\left(\mathrm{MBP_{UF}} + \mathrm{sMBR_{UF}}\right)} \times 100 \quad (9)$$

where UF and F denote unfiltered and filtered treatments, respectively.

Statistical analysis

Quantile regressions (tau = 0.5) were computed using the quantreg package (*76*) in R (*77*). Comparisons of means at the 0.05 level were conducted with the GraphPad Prism software using one-way ANOVA followed by a Tukey's multiple comparisons post hoc test, paired or unpaired *t* tests, and Kruskal-Wallis test followed by Dunn's multiple comparisons post hoc test. Data were $\log_{10}$ transformed before analysis.

Supplementary Materials

This PDF file includes:

Figs. S1 to S21
Tables S1 to S7
References

REFERENCES

1. M. Saunois, A. Martinez, B. Poulter, Z. Zhang, P. A. Raymond, P. Regnier, J. G. Canadell, R. B. Jackson, P. K. Patra, P. Bousquet, P. Ciais, E. J. Dlugokencky, X. Lan, G. H. Allen, D. Bastviken, D. J. Beerling, D. A. Belikov, D. R. Blake, S. Castaldi, M. Crippa, B. R. Deemer, F. Dennison, G. Etiope, N. Gedney, L. Höglund-Isaksson, M. A. Holgerson, P. O. Hopcroft, G. Hugelius, A. Ito, A. K. Jain, R. Janardanan, M. S. Johnson, T. Kleinen, P. B. Krummel, R. Lauerwald, T. Li, X. Liu, K. C. McDonald, J. R. Melton, J. Mühle, J. Müller, F. Murguia-Flores, Y. Niwa, S. Noce, S. Pan, R. J. Parker, C. Peng, M. Ramonet, W. J. Riley, G. Rocher-Ros, J. A. Rosentreter, M. Sasakawa, A. Segers, S. J. Smith, E. H. Stanley, J. Thanwerdas, H. Tian, A. Tsuruta, F. N. Tubiello, T. S. Weber, G. R. van der Werf, D. E. J. Worthy, Y. Xi, Y. Yoshida, W. Zhang, B. Zheng, Q. Zhu, Q. Zhu, Q. Zhuang, Global methane budget 2000–2020. *Earth Syst. Sci. Data* **17**, 1873–1958 (2025).
2. G. Rocher-Ros, E. H. Stanley, L. C. Loken, N. J. Casson, P. A. Raymond, S. Liu, G. Amatulli, R. A. Sponseller, Global methane emissions from rivers and streams. *Nature* **621**, 530–535 (2023).
3. M. S. Johnson, E. Matthews, J. Du, V. Genovese, D. Bastviken, Methane emission from global lakes: New spatiotemporal data and observation-driven modeling of methane dynamics indicates lower emissions. *J. Geophys. Res. Biogeosci.* **127**, e2022JG006793 (2022).
4. C. Duvert, A. V. Borges, E. Calamita, G. Rocher-Ros, A. Linkhorst, J. A. Rosentreter, S. Liu, K. Attermeyer, T. DelSontro, L. Deirmendjian, A. Dixon, C. Grasset, A. M. Herreid, L. C. Jeffrey, L. Marcon, R. M. Mwanake, J. R. Paranaíba, L. Ran, A. T. Rexroade, V. Solano, F. Ulloa-Cedamanos, J. Wang, K. M. Whitmore, L. Zhang, C. López-Lloreda, M. N. Macedo, D. Oviedo-Vargas, D. A. Riveros-Iregui, N. S. Marzolf, Hydroclimate and landscape diversity drive highly variable greenhouse gas emissions from tropical inland waters. *Nat. Water* **3**, 1303–1317 (2025).
5. F. Shelley, F. Abdullahi, J. Grey, M. Trimmer, Microbial methane cycling in the bed of a chalk river: Oxidation has the potential to match methanogenesis enhanced by warming. *Freshw. Biol.* **60**, 150–160 (2015).
6. L. Rovelli, L. A. Olde, C. M. Heppell, A. Binley, G. Yvon-Durocher, R. N. Glud, M. Trimmer, Contrasting biophysical controls on carbon dioxide and methane outgassing from streams. *J. Geophys. Res. Biogeosci.* **127**, e2021JG006328 (2022).
7. A. Bednařík, M. Blaser, A. Matoušů, P. Hekera, M. Rulík, Effect of weir impoundments on methane dynamics in a river. *Sci. Total Environ.* **584-585**, 164–174 (2017).
8. F. Shelley, J. Grey, M. Trimmer, Widespread methanotrophic primary production in lowland chalk rivers. *Proc. Biol. Sci.* **281**, 20132854 (2014).
9. P. Bodmer, J. Wilkinson, A. Lorke, Sediment properties drive spatial variability of potential methane production and oxidation in small streams. *J. Geophys. Res. Biogeosci.* **125**, e2019JG005213 (2020).
10. U. Zaiss, P. Winter, H. Kaltwasser, Microbial methane oxidation in the River Saar. *Z. Allg. Mikrobiol.* **22**, 139–148 (1982).
11. de M. A. S. Angelis, M. I. Cranton, Fate of methane in the Hudson River and estuary. *Glob. Biogeochem. Cycles* **7**, 509–523 (1993).
12. H. O. Sawakuchi, D. Bastviken, A. O. Sawakuchi, N. D. Ward, C. D. Borges, S. M. Tsai, J. E. Richey, M. V. R. Ballester, A. V. Krusche, Oxidative mitigation of aquatic methane emissions in large Amazonian rivers. *Glob. Change Biol.* **22**, 1075–1085 (2016).
13. L. Patel, R. Singh, S. C. Gowd, S. D. Thottathil, Environmental determinants of aerobic methane oxidation in a tropical river network. *Water Res.* **265**, 122257 (2024).
14. A. V. Borges, F. Darchambeau, C. R. Teodoru, T. R. Marwick, F. Tamooh, N. Geeraert, F. O. Omengo, F. Guérin, T. Lambert, C. Morana, E. Okuku, S. Bouillon, Globally significant greenhouse gas emissions from African inland waters. *Nat. Geosci.* **8**, 637–642 (2015).
15. A. V. Borges, F. Darchambeau, T. Lambert, C. Morana, G. H. Allen, E. Tambwe, A. Toengaho Sembaito, T. Mambo, J. Nlandu Wabakhangazi, J.-P. Descy, C. R. Teodoru, S. Bouillon, Variations in dissolved greenhouse gases (CO_2, CH_4, $N_{22}O$) in the Congo River network overwhelmingly driven by fluvial-wetland connectivity. *Biogeosciences* **16**, 3801–3834 (2019).
16. K. S. Aho, P. A. Raymond, Differential response of greenhouse gas evasion to storms in forested and wetland streams. *J. Geophys. Res. Biogeosci.* **124**, 649–662 (2019).
17. T. P. A. Nijman, T. A. Davidson, S. T. J. Weideveld, J. Audet, C. Esposito, E. E. Levi, A. Ho, L. P. M. Lamers, E. Jeppesen, A. J. Veraart, Warming and eutrophication interactively drive changes in the methane-oxidizing community of shallow lakes. *ISME Commun.* **1**, 32 (2021).
18. Y. Yao, H. Tian, X. Xu, Y. Li, S. Pan, Dynamics and controls of inland water CH_4 emissions across the conterminous United States: 1860–2019. *Water Res.* **224**, 119043 (2022).
19. J. R. Blaszczak, L. E. Koenig, F. H. Mejia, L. Gómez-Gener, C. L. Dutton, A. M. Carter, N. B. Grimm, J. W. Harvey, A. M. Helton, M. J. Cohen, Extent, patterns, and drivers of hypoxia in the world's streams and rivers. *Limnol. Oceanogr. Lett.* **8**, 453–463 (2023).
20. D. J. Graham, M. F. P. Bierkens, E. R. Jones, E. H. Sutanudjaja, M. T. H. van Vliet, Climate change drives low dissolved oxygen and increased hypoxia rates in rivers worldwide. *Nat. Clim. Change* **15**, 1348–1354 (2025).
21. S. D. Thottathil, P. C. J. Reis, Y. T. Prairie, Methane oxidation kinetics in northern freshwater lakes. *Biogeochemistry* **143**, 105–116 (2019).
22. H. O. Sawakuchi, G. Martin, S. Peura, S. Bertilsson, J. Karlsson, D. Bastviken, Phosphorus regulation of methane oxidation in water from ice-covered lakes. *J. Geophys. Res. Biogeosci.* **126**, e2020JG006190 (2021).
23. G. Abril, M. V. Commarieu, F. Guérin, Enhanced methane oxidation in an estuarine turbidity maximum. *Limnol. Oceanogr.* **52**, 470–475 (2007).
24. A. V. Borges, N. Gypens, T. Bauduin, Methanogenesis pathways and methane oxidation in urban ponds. *Aquat. Sci.* **88**, 29 (2026).
25. C. Morana, S. Bouillon, Methane paradox in tropical lakes? Sedimentary fluxes rather than pelagic production sustain methanotrophy. *Biogeosciences* **17**, 5209–5221 (2020).
26. G. Nyerges, S. Han, L. Y. Stein, Effects of ammonium and nitrite on growth and fitness of methanotrophic bacteria. *Appl. Environ. Microbiol.* **76**, 5648–5651 (2010).
27. P. Dunfield, R. Knowles, R. Dumont, T. R. Moore, Methane production and consumption in peat soils: Response to temperature and pH. *Soil Biol. Biochem.* **25**, 321–326 (1993).
28. T. Ren, J. A. Amaral, R. Knowles, Response of methane consumption by methanotrophic bacteria to oxygen. *Can. J. Microbiol.* **43**, 925–928 (1997).
29. A. Ho, F.-M. Kerckhof, C. Luke, A. Reim, S. Krause, N. Boon, P. L. E. Bodelier, Functional traits of methane-oxidizing bacteria as life strategies. *Environ. Microbiol. Rep.* **5**, 335–345 (2013).
30. S. Crevecoeur, C. Ruiz-González, Y. T. Prairie, P. A. Del Giorgio, Biogeography of methanotrophic bacteria across boreal waters. *Mol. Ecol.* **28**, 4181–4196 (2019).
31. M. Nagler, N. Praeg, G. H. Niedrist, K. Attermeyer, N. Catalán, F. Pilotto, C. G. Roberts, C. Bors, S. Fenoglio, M. Colls, S. Cauvy-Fraunié, B. Doyle, F. Romero, B. Machalett, T. Fuss, A. Bednařík, M. Klaus, P. Gilbert, D. Lamonica, A. C. Nydahl, C. R. González-Quijano, L. T. Bistarelli, L. Kenderov, E. Piano, J.-R. Mor, V. Evtimova, E. deEyto, A. Freixa, M. Rulík, J. Pegg, S. H. Ortega, L. Steinle, P. Bodmer, Abundance and biogeography of methanogenic and methanotrophic microorganisms across European streams. *J. Biogeogr.* **48**, 947–960 (2021).
32. M. Li, C. Peng, K. Zhang, L. Xu, J. Wang, Y. Yang, P. Li, Z. Liu, N. He, Headwater stream ecosystem: An important source of greenhouse gases to the atmosphere. *Water Res.* **190**, 116738 (2021).
33. M. Trimmer, S. Maanoja, A. G. Hildrew, J. L. Pretty, J. Grey, Potential carbon fixation via methane oxidation in well-oxygenated river bed gravels. *Limnol. Oceanogr.* **55**, 560–568 (2010).
34. E. Wohl, B. P. Bledsoe, R. B. Jacobson, N. L. Poff, S. L. Rathburn, D. M. Walters, A. C. Wilcox, The natural sediment regime in rivers: Broadening the foundation for ecosystem management. *Bioscience* **65**, 358–371 (2015).

35. F. Caillon, K. Besemer, P. Peduzzi, J. Schelker, Soil microbial inoculation during flood events shapes headwater stream microbial communities and diversity. *Microb. Ecol.* **82**, 591–601 (2021).
36. J. B. Gontijo, F. S. Paula, A. M. Venturini, C. A. Yoshiura, C. D. Borges, J. M. S. Moura, B. J. M. Bohannan, K. Nüsslein, J. L. Mazza Rodrigues, S. M. Tsai, Not just a methane source: Amazonian floodplain sediments harbour a high diversity of methanotrophs with different metabolic capabilities. *Mol. Ecol.* **30**, 2560–2572 (2021).
37. D. L. Kirchman, The uptake of inorganic nutrients by heterotrophic bacteria. *Microb. Ecol.* **28**, 255–271 (1994).
38. P. Heděnec, A. Alias, H. Almahasheer, C. Liu, P. S. Chee, M. Yao, X. Li, L. Vesterdal, J. Frouz, Y. Kou, K. Yue, Global assessment of soil methanotroph abundances across biomes and climatic zones: The role of climate and soil properties. *Appl. Soil Ecol.* **195**, 105243 (2024).
39. B. C. Crump, L. A. Amaral-Zettler, G. W. Kling, Microbial diversity in Arctic freshwaters is structured by inoculation of microbes from soils. *ISME J.* **6**, 1629–1639 (2012).
40. J. P. Niño-García, C. Ruiz-González, P. A. del Giorgio, Interactions between hydrology and water chemistry shape bacterioplankton biogeography across boreal freshwater networks. *ISME J.* **10**, 1755–1766 (2016).
41. T. Bambakidis, B. C. Crump, B. Yoon, E. D. Kyzivat, K. S. Aho, C. F. Leal, J. H. Fair, A. Stubbins, S. Wagner, P. A. Raymond, J. D. Hosen, Temperature, water travel time, and dissolved organic matter structure river microbial communities in a large temperate watershed. *Limnol. Oceanogr.* **69**, 1618–1635 (2024).
42. M. A. Borton, B. B. McGivern, K. R. Willi, B. J. Woodcroft, A. C. Mosier, D. M. Singleton, T. Bambakidis, A. Pelly, R. A. Daly, F. Liu, A. Freiburger, J. N. Edirisinghe, J. P. Faria, R. Danczak, I. Leleiwi, A. E. Goldman, M. J. Wilkins, E. K. Hall, C. Pennacchio, S. Roux, E. A. Eloe-Fadrosh, S. P. Good, M. B. Sullivan, E. M. Wood-Charlson, C. S. Miller, M. R. V. Ross, C. S. Henry, B. C. Crump, J. C. Stegen, K. C. Wrighton, A functional microbiome catalogue crowdsourced from North American rivers. *Nature* **637**, 110–112 (2025).
43. M. V. Kevbrina, A. A. Okhapkina, D. S. Akhlynin, Growth of mesophilic methanotrophs at low temperatures. *Microbiology* **70**, 384–391 (2001).
44. A. T. Tveit, A. Söllinger, E. M. Rainer, A. Didriksen, A. G. Hestnes, L. Motleleng, H.-J. Hellinger, T. Rattei, M. M. Svenning, Thermal acclimation of methanotrophs from the genus *Methylobacter*. *ISME J.* **17**, 502–513 (2023).
45. N. J. Bale, W. I. C. Rijpstra, D. X. Sahonero-Canavesi, I. Y. Oshkin, S. E. Belova, S. N. Dedysh, J. S. S. Damsté, Fatty acid and hopanoid adaption to cold in the methanotroph *Methylovulum psychrotolerans*. *Front. Microbiol.* **10**, 589 (2019).
46. N. Richter, L. Villanueva, E. C. Hopmans, N. J. Bale, J. S. S. Damsté, D. Rush, Methanotroph-methylotroph lipid adaptations to changing environmental conditions. *Front. Microbiol.* **16**, 1532719 (2025).
47. N. T. Duc, P. Crill, D. Bastviken, Implications of temperature and sediment characteristics on methane formation and oxidation in lake sediments. *Biogeochemistry* **100**, 185–196 (2010).
48. B. Jiang, H. Chen, Z. Wei, J. Zhang, M. Guo, T. Yang, X. Zhou, Higher temperature sensitivity of forest soil methane oxidation in colder climates. *Nat. Commun.* **16**, 2428 (2025).
49. J. Nauw, de H. Haas, G. Rehder, A review of oceanographic and meteorological controls on the North Sea circulation and hydrodynamics with a view to the fate of North Sea methane from well site 22/4b and other seabed sources. *Mar. Pet. Geol.* **68**, 861–882 (2015).
50. S. Elliott, M. Maltrud, M. Reagan, G. Moridis, P. Cameron-Smith, Marine methane cycle simulations during early global warming. *J. Geophys. Res.* **116**, G01010 (2011).
51. Y. Chen, M. G. Dumont, N. P. McNamara, P. M. Chamberlain, L. Bodrossy, N. Stralis-Pavese, J. C. Murrell, Diversity of the active methanotrophic community in acidic peatlands as assessed by mRNA and SIP-PLFA analyses. *Environ. Microbiol.* **10**, 446–459 (2008).
52. L.-M. Pigneur, E. Falisse, K. Roland, E. Everbecq, J.-F. Deliège, J. S. Smitz, K. Van Doninck, J.-P. Descy, Impact of invasive Asian clams (*Corbicula* spp.) on a large river ecosystem. *Freshw. Biol.* **59**, 573–583 (2014).
53. G. Abril, H. Etcheber, B. Delille, M. Frankignoulle, A. V. Borges, Carbonate dissolution in the turbid and eutrophic Loire estuary. *Mar. Ecol. Prog. Ser.* **259**, 129–138 (2003).
54. M. Meybeck, Carbon, nitrogen, and phosphorus transport by world rivers. *Am. J. Sci.* **282**, 401–450 (1982).
55. P. C. J. Reis, S. D. Thottathil, Y. T. Prairie, The role of methanotrophy in the microbial carbon metabolism of temperate lakes. *Nat. Commun.* **13**, 43 (2022).
56. S. R. Carpenter, Microcosm experiments have limited relevance for community and ecosystem ecology. *Ecology* **77**, 677–680 (1996).
57. T. G. Benton, M. Solan, J. M. J. Travis, S. M. Sait, Microcosm experiments can inform global ecological problems. *Trends Ecol. Evol.* **22**, 516–521 (2007).
58. R. L. Vannote, G. W. Minshall, K. W. Cummins, J. R. Sedell, C. E. Cushing, The river continuum concept. *Can. J. Fish. Aquat. Sci.* **37**, 130–137 (1980).
59. W. J. Junk, P. B. Bayley, R. E. Sparks, The flood pulse concept in river-floodplain systems. *Can. J. Fish. Aquat. Sci.* **106**, 110–127 (1989).
60. S. Linke, B. Lehner, C. Ouellet Dallaire, J. Ariwi, G. Grill, M. Anand, P. Beames, V. Burchard-Levine, S. Maxwell, H. Moidu, F. Tan, M. Thieme, Global hydro-environmental sub-basin and river reach characteristics at high spatial resolution. *Sci. Data* **6**, 283 (2019).
61. P. A. Raymond, C. J. Zappa, D. Butman, T. L. Bott, C. Potter, P. Mulholland, A. E. Laursen, W. H. McDowell, D. Newbold, Scaling the gas transfer velocity and hydraulic geometry in streams and small rivers. *Limnol. Oceanogr. Fluids Environ.* **2**, 41–53 (2012).
62. A. V. Borges, F. Darchambeau, T. Lambert, S. Bouillon, C. Morana, S. Brouyère, V. Hakoun, A. Jurado, H.-C. Tseng, J.-P. Descy, F. A. E. Roland, Effects of agricultural land use on fluvial carbon dioxide, methane and nitrous oxide concentrations in a large European river (Meuse, Belgium). *Sci. Total Environ.* **610-611**, 342–355 (2018).
63. G. Chiriboga, A. V. Borges, Andean headwater and piedmont streams are hot spots of carbon dioxide and methane emissions in the Amazon basin. *Commun. Earth Environ.* **4**, 76 (2023).
64. R. M. Mwanake, G. M. Gettel, C. Ishimwe, E. G. Wangari, K. Butterbach-Bahl, R. Kiese, Basin-scale estimates of greenhouse gas emissions from the Mara River, Kenya: Importance of discharge, stream size, and land use/land cover. *Limnol. Oceanogr.* **67**, 1776–1793 (2022).
65. American Public Health Association (APHA), *Standard Methods for the Examination of Water and Wastewater* (American Public Health Association, 1998).
66. Standing Committee of Analysts, "Ammonia in waters: Methods for the examination of waters and associated materials" (HMSO, 1981).
67. J. Koroleff, "Determination of total phosphorus by alkaline persulphate oxidation" in *Methods of Seawater Analysis* (Verlag Chemie, 1983), pp. 136–138.
68. H. Iwata, K. Nakazawa, H. Sato, M. Itoh, Y. Miyabara, R. Hirata, Y. Takahashi, T. Tokida, R. Endo, Temporal and spatial variations in methane emissions from the littoral zone of a shallow mid-latitude lake with steady methane bubble emission areas. *Agric. For. Meteorol.* **295**, 108184 (2020).
69. R. Segers, Methane production and methane consumption: A review of processes underlying wetland methane fluxes. *Biogeochemistry* **41**, 23–51 (1998).
70. S. Yamamoto, J. B. Alcauskas, T. E. Crozier, Solubility of methane in distilled water and seawater. *J. Chem. Eng. Data* **21**, 78–80 (1976).
71. R. Wanninkhof, Relationship between wind speed and gas exchange over the ocean. *J. Geophys. Res. Oceans* **97**, 7373–7382 (1992).
72. K. Liptay, J. Chanton, P. Czepiel, B. Mosher, Use of stable isotopes to determine methane oxidation in landfill cover soils. *J. Geophys. Res. Atmos.* **103**, 8243–8250 (1998).
73. C. Morana, A. V. Borges, F. A. E. Roland, F. Darchambeau, J.-P. Descy, S. Bouillon, Methanotrophy within the water column of a large meromictic tropical lake (Lake Kivu, East Africa). *Biogeosciences* **12**, 2077–2088 (2015).
74. S. Balathandayuthabani, B. Panneer Selvam, M. Gålfalk, P. Saetre, S. Peura, U. Kautsky, L. Klemedtsson, L. Arunachalam, G. Vellingiri, D. Bastviken, Methane in two stream networks: Similar contributions from groundwater and local sediments while oxidation was a large sink controlling atmospheric emissions. *J. Geophys. Res. Biogeosci.* **129**, e2023JG007836 (2024).
75. D. Bastviken, J. Ejlertsson, L. Tranvik, Measurement of methane oxidation in lakes: A comparison of methods. *Environ. Sci. Technol.* **36**, 3354–3361 (2002).
76. R. Koenker, *Quantile Regression* (Cambridge Univ. Press, 2005).
77. R Core Team, R: A language and environment for statistical computing (2022); https://r-project.org/.
78. M. I. Bird, P. Pousai, Variations of $\delta^{13}C$ in the surface soil organic carbon pool. *Glob. Biogeochem. Cycles* **11**, 313–322 (1997).
79. A. Bagnoud, P. Pramateftaki, M. J. Bogard, T. J. Battin, H. Peter, Microbial ecology of methanotrophy in streams along a gradient of CH_4 availability. *Front. Microbiol.* **11**, 771 (2020).
80. L.-D. Shen, L. Ouyang, Y. Zhu, M. Trimmer, Active pathways of anaerobic methane oxidation across contrasting riverbeds. *ISME J.* **13**, 752–766 (2019).
81. I. A. Sanders, C. M. Heppell, J. A. Cotton, G. Wharton, A. G. Hildrew, E. J. Flowers, M. Trimmer, Emission of methane from chalk streams has potential implications for agricultural practices. *Freshw. Biol.* **52**, 1176–1186 (2007).

Acknowledgments: We thank M.-V. Commarieu, T. Bousmanne, C. Schonbrodt, O. Efe, Y. Stroobandt, and Z. Kelemen for help in sample collection and/or laboratory analysis and the handling editor and the reviewers for constructive comments on the initial submission. A.V.B. is a research director at the FNRS. **Funding:** This work was supported by the Belgian Federal Science Policy Office BR/154/A1/HIPE (A.V.B., S.B., and W.O.), Fonds National de la Recherche Scientifique T.0037.24 (A.V.B.), Fonds National de la Recherche Scientifique J.0015.21 (A.V.B.), Fonds National de la Recherche Scientifique T.0027.20 (A.V.B.), Fonds National de la Recherche Scientifique J.0013.19 (A.V.B.), Fonds National de la Recherche Scientifique T.0156.18 (A.V.B.), Fonds National de la Recherche Scientifique X.3007.17 (A.V.B.), and Fund for Scientific Research, FWO-Vlaanderen, travel grants (S.B.). **Author contributions:** Conceptualization: A.V.B. Data curation: A.V.B. and S.B. Formal analysis: A.V.B. and J.-J.B. Funding acquisition: A.V.B. and S.B. Investigation: A.V.B., C.M., F.A.E.R., W.O., M.I., J.-J.B., L.K., P.O., W.C., and S.B. Methodology: A.V.B., C.M., F.A.E.R., W.O., M.I., J.-J.B., L.K., P.O., and W.C. Project administration: A.V.B. and S.B. Resources: C.M., F.A.E.R., W.O., M.I., J.-J.B., L.K., P.O., W.C., and S.B. Supervision: A.V.B. and S.B. Validation: A.V.B., C.M., F.A.E.R., W.O., M.I., L.K., P.O., and W.C. Visualization: A.V.B. Writing—original draft: A.V.B. Writing—review and editing: A.V.B., C.M., F.A.E.R., W.O., M.I., J.-J.B., L.K., P.O., W.C., and S.B. **Competing interests:** The authors declare that they have no

competing interests. **Data, code, and materials availability:** All data and code needed to evaluate and reproduce the results in the paper are present in the paper and/or the Supplementary Materials. The full dataset is available at https://zenodo.org/records/16893700. This study did not generate new materials.

Submitted 27 August 2025
Accepted 3 June 2026
Published 17 July 2026
10.1126/sciadv.aeb8250

Science Advances

Methane oxidation in African and European rivers depends on stream size and wetland connectivity

Alberto V. Borges, Cédric Morana, Fleur A. E. Roland, William Okello, Mwapu Isumbisho, Jean-Jacques Bowanga, Likoko Kashala, Patrick Omeja, Willy Champenois, and Steven Bouillon

Sci. Adv. **12** (29), eaeb8250. DOI: 10.1126/sciadv.aeb8250

Science Advances
AAAS

Supplementary Materials for

Methane oxidation in African and European rivers depends on stream size and wetland connectivity

Alberto V. Borges *et al.*

Corresponding author: Alberto V. Borges, alberto.borges@uliege.be

Sci. Adv. **12**, eaeb8250 (2026)
DOI: 10.1126/sciadv.aeb8250

This PDF file includes:

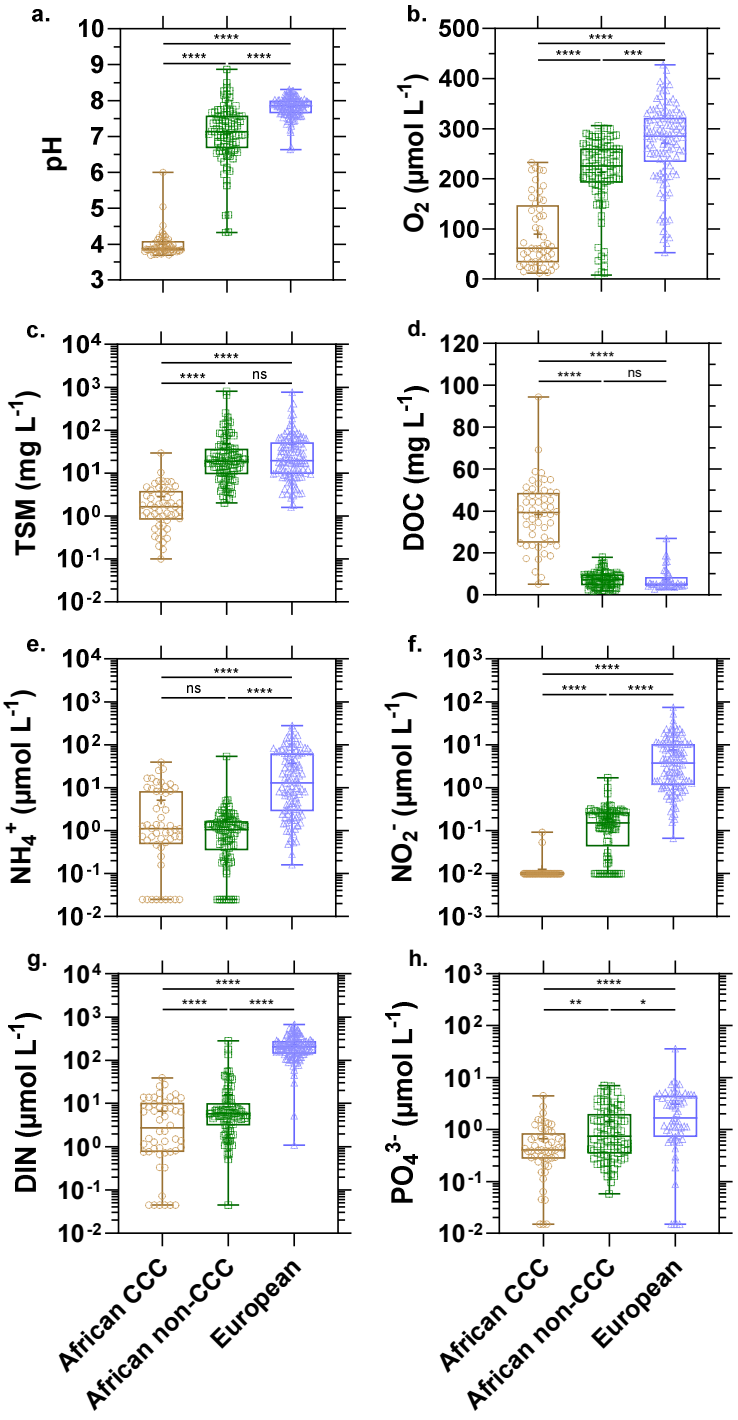

Figure S1 African and European streams show distinct biogeochemical characteristics. Box-plots of pH (**a**), dissolved O_2 (µmol L^{-1}) (**b**), total suspended matter (TSM in mg L^{-1}) (**c**), dissolved organic carbon (DOC in mg L^{-1}) (**d**), NH_4^+ (µmol L^{-1}) (**e**), NO_2^- (µmol L^{-1}) (**f**), dissolved inorganic nitrogen (DIN in µmol L^{-1}) (**g**), and PO_4^{3-} (µmol L^{-1}) (**h**) in African streams draining the flooded forest of the Cuvette Centrale Congolaise (CCC), other African streams, and European streams (Fig. 1). The box represents the first and third quartile, horizontal line corresponds to the median, the cross to the mean, error bars correspond to the maximum and minimum, symbols show all data points. Results of the statistical comparison of means are summarized on top of the figures and detailed in Table S3.

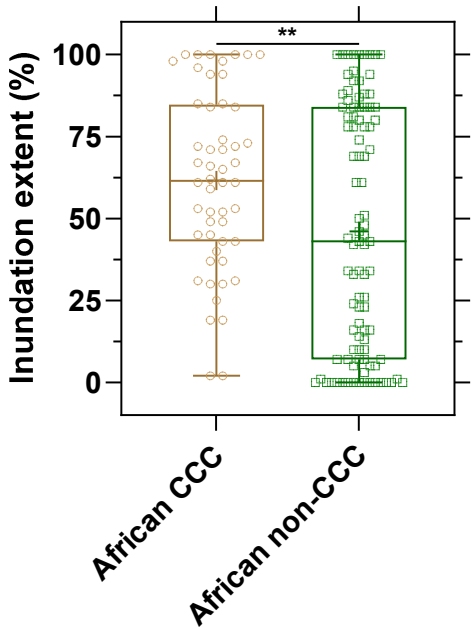

Figure S2 African streams within and outside Cuvette Centrale Congolaise (CCC) have different inundation patterns. Annual maximum of inundation extent in reach catchment (inu_pc_cmx) extracted from RiverATLAS (60) (%) in African streams draining the flooded forest of the CCC, other African streams (non-CCC) (Fig. 1). The box represents the first and third quartile, horizontal line corresponds to the median, the cross to the mean, error bars correspond to the maximum and minimum, symbols show all data points. Results of the statistical comparison of means are summarized on top of the figure and detailed in Table S5.

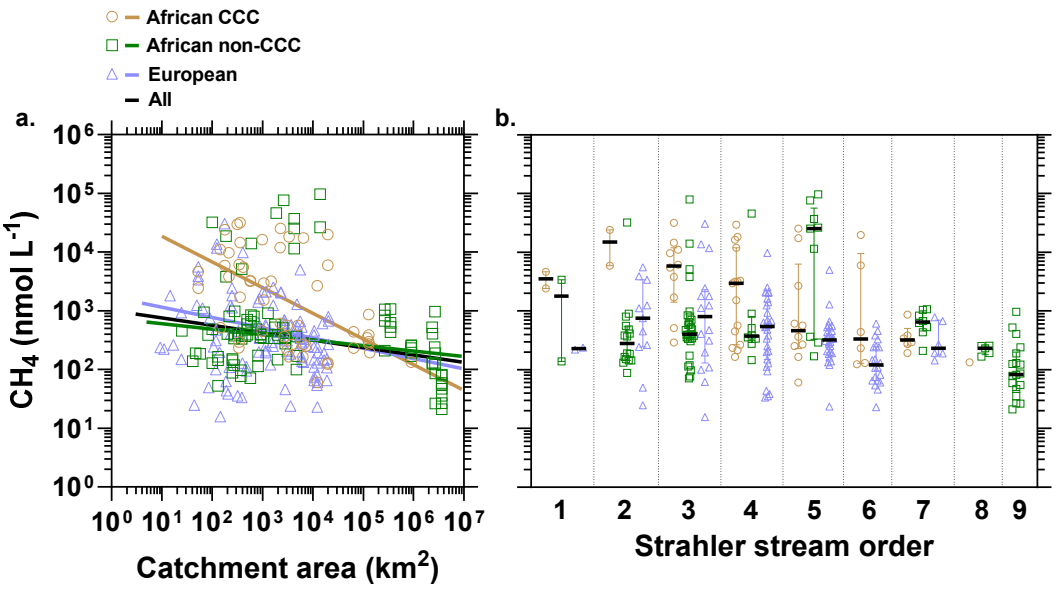

Figure S3 Dissolved methane concentrations decrease with river size. Dissolved methane concentration (CH_4 in nmol L^{-1}) versus catchment area (km^2) (**a**) and stream order (**b**) in African streams draining the flooded forest of the Cuvette Centrale Congolaise (CCC), other African streams, and European streams (Fig. 1). Lines show the quantile linear regressions (Table S4).

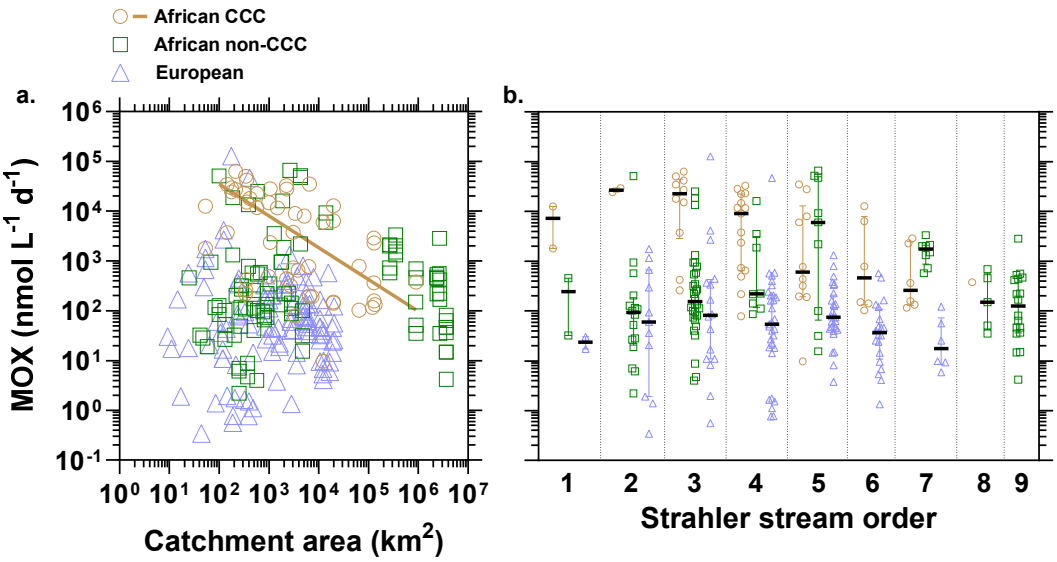

Figure S4 Methane oxidation (MOX) is invariant with river size. MOX (nmol L^{-1} d^{-1}) *versus* catchment area (km^2) (**a**) and stream order (**b**) in African streams draining the flooded forest of the Cuvette Centrale Congolaise (CCC), other African streams, and European streams (Fig. 1). Horizontal line corresponds to the median, error bars to first and third quartile, symbols show all data points. Other line shows the quantile linear regression (Table S4).

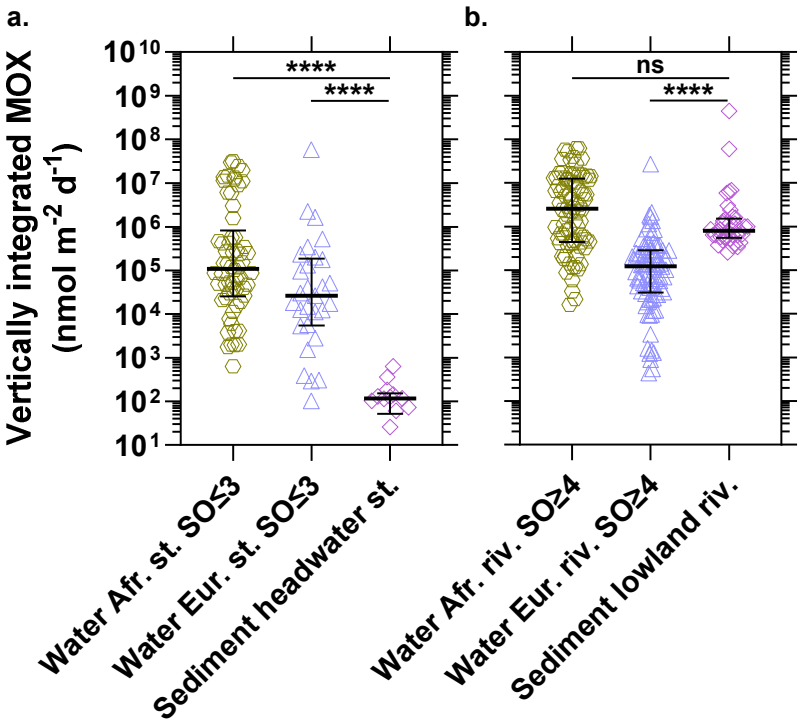

Figure S5 Methane oxidation (MOX) in rivers in the water column is equivalent to or higher than in sediments. Vertically integrated MOX (nmol L^{-1} m^{-2}) in the water column of African (Afr.) and European (Eur.) streams (st.) and rivers (riv.) and in sediments (Table S2) separated in small (headwaters or Strahler stream order (SO)≤3) (**a**) and large (lowland riv. or SO≥4) (**b**) systems. Results of the statistical comparison of means are summarized on top of the figure and detailed in Table S4.

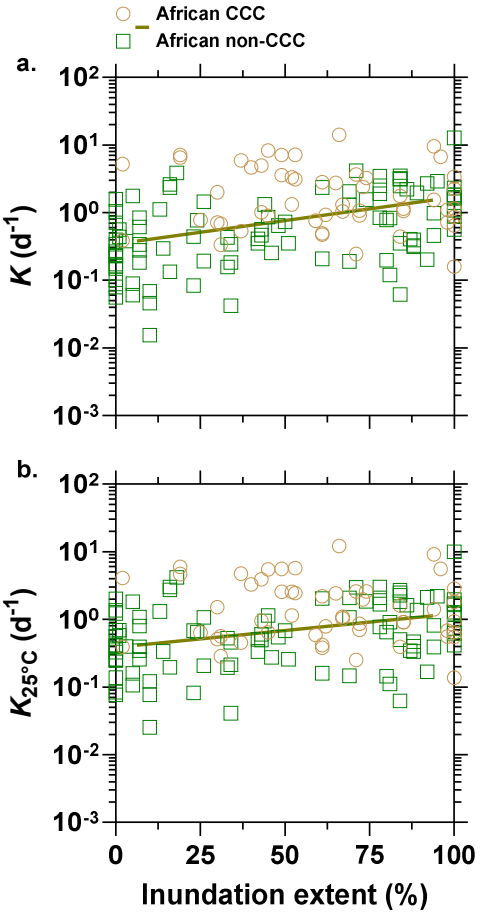

Figure S6 Methane oxidation apparent rate constant (*K*) in African rivers increases with wetland inundation. *K* (d^{-1}) (**a**) and *K* normalized to a constant temperature of 25°C ($K_{25°C}$ in d^{-1}) (**b**) *versus* annual maximum of inundation extent in reach catchment (inu_pc_cmx) extracted from RiverATLAS (60) (%) in African streams draining the flooded forest of the Cuvette Centrale Congolaise (CCC), other African streams (non-CCC) (Fig. 1). Lines show the quantile linear regressions (Table S4).

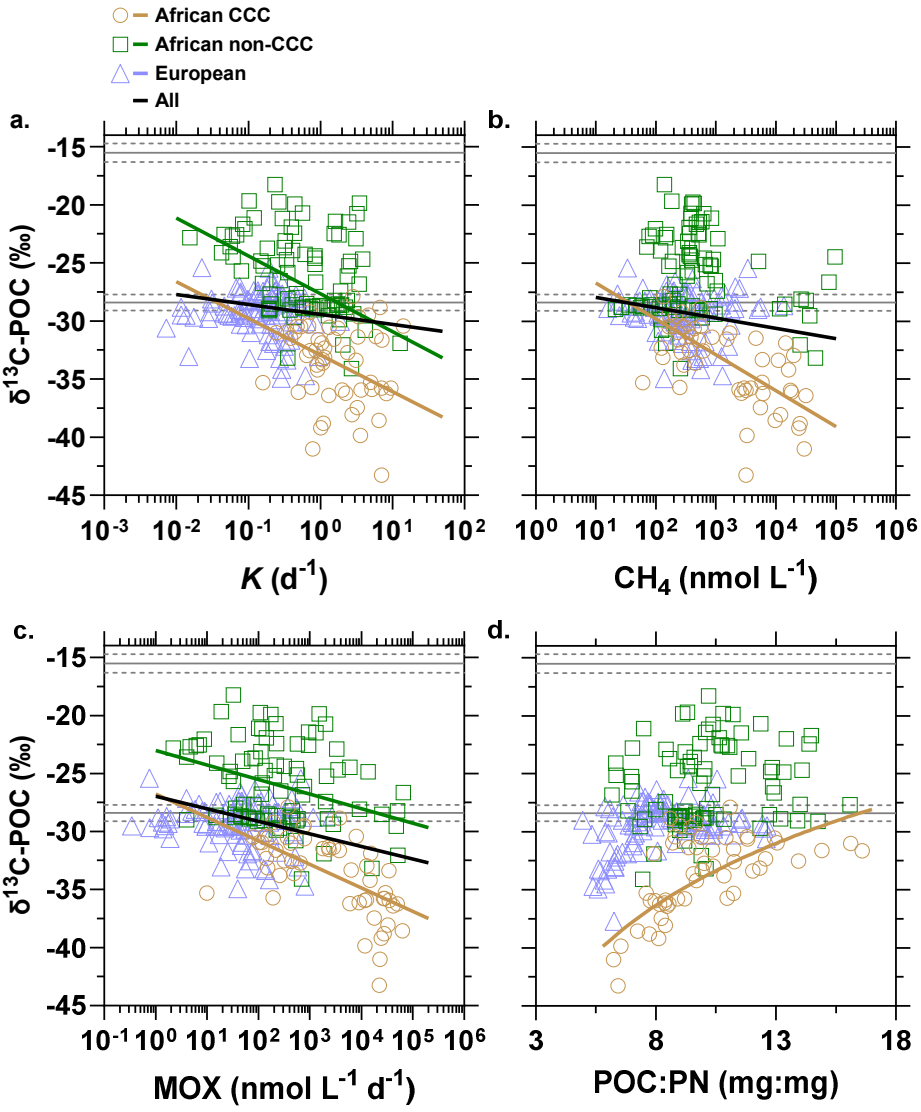

Figure S7 $^{13}C/^{12}C$ ratio of particulate organic carbon ($\delta^{13}C$-POC) decreases with the abundance of methanotrophs in African rivers draining flooded forests. $\delta^{13}C$-POC *versus* methane oxidation (MOX) apparent rate constant (K in d^{-1}) (**a**), CH_4 dissolved concentration (nmol L^{-1}) (**b**), MOX (nmol L^{-1} d^{-1}) (**c**), and particulate organic carbon to particulate nitrogen ratio (POC:PN in mg:mg) (**d**) in African streams draining the flooded forest of the Cuvette Centrale Congolaise (CCC), other African streams, and European streams (Fig. 1). Horizontal grey lines indicate mean (full line) and standard deviation (dotted lines) of average soil organic carbon stable isotope composition with a dominance of C4 (-15:5±0.8 ‰) and C3 plants (-28.4±0.7 ‰) (78). Lines show the quantile linear regressions (Table S4). Plot with K values normalized to a temperature of 25°C is shown in Figure S18.

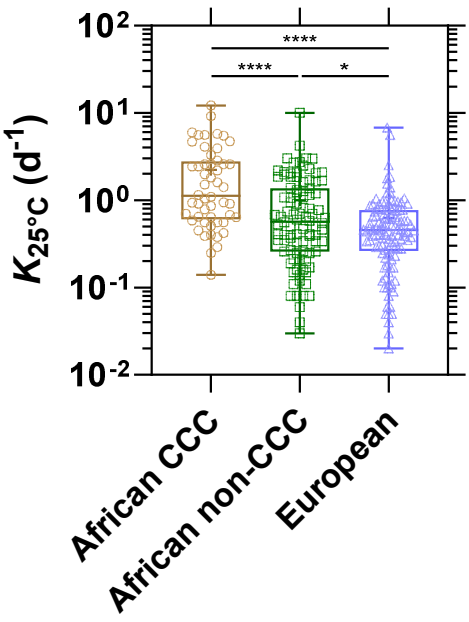

Figure S8 Methane oxidation apparent rate (*K*) is higher in African rivers draining flooded forests. *K* normalized to a constant temperature of 25°C ($K_{25°C}$ in d^{-1}) in African streams draining the flooded forest of the Cuvette Centrale Congolaise (CCC), other African streams, and European streams (Fig. 1). The box represents the first and third quartile, horizontal line corresponds to the median, the cross to the mean, error bars correspond to the maximum and minimum, symbols show all data points. Results of the statistical comparison of means are summarized on top of the figures and detailed in Table S3.

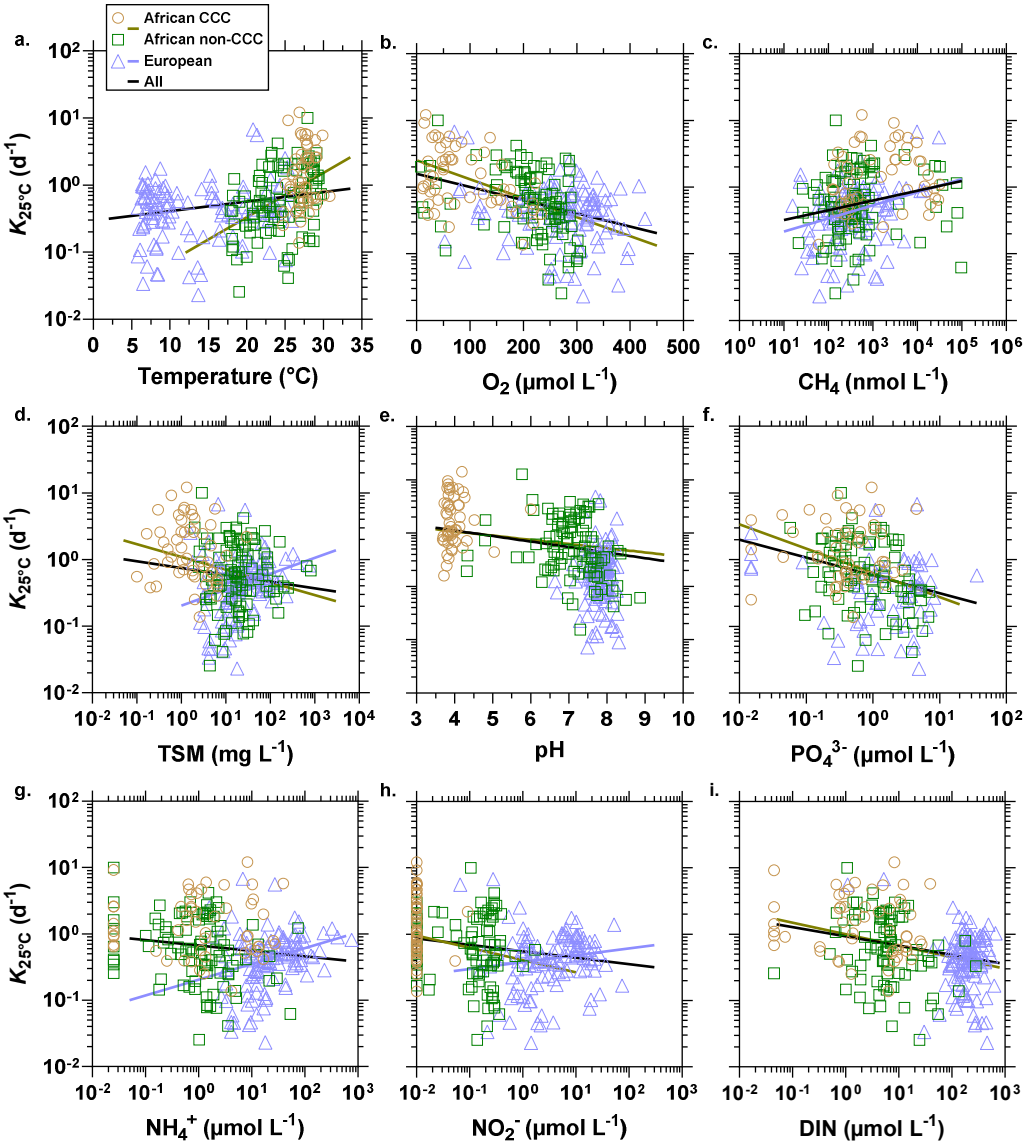

Figure S9 Methane oxidation apparent rate constant (*K*) dependency on several biogeochemical variables. *K* normalized to a temperature of 25°C ($K_{25°C}$ in d^{-1}) *versus* water temperature (°C) (**a**), dissolved O_2 (µmol L^{-1}) (**b**), dissolved CH_4 (nmol L^{-1}) (**c**), total suspended matter (TSM in mg L^{-1}) (**d**), pH (**e**), PO_4^{3-} (µmol L^{-1}) (**f**); NH_4^+ (µmol L^{-1}) (**g**), NO_2^- (µmol L^{-1}) (**h**), dissolved inorganic nitrogen (DIN in µmol L^{-1}) (**i**), in African streams draining the flooded forest of the Cuvette Centrale Congolaise (CCC), other African streams, and European streams (Fig. 1) Lines show the quantile linear regressions (Table S4).

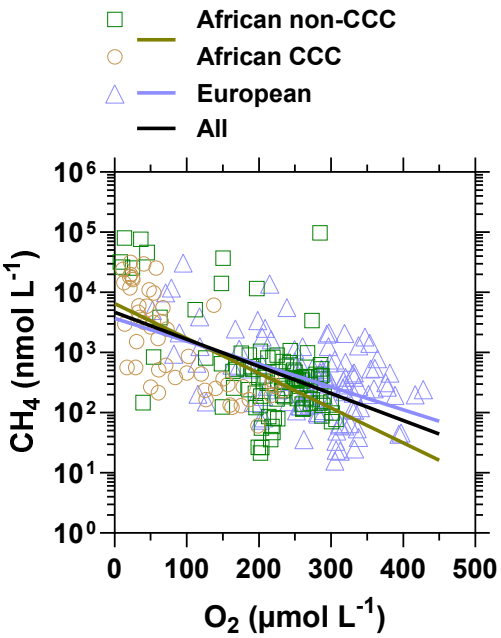

Figure S10 Dissolved methane concentration increases at low O_2 concentrations in African and European rivers. Dissolved CH_4 concentration (nmol L^{-1}) *versus* dissolved O_2 concentration (µmol L^{-1}) in African streams draining the flooded forest of the Cuvette Centrale Congolaise (CCC), other African streams, and European streams (Fig. 1) Lines show the quantile linear regressions (Table S4).

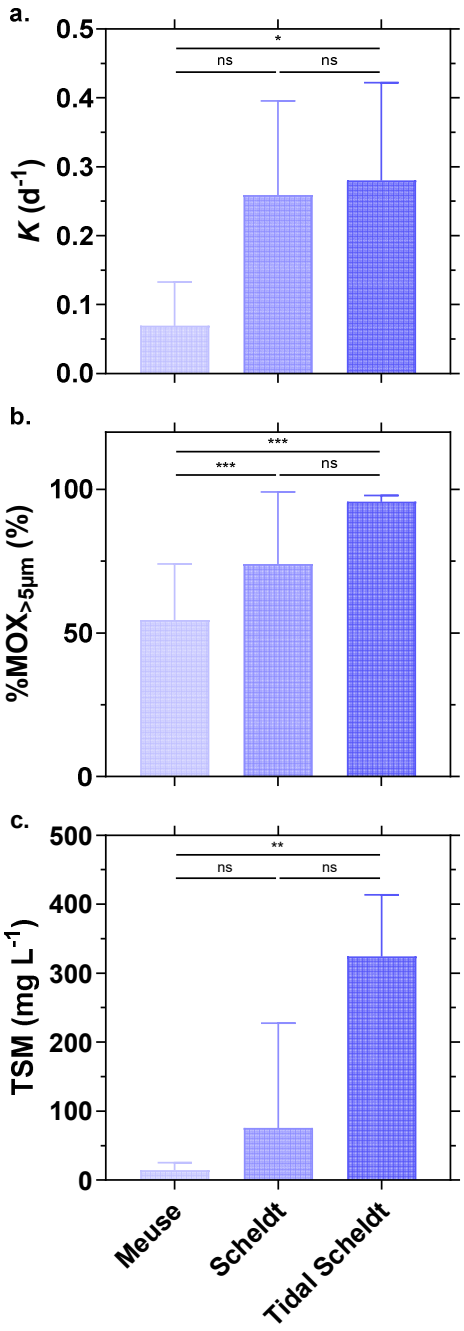

Figure S11 Methane oxidation (MOX) in European rivers increases with particles. MOX apparent rate constant (K in d^{-1}) (**a**), contribution of particle-attached MOB (>5 µm) to MOX (%$MOX_{>5µm}$ in %) (**b**), and total suspended matter (TSM in mg L^{-1}) (**c**) in the Meuse, Scheldt proper, and tidal Scheldt rivers. Results of the statistical comparison of means are summarized on top of the figures and detailed in Table S6.

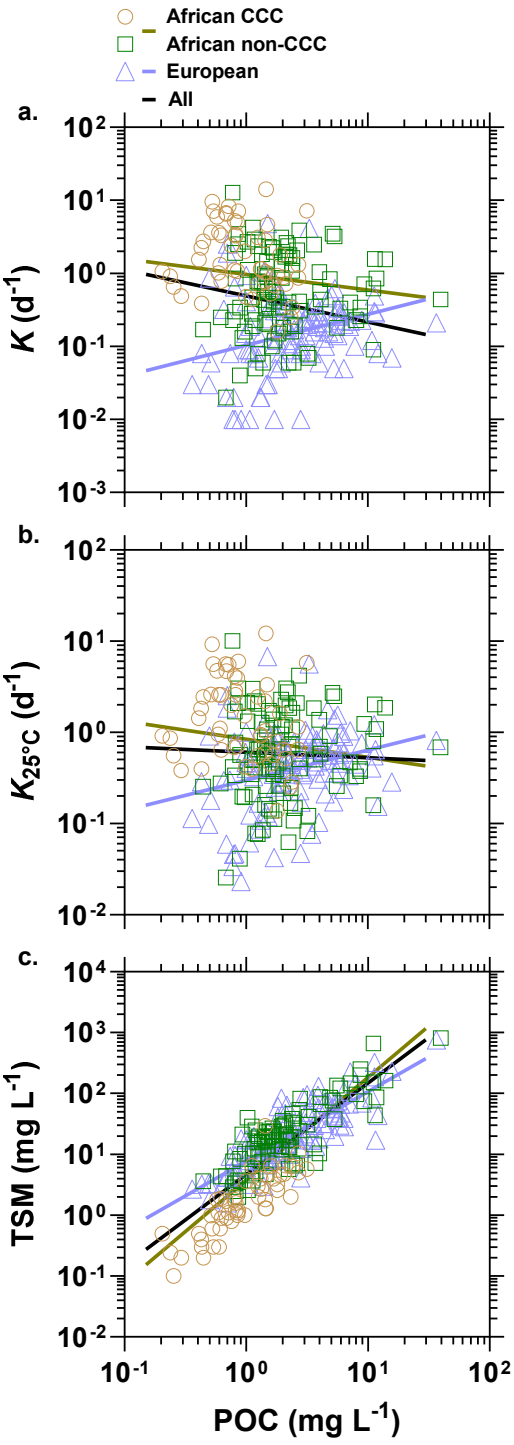

Figure S12 Methane oxidation apparent rate constant (*K*) dependency on particulate organic carbon (POC) in rivers. *K* (d^{-1}) (**a**), *K* normalized to a temperature of 25°C ($K_{25°C}$ in d^{-1}) (**b**), and total suspended matter (TSM in mg L^{-1}) (**c**) *versus* POC (mg L^{-1}) in African streams draining the flooded forest of the Cuvette Centrale Congolaise (CCC), other African streams, and European streams (Fig. 1) Lines show the quantile linear regressions (Table S4).

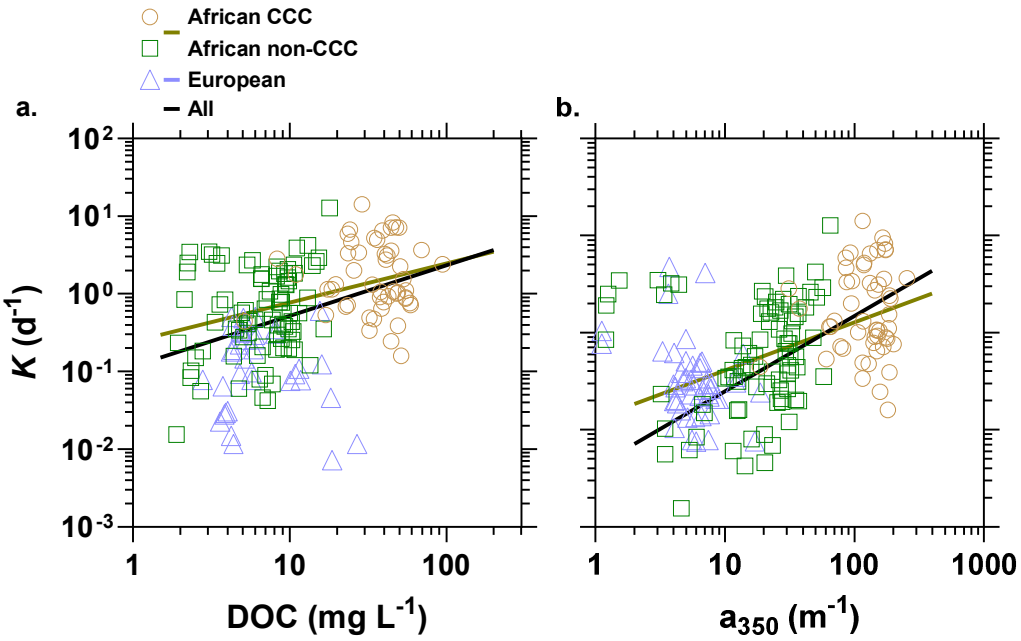

Figure S13 Methane oxidation apparent rate constant (*K*) dependency on dissolved organic carbon (DOC) in rivers. *K* (d^{-1}) *versus* dissolved organic carbon (DOC in mg L^{-1}) (**a**) and colored dissolved organic matter absorbance at 350 nm (a_{350} in m^{-1}) (**b**) in African streams draining the flooded forest of the Cuvette Centrale Congolaise (CCC), other African streams, and European streams (Fig. 1) Lines show the quantile linear regressions (Table S4). Plots with *K* values normalized to a temperature of 25°C are shown in Figure S20.

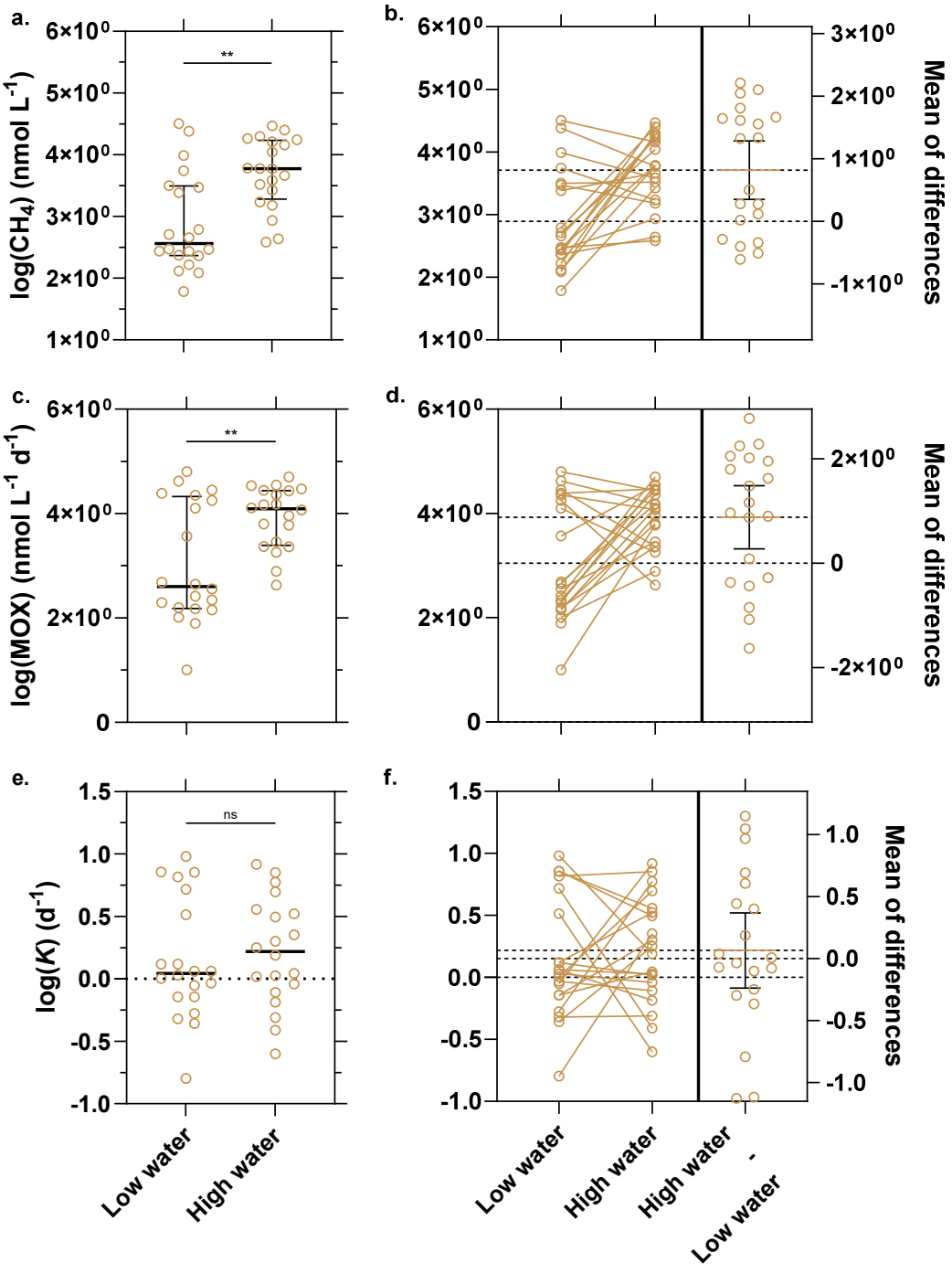

Figure S14 Dissolved CH_4 concentration and methane oxidation (MOX) are higher during high water than low water period in African rivers draining flooded forests. Distribution and estimation plots of dissolved CH_4 concentration (nmol L^{-1}) (**a**,**b**), MOX (nmol L^{-1} d^{-1}) (**c**,**d**), and MOX apparent rate constant (*K* in d^{-1}) (**e**,**f**) during the low water and high water period in the streams and rivers draining the Cuvette Centrale Congolaise (paired measurements). On the left plots, the horizontal black line corresponds to the median, error bars to first and third quartile, on the right plots, the horizontal black line corresponds to the mean and 95% confidence interval of the differences between low water and high water periods, symbols show all data points. Results of the statistical comparison of means are summarized on top of the figures and detailed in Table S7.

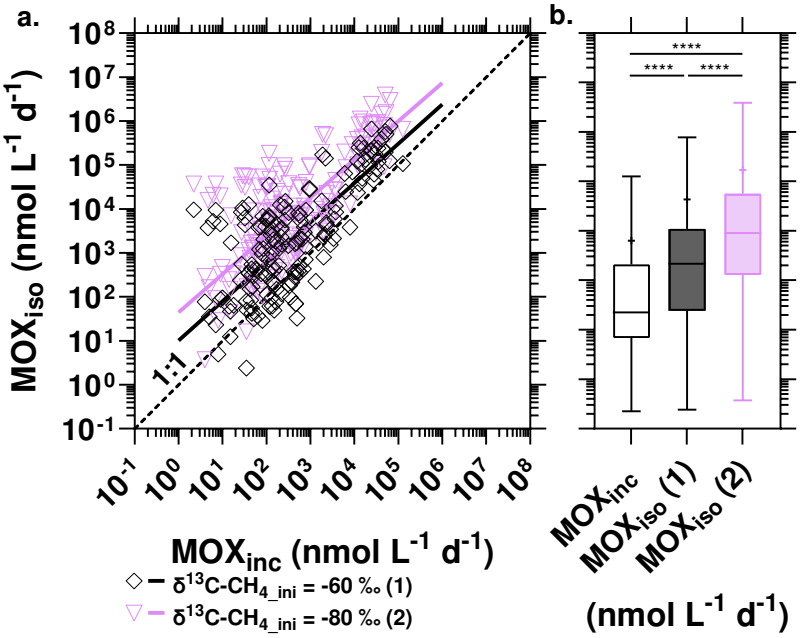

Figure S15 Methane oxidation (MOX) estimated from isotopic fractionation is higher than measured by incubations. MOX (nmol L^{-1} d^{-1}) from incubations (MOX_{inc}) versus MOX from Rayleigh fractionation model (72) (MOX_{iso}) using two values for initial $^{13}C/^{12}C$ ratio of CH_4 ($\delta^{13}C\text{-}CH_4$) of -80 and -60 ‰ (**a**), and corresponding box-plots (**b**). In plot (**a**) solid lines show the quantile linear regressions (Table S3) and dotted line the 1:1 line. In plot (**b**), the box represents the first and third quartile, horizontal line corresponds to the median, the cross to the mean, error bars correspond to the maximum and minimum. Were excluded from the analysis four negative values of MOX_{iso} based on initial $\delta^{13}C\text{-}CH_4$ of -60‰. Results of the statistical comparison of means are summarized on top of the figures and detailed in Table S3.

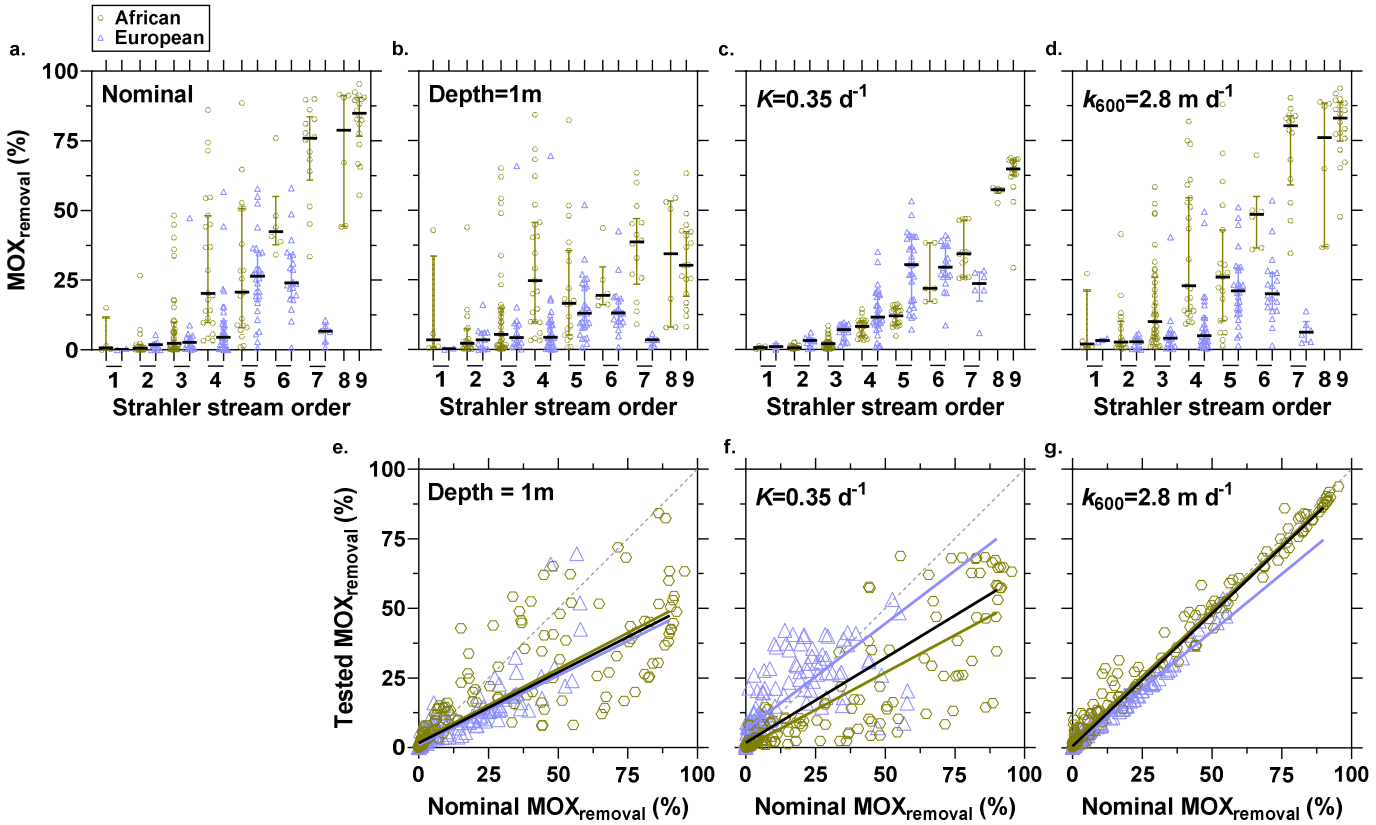

Figure S16 Contribution of methane oxidation to total dissolved CH_4 methane removal mainly depends on depth and methane oxidation apparent rate constant (*K*) and marginally on gas transfer velocity gas transfer velocity (k_{600}). Contribution of methane oxidation to total dissolved CH_4 methane removal including degassing to the atmosphere ($MOX_{removal}$ in %) based on initial stream depth (m), *K* (d^{-1}), and k_{600} (m d^{-1}) values (nominal) (**a**), re-computed using a constant depth of 1 m (**b**) or a *K* of 0.35 d^{-1} (**c**), or a constant k_{600} of 2.8 m d^{-1} (**d**) (median values of the whole data set) as a function of Strahler stream order in African and European streams (Fig. 1), and re-computed (tested) $MOX_{removal}$ values plotted *versus* nominal ones (**e**,**f**,**g**). In plots **a**, **b**, **c**, and **d** horizontal black line corresponds to the median, error bars to first and third quartile, symbols show all data points. In plots e, f, and g, solid lines show the quantile linear regressions (Table S4) and the 1:1 line is represented by the dotted line.

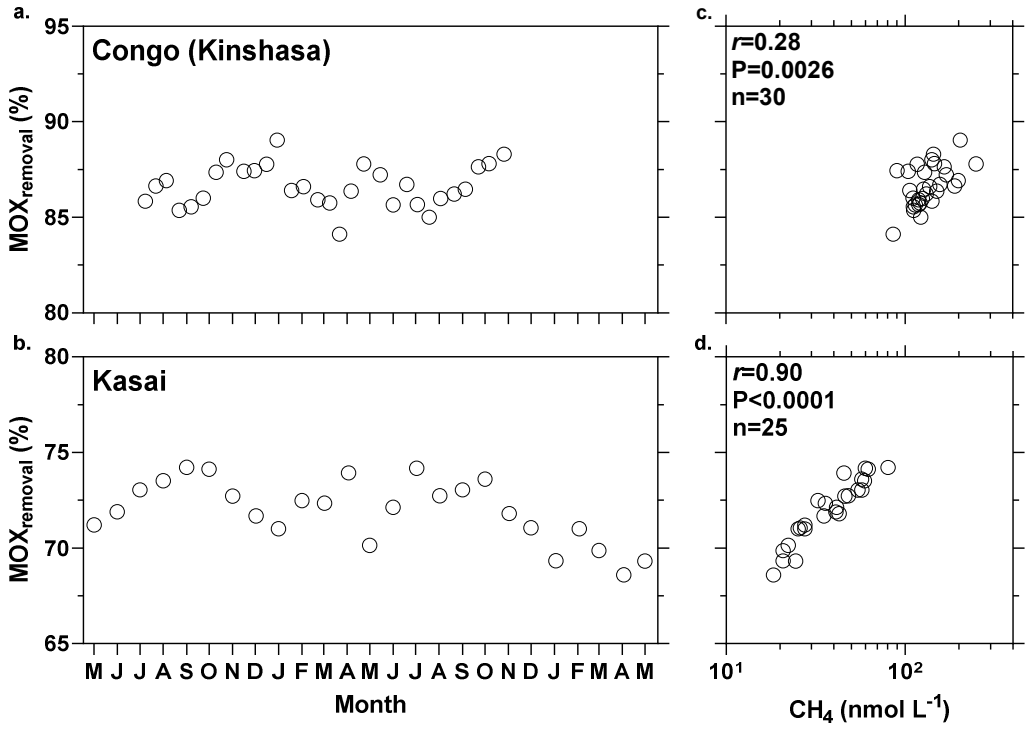

Figure S17 Contribution of methane oxidation to total dissolved CH_4 methane removal shows low seasonal variability in African rivers. Time-series of the contribution of methane oxidation to total dissolved CH_4 methane removal including degassing to the atmosphere ($MOX_{removal}$ in %) in the Congo River at Kinshasa (22-07-2011 to 09-11-2012, averaged depth = 13.9 m) (**a**) and the Kasai River (14-05-2015 to 15-05-2017, average depth = 9.5 m) (**b**), and correlation of $MOX_{removal}$ with dissolved CH_4 concentration (**c**,**d**). MOX was calculated from dissolved CH_4 concentrations based the linear quantile regression derived from MOX and CH_4 measurements in the Congo mainstem and the Kasai River ($\log(MOX) = -0.61\pm0.47 + 1.36\pm0.22 \times \log(CH_4)$, $P<0.00001$, $n=24$). The diffusive CH_4 emissions were calculated from gas transfer velocities derived from measured freshwater discharge contemporary to sampling for dissolved CH_4 concentrations. The conversion of the diffusive CH_4 emissions from areal to volumetric units accounted for seasonal variations of river depth. Time series of dissolved CH_4 concentration were reported by Reference (15).

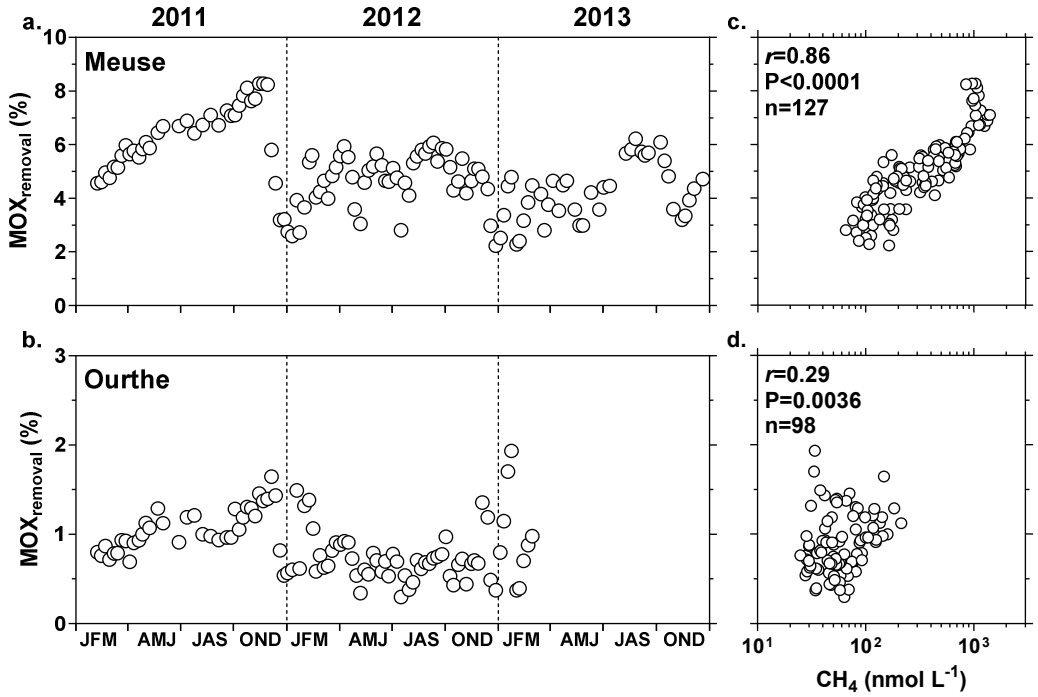

Figure S18 Contribution of methane oxidation to total dissolved CH_4 methane removal shows low seasonal variability in European rivers. Time-series of the contribution of methane oxidation to total dissolved CH_4 methane removal including degassing to the atmosphere ($MOX_{removal}$ in %) in the Meuse (07/02/2011 to 28/02/2013, average depth = 2.6 m) (**a**) and the Ourthe rivers (07/02/2011 to 20/12/2013, average depth = 0.95 m) (**b**), and correlation of $MOX_{removal}$ with dissolved CH_4 concentration (c,d). MOX was calculated from dissolved CH_4 concentrations based the linear quantile regression derived from MOX and CH_4 measurements in the Meuse and Ourthe rivers ($\log(MOX) = -2.10\pm0.30 + 1.30\pm0.12 \times \log(CH_4)$, $P<0.00001$, $n=21$). The diffusive CH_4 emissions were calculated from gas transfer velocities derived from measured freshwater discharge contemporary to sampling for dissolved CH_4 concentrations. The conversion of the diffusive CH_4 emissions from areal to volumetric units accounted for seasonal variations of river depth. Time series of dissolved CH_4 concentration were reported by Reference (62).

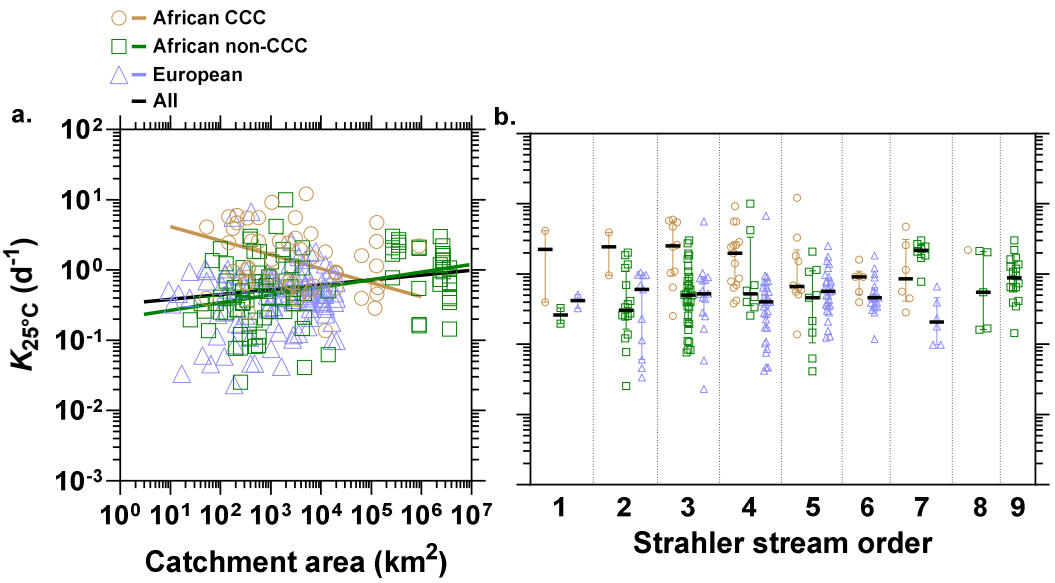

Figure S19 Methane oxidation apparent rate constant (*K*) increases with stream size. *K* normalized to a temperature of 25°C ($K_{25°C}$ in d^{-1}) in African streams draining the flooded forest of the Cuvette Centrale Congolaise (CCC), other African streams, and European streams (Fig. 1) versus catchment area (km^2) (**a**) and stream order (**b**). Horizontal black line corresponds to the median, error bars to first and third quartile, symbols show all data points. Other lines show the quantile linear regressions (Table S4).

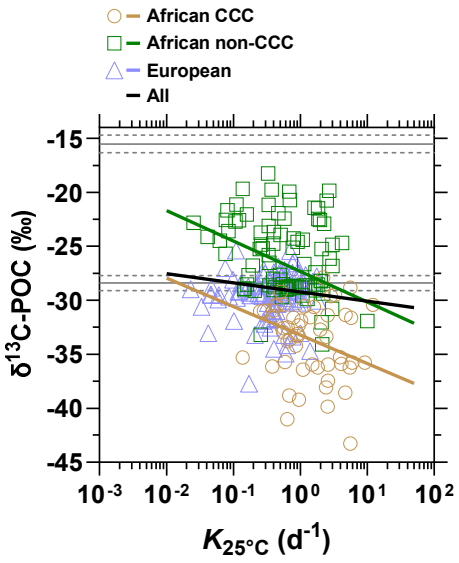

Figure S20 $^{13}C/^{12}C$ ratio of particulate organic carbon ($\delta^{13}C$-POC) decreases with methane oxidation apparent rate constant (*K*) in streams. $\delta^{13}C$-POC *versus* *K* normalized to a temperature of 25°C ($K_{25°C}$ in d^{-1}) in African streams draining the flooded forest of the Cuvette Centrale Congolaise (CCC), other African streams, and European streams (Fig. 1). Horizontal grey lines indicate mean (full line) and standard deviation (dotted lines) of average soil organic carbon stable isotope composition with a dominance of C4 (-15:5±0.8 ‰) and C3 plants (-28.4±0.7 ‰) (78). Lines show the quantile linear regressions (Table S4).

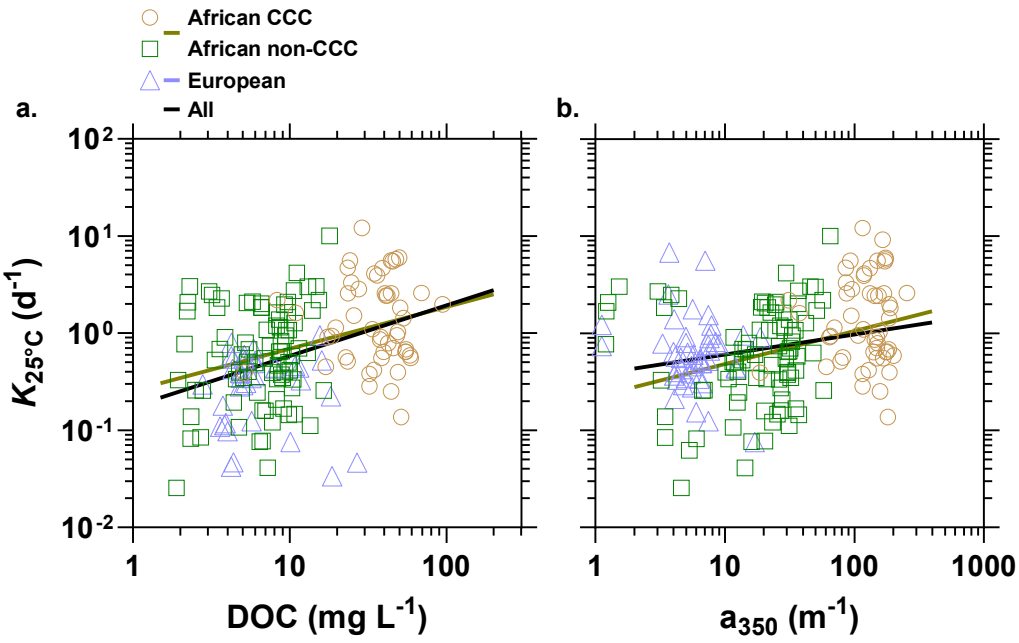

Figure S21 Methane oxidation apparent rate constant (*K*) dependency on dissolved organic carbon (DOC) in rivers. *K* normalized to a temperature of 25°C ($K_{25°C}$ in d^{-1}) *versus* DOC (mg L^{-1}) (**a**) and colored dissolved organic matter absorbance at 350 nm (a_{350} in m^{-1}) (**b**) in African streams draining the flooded forest of the Cuvette Centrale Congolaise (CCC), other African streams, and European streams (Fig. 1) Lines show the quantile linear regressions (Table S4).

Table S1 Sample identifier (Sample_ID), region, sampling date, stream name, latitude and longitude, and relevant stream characteristics derived from RiverATLAS: reach identifier (HYRIV_ID), upstream catchment area (km^2), Strahler stream order, annual average freshwater discharge at reach point ($m^3\ s^{-1}$), stream gradient (decimeters km^{-1}), land cover extent in total watershed upstream of reach pour point (in % cover) aggregated into three classes (forest, shrub and herbaceous, cropland).

Sample_ID	Region	Samplig date	Name	Latitude	Longitude	HYRIV_ID	Catchment area	Strahler order	Annual discharge	Stream Gradient	Forest cover	Shrub and herbaceous cover	Cropland cover
		dd-mm-yyyy		°N	°E		km^2		$m^3\ s^{-1}$	dm km^{-1}	% cover	% cover	% cover
RIVER_1	African non-CCC	27-10-2016	Ntungwe	-0.57458	29.72385	11008816	2819.5	4	20.4	22	10	40	51
RIVER_2	African non-CCC	27-10-2016	Ishasha	-0.61627	29.65745	11013050	918.6	3	7.5	29	37	16	46
RIVER_3	African non-CCC	28-10-2016	Nyamugasani	-0.12287	29.84283	10996499	497.4	3	2.5	53	54	17	21
RIVER_4	African non-CCC	28-10-2016	Nyamugasani	-0.00895	29.89895	10992953	336.6	2	1.6	49	44	23	24
RIVER_5	African non-CCC	29-10-2016	Nyamwamba	0.19460	30.10448	10989781	251.1	2	1.0	76	31	0	52
RIVER_6	African non-CCC	29-10-2016	Sebwe	0.25242	30.11657	10986222	372.9	3	1.5	134	45	1	30
RIVER_7	African non-CCC	22-03-2017	Nyamugasani	-0.12287	29.84283	10996499	497.4	3	2.5	53	54	17	21
RIVER_8	African non-CCC	23-03-2017	Isasha	-0.61612	29.65788	11013050	918.6	3	7.5	29	37	16	46
RIVER_9	African non-CCC	23-03-2017	Ntungwe	-0.57462	29.72410	11008816	2819.5	4	20.4	22	10	40	51
RIVER_10	African non-CCC	23-03-2017	Nchwera	-0.45847	29.80139	11005453	461.5	2	3.0	32	43	12	42
RIVER_11	African non-CCC	23-03-2017	Nyamweru	-0.31278	29.87104	11001080	280.3	3	1.6	46	95	0	4
RIVER_12	African non-CCC	25-03-2017	Nyamwamba	0.19472	30.10452	10989781	251.1	2	1.0	76	31	0	52
RIVER_13	African non-CCC	25-03-2017	Ssebo	0.25192	30.11678	10986222	372.9	3	1.5	134	45	1	30
RIVER_14	African non-CCC	25-03-2017	Nsongya	0.54330	30.16837	10977658	47.0	2	0.2	169	78	0	22
RIVER_15	African non-CCC	27-03-2017	tributary of Dura	0.45860	30.37982	10979790	129.9	2	0.6	87	94	0	5
RIVER_16	African non-CCC	27-03-2017	Mpanga	0.10058	30.46215	10989376	4727.8	5	21.5	5	20	19	62
RIVER_17	African non-CCC	18-01-2018	Ishasha	-0.61612	29.65788	11013050	918.6	3	7.5	29	37	16	46
RIVER_18	African non-CCC	18-01-2018	Ntungwe	-0.57462	29.72410	11008816	2819.5	4	20.4	22	10	40	51
RIVER_19	African non-CCC	18-01-2018	Rwampuru	-0.38402	29.87593	11003028	200.7	3	1.2	51	68	9	24
RIVER_20	African non-CCC	19-01-2018	Kihizi	-0.42304	29.86777	11004438	99.4	2	0.6	68	93	0	6
RIVER_21	African non-CCC	19-01-2018	Nyamweru	-0.31278	29.87104	11001080	280.3	3	1.6	46	95	0	4
RIVER_22	African non-CCC	20-01-2018	Nyamwamba	0.19472	30.10452	10989781	251.1	2	1.0	76	31	0	52
RIVER_23	African non-CCC	21-01-2018	Ntabago	0.37300	30.22882	10982150	40.8	1	0.2	204	41	0	59
RIVER_24	African non-CCC	21-01-2018	Ntabago	0.35383	30.27268	10982469	57.5	2	0.2	130	36	0	64
RIVER_25	African non-CCC	21-01-2018	Nsongya	0.35015	30.27837	10982702	572.3	3	2.5	56	57	0	43
RIVER_26	African non-CCC	02-11-2018	Katonga	-0.04160	32.02000	10993577	13953.0	5	116.8	10	19	39	42
RIVER_27	African non-CCC	09-06-2019	Katonga	-0.04178	32.02030	10993577	13953.0	5	116.8	10	19	39	42
RIVER_28	African non-CCC	10-08-2022	Congo	-3.80880	15.95401	11098042	3611637.0	9	38289.7	0	83	9	6
RIVER_29	African CCC	16-08-2022	Lokoro	-1.69270	18.54409	11042636	19857.8	6	261.0	3	95	0	4
RIVER_30	African CCC	16-08-2022	Lokoro	-1.69569	18.49640	11042891	19878.9	6	261.7	6	95	0	4
RIVER_31	African CCC	17-08-2022	Bolongo Baambi	-1.44159	18.72099	11034980	3821.0	4	54.8	6	98	0	2
RIVER_32	African CCC	17-08-2022	Lotoi	-1.44337	18.72723	11034981	7312.4	5	108.3	3	99	0	0
RIVER_33	African CCC	18-08-2022	Donkese	-1.57094	18.50392	11039334	12157.6	5	177.2	6	97	0	1
RIVER_34	African CCC	18-08-2022	Mbalenzale	-1.52505	18.25787	11038487	342.1	3	4.8	21	96	0	1
RIVER_35	African CCC	19-08-2022	Nkoto	-1.54101	18.01154	11037976	2260.4	5	35.5	3	96	0	4
RIVER_36	African CCC	19-08-2022	Isaba	-1.60006	18.05652	11040122	2697.1	5	42.4	5	93	0	4
RIVER_37	African CCC	20-08-2022	Olongo Lule	-1.66870	17.96399	11042074	3038.4	4	41.6	2	88	2	9
RIVER_38	African CCC	20-08-2022	Olongo Lule	-1.67473	18.02254	11042359	3093.3	4	43.0	7	88	2	9
RIVER_39	African CCC	20-08-2022	Bosongo	-1.90130	18.15664	11049173	144.6	3	2.2	15	77	0	20
RIVER_40	African CCC	21-08-2022	Mpongo Boli	-1.99835	18.16323	11052103	338.5	4	5.0	12	94	0	5
RIVER_41	African CCC	21-08-2022	Lobeke	-2.37716	18.24657	11063613	992.9	4	14.3	5	96	1	2
RIVER_42	African CCC	22-08-2022	Luabu	-2.76986	18.34906	11073988	3358.6	4	43.5	7	96	0	3
RIVER_43	African CCC	22-08-2022	Lukenie	-2.78449	18.35374	11074446	64865.9	6	852.6	0	87	4	8
RIVER_44	African CCC	22-08-2022	Fimi	-2.77268	17.88950	11073981	120177.6	7	1669.3	2	89	3	6
RIVER_45	African CCC	23-08-2022	Molibampê	-2.57393	17.74092	11068678	5092.1	5	67.1	2	90	8	2
RIVER_46	African CCC	23-08-2022	Molibampê	-2.71432	17.70250	11072940	6528.9	5	85.5	2	89	9	2
RIVER_47	African CCC	23-08-2022	Molibampê	-2.66543	17.74315	11071278	6307.6	5	82.6	5	89	9	2
RIVER_48	African CCC	24-08-2022	Fimi	-2.74306	17.59891	11073370	127821.1	7	1768.4	3	89	3	6
RIVER_49	African CCC	24-08-2022	Fimi	-2.89225	17.32755	11077088	129982.8	7	1799.0	2	88	4	6
RIVER_50	African CCC	24-08-2022	Fimi	-2.99570	17.05443	11079580	135904.0	7	1870.5	2	88	4	5
RIVER_51	African non-CCC	24-08-2022	Kwa	-3.05113	16.83249	11081974	890260.4	8	8847.1	1	82	15	2
RIVER_52	African non-CCC	24-08-2022	Kwa	-3.05252	16.48862	11081248	893411.9	8	8882.9	0	82	16	2
RIVER_53	African non-CCC	25-08-2022	Kwa	-3.16890	16.20823	11084458	894486.6	8	8896.9	0	82	16	2
RIVER_54	African non-CCC	25-08-2022	Congo	-3.42631	16.16607	11089852	3604648.0	9	38148.7	0	83	9	6
RIVER_55	African non-CCC	25-08-2022	Congo	-3.81038	15.95265	11098042	3611637.0	9	38289.7	0	83	9	6
RIVER_56	African non-CCC	25-08-2022	Congo	-4.01698	15.61402	11101977	3625209.0	9	38524.2	0	83	9	6
RIVER_57	African non-CCC	26-08-2022	Congo	-4.19946	15.51006	11105517	3625626.0	9	38526.5	1	83	9	6
RIVER_58	African non-CCC	22-03-2023	Kwa	-3.05569	16.49010	11081248	893411.9	8	8882.9	0	82	16	2
RIVER_59	African CCC	23-03-2023	Fimi	-2.89056	17.32885	11077088	129982.8	7	1799.0	2	88	4	6
RIVER_60	African CCC	23-03-2023	Fimi	-2.74441	17.60095	11073370	127821.1	7	1768.4	3	89	3	6
RIVER_61	African CCC	24-03-2023	Bowele	-2.22165	18.52707	11058649	1486.4	4	20.3	3	94	1	5
RIVER_62	African CCC	25-03-2023	Mpongo-Boli	-1.99688	18.15643	11052102	316.9	4	4.7	0	96	0	4
RIVER_63	African CCC	25-03-2023	Bosongo	-1.90074	18.15611	11049173	144.6	3	2.2	15	77	0	20
RIVER_64	African CCC	26-03-2023	Lokoro	-1.69230	18.54378	11042636	19857.8	6	261.0	3	95	0	4
RIVER_65	African CCC	27-03-2023	Lokoro	-1.69490	18.49557	11042891	19878.9	6	261.7	6	95	0	4
RIVER_66	African CCC	27-03-2023	Ndongese	-1.57081	18.50362	11039334	12157.6	5	177.2	6	97	0	1
RIVER_67	African CCC	28-03-2023	Mbalenzale	-1.52347	18.26152	11038487	342.1	3	4.8	21	96	0	1
RIVER_68	African CCC	28-03-2023	Nkoto	-1.53914	18.01027	11037976	2260.4	5	35.5	3	96	0	4
RIVER_69	African CCC	31-03-2023	Lobeke	-2.37704	18.24479	11063613	992.9	4	14.3	5	96	1	2
RIVER_70	African CCC	01-04-2023	Luabu	-2.76966	18.34890	11073988	3358.6	4	43.5	7	96	0	3
RIVER_71	African CCC	01-04-2023	Lukenie	-2.78617	18.35295	11074446	64865.9	6	852.6	0	87	4	8
RIVER_72	African CCC	02-04-2023	Molibampê	-2.71488	17.70248	11072940	6528.9	5	85.5	2	89	9	2
RIVER_73	African CCC	03-04-2023	Kwa	-3.17526	16.19696	11084458	894486.6	8	8896.9	0	82	16	2
RIVER_74	African CCC	07-04-2023	Moninga	-0.82116	17.85945	11015987	355.0	3	4.4	5	99	0	2
RIVER_75	African CCC	07-04-2023	Ngoie	-0.88430	17.94549	11018021	356.7	3	4.6	0	98	0	2
RIVER_76	African CCC	08-04-2023	Lobambo	-0.94313	18.03740	11019799	214.4	3	2.8	6	97	0	3
RIVER_77	African CCC	08-04-2023	Bituka	-1.01817	18.10784	11022238	573.7	4	7.5	7	98	0	2
RIVER_78	African CCC	08-04-2023	Bembe	-0.98960	18.16252	11024228	52.6	1	0.7	17	99	0	0
RIVER_79	African CCC	08-04-2023	Lolo	-0.95640	18.19248	11020038	2251.0	4	29.4	6	94	0	5
RIVER_80	African CCC	09-04-2023	Ehanga	-0.64323	18.14530	11010617	176.7	2	2.1	18	79	0	18
RIVER_81	African CCC	09-04-2023	Zobo	-0.61134	18.09904	11010476	1055.9	4	12.4	6	84	0	15
RIVER_82	African non-CCC	10-04-2023	Congo	-0.65406	17.66233	11011415	2349833.0	9	23947.4	0	85	7	6
RIVER_83	African non-CCC	11-04-2023	Congo	-1.85945	16.54353	11048467	2668710.0	9	28396.5	0	84	7	6
RIVER_84	African CCC	21-08-2023	Moninga	-0.82025	17.85999	11015987	355.0	3	4.4	5	99	0	2
RIVER_85	African CCC	22-08-2023	Ngoie	-0.88441	17.94540	11017752	412.7	3	5.3	2	93	0	2

Table S1 (continued)

RIVER_86	African CCC	22-08-2023	Lobambo	-0.94304	18.03786	11019799	214.4	3	2.8	6	97	0	3
RIVER_87	African CCC	23-08-2023	Bituka	-1.01758	18.10782	11022238	573.7	4	7.5	7	98	0	2
RIVER_88	African CCC	23-08-2023	Bembe	-0.98960	18.16253	11024228	52.6	1	0.7	17	99	0	0
RIVER_89	African CCC	24-08-2023	Ehanga	-0.64298	18.14551	11010617	176.7	2	2.1	18	79	0	18
RIVER_90	African CCC	24-08-2023	Zobo	-0.61090	18.09317	11010476	1055.9	4	12.4	6	84	0	15
RIVER_91	African non-CCC	25-08-2023	Congo	-0.63883	17.66903	11010766	2341691.0	9	23758.8	0	85	7	6
RIVER_92	African non-CCC	25-08-2023	Congo	-0.92303	17.38118	11019251	2351022.0	9	24377.5	0	85	7	6
RIVER_93	African non-CCC	26-08-2023	Moliba Mbo	-1.07050	17.25795	11022617	1989.3	4	22.3	0	96	0	2
RIVER_94	African non-CCC	26-08-2023	Congo	-1.13078	17.00014	11025361	2355373.0	9	24421.3	10	84	7	6
RIVER_95	African non-CCC	26-08-2023	Congo	-1.46212	16.73846	11035999	2640976.0	9	27728.0	0	85	6	6
RIVER_96	African non-CCC	26-08-2023	Sangasi	-1.72084	16.66424	11043871	1893.1	4	18.3	2	89	4	6
RIVER_97	African non-CCC	27-08-2023	Congo	-1.91608	16.52484	11050079	2672933.0	9	28436.5	2	84	7	6
RIVER_98	African non-CCC	27-08-2023	Congo	-2.13562	16.21698	11056841	2685993.0	9	28701.1	1	84	7	6
RIVER_99	African non-CCC	27-08-2023	Congo	-2.58084	16.22826	11069117	2689202.0	9	28744.9	0	83	7	6
RIVER_100	African non-CCC	27-08-2023	Mbali	-2.85302	16.19790	11076147	671.3	3	8.6	34	84	15	0
RIVER_101	African non-CCC	27-08-2023	Congo	-3.04558	16.18341	11081760	2708229.0	9	29221.3	0	83	8	6
RIVER_102	African non-CCC	28-08-2023	Kwa	-3.17111	16.20117	11084458	894486.6	8	8896.9	0	82	16	2
RIVER_103	African non-CCC	28-09-2023	Tomo	-3.30069	16.23139	11087176	591.9	3	7.9	34	86	14	0
RIVER_104	African non-CCC	28-09-2023	Congo	-3.43277	16.15636	11090242	3604674.0	9	38149.1	0	83	9	6
RIVER_105	African non-CCC	28-09-2023	Mpunu	-3.56317	16.09752	11093597	1686.0	3	24.5	69	69	31	0
RIVER_106	African non-CCC	28-09-2023	Mai Ndombe	-3.75683	15.98883	11096953	759.7	3	13.0	121	80	21	0
RIVER_107	African non-CCC	28-09-2023	Congo	-3.83046	15.93997	11098360	3611678.0	9	38290.5	0	83	9	6
RIVER_108	African non-CCC	28-09-2023	Congo	-4.01963	15.61141	11101977	3625209.0	9	38524.2	0	83	9	6
RIVER_109	African non-CCC	22-11-2021	Victoria Nile	2.21105	31.40712	10934232	351575.5	7	2031.5	4	17	24	40
RIVER_110	African non-CCC	02-12-2021	Victoria Nile	1.38557	32.84643	10955649	268980.6	7	3140.6	0	15	26	34
RIVER_111	African non-CCC	02-12-2021	Sezibwa	1.32115	32.76770	10956384	4258.0	5	27.9	0	63	1	35
RIVER_112	African non-CCC	25-05-2022	Victoria Nile	2.21480	31.40619	10934232	351575.5	7	2031.5	4	17	24	40
RIVER_113	African non-CCC	07-06-2022	Victoria Nile	1.37983	32.84656	10955649	268980.6	7	3140.6	0	15	26	34
RIVER_114	African non-CCC	10-04-2024	Victoria Nile	2.21520	31.41295	10934232	351575.5	7	2031.5	4	17	24	40
RIVER_115	African non-CCC	24-04-2024	Victoria Nile	1.37941	32.84820	10955649	268980.6	7	3140.6	0	15	26	34
RIVER_116	African non-CCC	24-04-2024	Sezibwa	1.31790	32.76706	10956384	4258.0	5	27.9	0	63	1	35
RIVER_117	African non-CCC	09-04-2024	Bubwe	1.84149	31.39393	10944699	82.4	2	0.3	213	34	3	59
RIVER_118	African non-CCC	09-04-2024	Somosio	1.88131	31.40648	10941929	216.1	2	0.9	32	63	0	36
RIVER_119	African non-CCC	09-04-2024	Wasoke	1.92998	31.42801	10940718	583.2	3	2.5	19	49	0	51
RIVER_120	African non-CCC	09-04-2024	Waiga	1.99223	31.47529	10939041	1755.4	3	4.6	27	43	0	57
RIVER_121	African non-CCC	13-04-2024	Waaki	1.70921	31.37616	10946408	493.7	3	2.1	210	76	0	24
RIVER_122	African non-CCC	13-04-2024	Wambaby	1.52999	31.11483	10950826	812.9	3	3.6	457	96	0	3
RIVER_123	African non-CCC	14-04-2024	Lutowa	1.41143	31.00144	10953837	271.7	3	1.3	147	100	0	0
RIVER_124	African non-CCC	14-04-2024	Nkusi	1.12955	30.99482	10962320	387.6	3	1.8	59	100	0	0
RIVER_125	African non-CCC	30-04-2024	Rwizi	-0.61931	30.61091	11009786	2024.5	4	12.8	5	1	17	82
RIVER_126	African non-CCC	09-06-2024	Victoria Nile	2.21493	31.40497	10934232	351575.5	7	2031.5	4	17	24	40
RIVER_127	African non-CCC	25-06-2024	Victoria Nile	1.37410	32.85071	10955649	268980.6	7	3140.6	0	15	26	34
RIVER_128	African non-CCC	25-06-2024	Sezibwa	1.31770	32.76645	10956384	4258.0	5	27.9	0	63	1	35
RIVER_129	African non-CCC	13-06-2024	Waiga	1.99204	31.47542	10939041	1755.4	3	4.6	27	43	0	57
RIVER_130	African non-CCC	13-06-2024	Wasoke	1.92991	31.42791	10940718	583.2	3	2.5	19	49	0	51
RIVER_131	African non-CCC	13-06-2024	Waaki	1.70911	31.37632	10946408	493.7	3	2.1	210	76	0	24
RIVER_132	African non-CCC	13-06-2024	Wambabyar	1.52988	31.11522	10950826	812.9	3	3.6	457	96	0	3
RIVER_133	African non-CCC	14-06-2024	Lutowa	1.41227	31.00199	10953837	271.7	3	1.3	147	100	0	0
RIVER_134	African non-CCC	14-06-2024	Nkusi	1.12971	30.99440	10962320	387.6	3	1.8	59	100	0	0
RIVER_135	African non-CCC	14-06-2024	Nkusi	1.08407	31.11523	10963583	1283.3	4	4.8	14	98	0	2
RIVER_136	African non-CCC	19-06-2024	Muzizi	0.87091	30.72935	10968507	2655.6	5	13.5	18	86	0	13
RIVER_137	African non-CCC	01-07-2024	Rwizi	-0.68622	30.88713	11012423	2513.9	4	15.5	16	1	21	78
RIVER_138	African non-CCC	21-03-2025	Kagara	-1.03835	30.18469	11023039	98.9	2	0.7	30	0	64	37
RIVER_139	African non-CCC	21-03-2025	Mugoyo	-0.92741	30.22250	11018919	187.2	3	1.3	10	0	23	77
RIVER_140	African non-CCC	02-04-2025	Dura	0.45821	30.38014	10979790	129.9	2	0.6	87	94	0	5
RIVER_141	African non-CCC	02-04-2025	Mpanga	0.10068	30.46235	10989376	4727.8	5	21.5	5	20	19	62
RIVER_256	African non-CCC	11-06-2025	Mucha	-1.22404	29.71601	11028503	68.5	2	0.6	58	98	0	2
RIVER_257	African non-CCC	11-06-2025	Rutchuru	-1.24381	29.65607	11028746	1040.6	3	7.7	98	44	16	25
RIVER_258	African non-CCC	12-06-2025	Kabere	-1.22460	29.87940	11028373	24.9	1	0.2	65	18	67	11
RIVER_259	African non-CCC	13-06-2025	Kagara	-1.03799	30.18466	11023039	98.9	2	0.7	30	0	64	37
RIVER_260	African non-CCC	13-06-2025	Mugoyo	-0.92746	30.22252	11018919	187.2	3	1.3	10	0	23	77
RIVER_261	African non-CCC	25-06-2025	Dura	0.45858	30.38002	10979790	129.9	2	0.6	87	94	0	5
RIVER_262	African non-CCC	25-06-2025	Mpanga	0.10075	30.46218	10989376	4727.8	5	21.5	5	20	19	62
RIVER_142	European	15-03-2017	Eau Noire	50.07790	4.55135	20372178	221.9	2	2.3	36	62	24	14
RIVER_143	European	24-03-2017	Geer	50.73460	5.39389	20355570	266.2	3	2.9	13	0	2	98
RIVER_144	European	09-03-2017	Gueule	50.75050	5.94087	20355869	153.2	2	2.0	58	27	53	18
RIVER_145	European	14-03-2017	Lhomme	50.13930	5.16413	20370167	474.6	3	5.7	35	62	9	29
RIVER_146	European	10-03-2017	Lhomme	49.97200	5.39110	20374412	26.8	1	0.3	88	54	39	7
RIVER_147	European	09-03-2017	Lienne	50.40960	5.76924	20364602	152.4	2	1.8	79	65	16	18
RIVER_148	European	09-03-2017	Meuse	50.73730	5.69026	20356226	20483.1	6	240.3	8	31	29	37
RIVER_149	European	24-03-2017	Meuse	50.62090	5.57959	20358760	16776.0	5	194.6	12	28	30	39
RIVER_150	European	10-03-2017	Ourthe	50.10680	5.64624	20371232	403.1	3	5.1	48	37	51	12
RIVER_151	European	10-03-2017	Ourthe	50.13670	5.72208	20370454	331.2	3	4.1	42	47	32	20
RIVER_152	European	31-03-2017	Sambre	50.40790	4.39512	20363761	1691.6	4	20.0	13	12	50	35
RIVER_153	European	31-03-2017	Sambre	50.41940	4.54671	20363646	2390.1	4	28.2	7	10	38	43
RIVER_154	European	17-03-2017	Sambre	50.44595	4.69585	20362862	2777.7	4	32.8	13	10	33	49
RIVER_155	European	15-03-2017	Eau Noire	50.00480	4.42533	20373803	114.7	2	1.2	62	63	30	7
RIVER_156	European	24-03-2017	Geer	50.68610	5.23110	20357259	56.2	1	0.6	13	0	1	97
RIVER_157	European	10-03-2017	Lesse	49.92307	5.28176	20375401	41.2	1	0.5	86	70	16	13
RIVER_158	European	14-03-2017	Lesse	50.12620	5.18501	20370881	389.6	3	4.8	53	71	9	20
RIVER_159	European	14-03-2017	Lesse	50.17360	5.04672	20369667	1164.6	4	13.9	16	61	13	26
RIVER_160	European	13-11-2017	Biran	50.15880	5.05997	20370548	50.4	1	0.6	23	24	42	34
RIVER_161	European	28-11-2017	Eau d'Heure	50.36730	4.39651	20366026	336.8	3	3.8	34	13	15	67
RIVER_162	European	20-11-2017	Eau d'Heure	50.17540	4.40847	20369489	20.4	1	0.2	32	27	30	43
RIVER_163	European	29-11-2017	Geer	50.73460	5.39389	20355570	266.2	3	2.9	13	0	2	98
RIVER_164	European	29-11-2017	Gueule	50.75050	5.94087	20355869	153.2	2	2.0	58	27	53	18
RIVER_165	European	28-11-2017	Hantes	50.29910	4.17308	20366535	139.8	2	1.6	52	7	62	31
RIVER_166	European	24-11-2017	Hoëgne	50.55360	5.80467	20360358	206.0	3	2.6	39	68	11	18
RIVER_167	European	13-11-2017	Lhomme	50.13930	5.16413	20370167	474.6	3	5.7	35	62	9	29
RIVER_168	European	13-11-2017	Masblette	50.11510	5.29752	20371800	45.6	1	0.6	185	86	0	14
RIVER_169	European	29-11-2017	Meuse	50.73730	5.69026	20356226	20483.1	6	240.3	8	31	29	37
RIVER_170	European	10-11-2017	Meuse	50.58070	5.40556	20359963	16641.1	5	193.6	8	26	30	39
RIVER_171	European	30-11-2017	Meuse	50.39604	4.87994	20364096	12664.7	5	149.2	6	34	32	34
RIVER_172	European	28-11-2017	Sambre	50.30470	4.11747	20366751	1243.8	4	14.9	6	14	57	27

Table S1 (continued)

RIVER_173	European	28-11-2017	Sambre	50.40790	4.39512	20363761	1691.6	4	20.0	13	12	50	35
RIVER_174	European	21-11-2017	Sambre	50.41940	4.54671	20363646	2390.1	4	28.2	7	10	38	43
RIVER_175	European	28-11-2017	Sambre	50.44595	4.69585	20362862	2777.7	4	32.8	13	10	33	49
RIVER_176	European	29-11-2017	Geer	50.68610	5.23110	20357259	56.2	1	0.6	13	0	1	97
RIVER_177	European	13-11-2017	Lesse	50.12620	5.18501	20370881	389.6	3	4.8	53	71	9	20
RIVER_178	European	13-11-2017	Lesse	50.17360	5.04672	20369667	1164.6	4	13.9	16	61	13	26
RIVER_179	European	24-11-2017	Ourthe	50.37660	5.52015	20364920	1259.3	4	15.3	14	45	31	24
RIVER_180	European	31-10-2017	Rulles	49.72080	5.59432	20380254	112.7	2	1.6	43	82	13	6
RIVER_181	European	20-11-2017	Ry de Rome	50.03750	4.50192	20372884	16.4	1	0.2	115	93	0	8
RIVER_182	European	01-12-2017	Warche	50.38710	5.99168	20364212	187.3	2	2.6	50	42	42	15
RIVER_183	European	29-11-2017	Geer	50.71949	5.31716	20355997	127.7	2	1.4	11	0	1	97
RIVER_184	European	17-11-2017	Ourthe	50.53159	5.56800	20361207	2786.9	5	34.3	22	51	27	22
RIVER_185	European	10-09-2018	Geer	50.73460	5.39389	20355570	266.2	3	2.9	13	0	2	98
RIVER_186	European	10-09-2018	Gueule	50.75050	5.94087	20355869	153.2	2	2.0	58	27	53	18
RIVER_187	European	31-08-2018	Sambre	50.30470	4.11747	20366751	1243.8	4	14.9	6	14	57	27
RIVER_188	European	31-08-2018	Sambre	50.40790	4.39512	20363761	1691.6	4	20.0	13	12	50	35
RIVER_189	European	28-08-2018	Sambre	50.44595	4.69585	20362862	2777.7	4	32.8	13	10	33	49
RIVER_190	European	07-09-2018	Bocq	50.32130	4.94365	20365829	189.0	3	2.1	74	5	25	69
RIVER_191	European	07-09-2018	Burnot	50.36360	4.84701	20364812	69.8	2	0.8	163	12	25	60
RIVER_192	European	10-09-2018	Geer	50.68610	5.23110	20357259	56.2	1	0.6	13	0	1	97
RIVER_193	European	29-08-2018	Ton	49.55890	5.53155	20384243	92.8	2	1.3	26	82	11	7
RIVER_194	European	10-09-2018	Geer	50.71949	5.31716	20355997	127.7	2	1.4	11	0	1	97
RIVER_195	European	10-08-2020	Meuse	48.11840	5.55633	20422887	176.0	3	2.1	7	0	88	12
RIVER_196	European	10-08-2020	Meuse	48.26337	5.63325	20420086	410.3	3	4.7	13	4	78	17
RIVER_197	European	10-08-2020	Meuse	48.70590	5.69701	20406535	2111.1	5	23.6	6	16	48	35
RIVER_198	European	10-08-2020	Meuse	48.80055	5.54636	20403704	2390.5	5	26.4	14	17	44	39
RIVER_199	European	10-08-2020	Meuse	48.89366	5.53927	20401782	2591.0	5	28.4	8	17	41	41
RIVER_200	European	11-08-2020	Meuse	49.07063	5.41457	20396906	3060.3	5	33.5	11	17	39	43
RIVER_201	European	11-08-2020	Meuse	49.38860	5.17829	20388705	3704.7	5	40.8	7	17	36	46
RIVER_202	European	11-08-2020	Meuse	49.66685	4.98247	20381654	6474.3	5	76.5	12	17	38	44
RIVER_203	European	11-08-2020	Meuse	49.84005	4.76203	20377902	7872.7	5	91.9	6	19	41	40
RIVER_204	European	19-08-2020	Meuse	50.21056	4.82128	20368695	10642.0	5	125.6	19	31	35	34
RIVER_205	European	19-08-2020	Meuse	50.46161	4.87049	20362234	15629.9	5	184.3	19	28	32	38
RIVER_206	European	23-08-2020	Meuse	50.62090	5.57959	20358418	20418.3	6	239.6	12	31	29	37
RIVER_207	European	18-06-2019	Senne	50.69411	4.20067	20356654	233.3	3	3.2	24	0	4	95
RIVER_208	European	18-06-2019	Dendre	50.79321	3.90103	20354830	838.4	3	11.4	16	1	4	93
RIVER_209	European	18-06-2019	Dendre	50.89195	4.08171	20351525	1149.6	3	15.7	21	0	6	90
RIVER_210	European	18-06-2019	Senne	50.91775	4.42046	20350678	1022.7	4	13.9	38	3	2	69
RIVER_211	European	20-06-2019	Dyle	51.01151	4.52103	20347967	3576.5	5	45.4	10	9	2	78
RIVER_212	European	20-06-2019	Senne	51.03492	4.42257	20348342	24.2	1	0.3	15	4	0	89
RIVER_213	European	20-06-2019	Dyle	50.86189	4.68130	20352220	804.5	4	10.7	16	10	1	73
RIVER_214	European	25-06-2019	Dyle	50.71068	2.99805	20356438	870.0	3	12.4	7	0	0	77
RIVER_215	European	27-06-2019	Scheldt	50.95648	3.65665	20349897	6079.0	5	82.5	2	3	3	86
RIVER_216	European	27-06-2019	Scheldt	50.77428	3.47256	20354613	5632.4	5	76.3	4	3	4	86
RIVER_217	European	27-06-2019	Scheldt	50.51595	3.42312	20361005	4850.5	5	65.1	13	4	4	85
RIVER_218	European	02-07-2019	Scheldt	51.01319	3.93034	20347966	10463.0	5	148.6	0	2	3	86
RIVER_219	European	02-07-2019	Scheldt	51.02957	4.04219	20348219	10616.6	5	150.7	3	2	3	86
RIVER_220	European	02-07-2019	Scheldt	51.03922	4.16509	20347381	12042.0	5	170.2	5	2	3	87
RIVER_221	European	02-07-2019	Scheldt	51.12286	4.21474	20345726	12275.4	5	173.5	1	2	3	87
RIVER_222	European	04-07-2019	Scheldt	51.23373	4.39544	20342955	19001.2	6	262.5	3	5	2	82
RIVER_223	European	04-07-2019	Scheldt	51.14311	4.33105	20344885	18909.9	6	261.2	5	5	2	82
RIVER_224	European	04-07-2019	Rupel	51.08408	4.36613	20346241	6486.2	5	85.7	0	11	1	75
RIVER_225	European	04-07-2019	Scheldt	51.12230	4.28747	20345396	12305.5	5	173.9	2	2	3	87
RIVER_226	European	03-02-2020	Scheldt	50.51595	3.42312	20361005	4850.5	5	65.1	13	4	4	85
RIVER_227	European	03-02-2020	Lys	50.66061	2.76647	20357765	1546.9	4	25.4	3	0	1	94
RIVER_228	European	03-02-2020	Dyle	50.71068	2.99805	20356438	870.0	3	12.4	7	0	0	77
RIVER_229	European	03-02-2020	Lys	50.80131	3.18929	20353766	3043.5	4	47.0	9	0	0	89
RIVER_230	European	03-02-2020	Scheldt	50.77428	3.47256	20354613	5632.4	5	76.3	4	3	4	86
RIVER_231	European	04-02-2020	Scheldt	50.95648	3.65665	20349897	6079.0	5	82.5	2	3	3	86
RIVER_232	European	10-02-2020	Scheldt	51.23373	4.39544	20342955	19001.2	6	262.5	3	5	2	82
RIVER_233	European	10-02-2020	Scheldt	51.14311	4.33105	20345396	12305.5	5	173.9	2	2	3	87
RIVER_234	European	10-02-2020	Scheldt	51.12286	4.21474	20345726	12275.4	5	173.5	1	2	3	87
RIVER_235	European	10-02-2020	Senne	51.03492	4.42257	20348342	24.2	1	0.3	15	4	0	89
RIVER_236	European	12-02-2020	Scheldt	51.01319	3.93034	20347966	10463.0	5	148.6	0	2	3	86
RIVER_237	European	12-02-2020	Scheldt	51.03922	4.16509	20347381	12042.0	5	170.2	5	2	3	87
RIVER_238	European	12-02-2020	Dyle	51.01151	4.52103	20347967	3576.5	5	45.4	10	9	2	78
RIVER_239	European	12-02-2020	Dyle	50.86189	4.68130	20352220	804.5	4	10.7	16	10	1	73
RIVER_240	European	17-02-2020	Senne	50.69411	4.20067	20356654	233.3	3	3.2	24	0	4	95
RIVER_241	European	17-02-2020	Dendre	50.89195	4.08171	20351525	1149.6	3	15.7	21	0	6	90
RIVER_242	European	17-02-2020	Dendre	50.79321	3.90103	20354830	838.4	3	11.4	16	1	4	93
RIVER_243	European	17-02-2020	Senne	50.91775	4.42046	20350678	1022.7	4	13.9	38	3	2	69
RIVER_244	European	24-04-2020	Scheldt	50.51595	3.42312	20361005	4850.5	5	65.1	13	4	4	85
RIVER_245	European	24-04-2020	Scheldt	50.77428	3.47256	20354613	5632.4	5	76.3	4	3	4	86
RIVER_246	European	24-04-2020	Scheldt	50.95648	3.65665	20349897	6079.0	5	82.5	2	3	3	86
RIVER_247	European	24-04-2020	Scheldt	51.01319	3.93034	20347966	10463.0	5	148.6	0	2	3	86
RIVER_248	European	29-04-2020	Scheldt	50.51595	3.42312	20361005	4850.5	5	65.1	13	4	4	85
RIVER_249	European	29-04-2020	Scheldt	50.77428	3.47256	20354613	5632.4	5	76.3	4	3	4	86
RIVER_250	European	29-04-2020	Scheldt	50.95648	3.65665	20349897	6079.0	5	82.5	2	3	3	86
RIVER_251	European	29-04-2020	Scheldt	51.01319	3.93034	20347966	10463.0	5	148.6	0	2	3	86
RIVER_252	European	15-05-2020	Scheldt	50.51595	3.42312	20361005	4850.5	5	65.1	13	4	4	85
RIVER_253	European	15-05-2020	Scheldt	50.77428	3.47256	20354613	5632.4	5	76.3	4	3	4	86
RIVER_254	European	15-05-2020	Scheldt	50.95648	3.65665	20349897	6079.0	5	82.5	2	3	3	86
RIVER_255	European	15-05-2020	Scheldt	51.01319	3.93034	20347966	10463.0	5	148.6	0	2	3	86

Table S2 Vertically integrated methane oxidation (MOX in nmol m^{-2} d^{-1}) in river sediments reported in literature. The values given per g of sediment were converted per m^2 with a sediment density of 0.95 g cm^{-3} integrated over a depth of 15 cm (8). Data reported by Reference (9) were excluded because the incubations were spiked with CH_4 and reported rates were not correct to in-situ CH_4 levels.

Name	Region	Stream size	MOX recalculated units		MOX original units		Reference
And-1	Switzerland	Headwaters	0	nmol/m2/d	0.000	nmol/m2/h	(79)
Com-1	Switzerland	Headwaters	74	nmol/m2/d	3.070	nmol/m2/h	(79)
Com-2	Switzerland	Headwaters	116	nmol/m2/d	4.850	nmol/m2/h	(79)
Geb-1	Switzerland	Headwaters	117	nmol/m2/d	4.860	nmol/m2/h	(79)
Sen-1	Switzerland	Headwaters	361	nmol/m2/d	15.060	nmol/m2/h	(79)
Sor-1	Switzerland	Headwaters	104	nmol/m2/d	4.340	nmol/m2/h	(79)
Sor-2	Switzerland	Headwaters	184	nmol/m2/d	7.680	nmol/m2/h	(79)
Sor-3	Switzerland	Headwaters	145	nmol/m2/d	6.030	nmol/m2/h	(79)
Tal-1	Switzerland	Headwaters	26	nmol/m2/d	1.100	nmol/m2/h	(79)
Ven-1	Switzerland	Headwaters	126	nmol/m2/d	5.240	nmol/m2/h	(79)
Ven-2	Switzerland	Headwaters	61	nmol/m2/d	2.560	nmol/m2/h	(79)
Vev-1	Switzerland	Headwaters	0	nmol/m2/d	0.000	nmol/m2/h	(79)
Vey-1	Switzerland	Headwaters	129	nmol/m2/d	5.390	nmol/m2/h	(79)
Vey-2	Switzerland	Headwaters	637	nmol/m2/d	26.550	nmol/m2/h	(79)
Ash	Southern England	Lowland rivers	254,328	nmol/m2/d	0.074	nmol/g/h	(8)
Pang at Brafield	Southern England	Lowland rivers	340,057	nmol/m2/d	0.099	nmol/g/h	(8)
Philhill	Southern England	Lowland rivers	358,917	nmol/m2/d	0.105	nmol/g/h	(8)
Piddle at Piddlethenthide	Southern England	Lowland rivers	370,919	nmol/m2/d	0.108	nmol/g/h	(8)
Cam	Southern England	Lowland rivers	394,923	nmol/m2/d	0.115	nmol/g/h	(8)
Wallop	Southern England	Lowland rivers	427,500	nmol/m2/d	0.125	nmol/g/h	(8)
Ver	Southern England	Lowland rivers	472,079	nmol/m2/d	0.138	nmol/g/h	(8)
Lambourn at Westbrook	Southern England	Lowland rivers	520,087	nmol/m2/d	0.152	nmol/g/h	(8)
Bere	Southern England	Lowland rivers	535,518	nmol/m2/d	0.157	nmol/g/h	(8)
Allen	Southern England	Lowland rivers	574,953	nmol/m2/d	0.168	nmol/g/h	(8)
Pang at Tidmarsh	Southern England	Lowland rivers	585,241	nmol/m2/d	0.171	nmol/g/h	(8)
Granta	Southern England	Lowland rivers	634,963	nmol/m2/d	0.186	nmol/g/h	(8)
Meon	Southern England	Lowland rivers	634,963	nmol/m2/d	0.186	nmol/g/h	(8)
Lea	Southern England	Lowland rivers	634,963	nmol/m2/d	0.186	nmol/g/h	(8)
Gade	Southern England	Lowland rivers	638,392	nmol/m2/d	0.187	nmol/g/h	(8)
Mimran	Southern England	Lowland rivers	667,540	nmol/m2/d	0.195	nmol/g/h	(8)
Test	Southern England	Lowland rivers	777,273	nmol/m2/d	0.227	nmol/g/h	(8)
Chees at Chenies	Southern England	Lowland rivers	790,989	nmol/m2/d	0.231	nmol/g/h	(8)
Darenth	Southern England	Lowland rivers	794,418	nmol/m2/d	0.232	nmol/g/h	(8)
Kennet Tributary	Southern England	Lowland rivers	840,712	nmol/m2/d	0.246	nmol/g/h	(8)
Kennet	Southern England	Lowland rivers	852,714	nmol/m2/d	0.249	nmol/g/h	(8)
Cray	Southern England	Lowland rivers	993,309	nmol/m2/d	0.290	nmol/g/h	(8)
Itchen at Itchen Stoke	Southern England	Lowland rivers	996,738	nmol/m2/d	0.291	nmol/g/h	(8)
Stort	Southern England	Lowland rivers	1,156,193	nmol/m2/d	0.338	nmol/g/h	(8)
Chess	Southern England	Lowland rivers	1,181,912	nmol/m2/d	0.346	nmol/g/h	(8)
Frome	Southern England	Lowland rivers	1,199,057	nmol/m2/d	0.351	nmol/g/h	(8)
Piddle	Southern England	Lowland rivers	1,346,511	nmol/m2/d	0.394	nmol/g/h	(8)
Bourne	Southern England	Lowland rivers	1,445,956	nmol/m2/d	0.423	nmol/g/h	(8)
Itchen	Southern England	Lowland rivers	1,593,409	nmol/m2/d	0.466	nmol/g/h	(8)
Misbourne	Southern England	Lowland rivers	1,685,996	nmol/m2/d	0.493	nmol/g/h	(8)
Tadnoll	Southern England	Lowland rivers	2,397,543	nmol/m2/d	0.701	nmol/g/h	(8)
Bulbourne	Southern England	Lowland rivers	3,002,787	nmol/m2/d	0.878	nmol/g/h	(8)
Hammer	Southern England	Lowland rivers	6,371,505	nmol/m2/d	44.712	nmol/g/d	(80)
Marden	Southern England	Lowland rivers	5,769,473	nmol/m2/d	40.488	nmol/g/d	(80)
Nadder	Southern England	Lowland rivers	6,760,471	nmol/m2/d	47.442	nmol/g/d	(80)
Frome	Southern England	Lowland rivers	59,304,000	nmol/m2/d	2471.000	µmol/m2/h	(81)
Morava	Czech Republic	Lowland rivers	441,750,000	nmol/m2/d	3.100	µmol/g/d	(7)

Table S3 Results of one-way analysis of variance (ANOVA) and Tukey's multiple comparisons test (F value, degree of freedom (DF) of treatment (between columns) (DFn) and of residual (within columns) (DFd), mean 1 and 2, mean and standard error (SE) of difference of means (diff.), n1, n2, adjusted (adj.) P value, and corresponding summary as shown in figures).

Figure	Variable tested	F (DFn, DFd)	P value	Tukey's multiple comparisons test	Mean 1	Mean 2	Mean±SE of diff.	n1	n2	Summary	Adj. P Value
2 a	log(MOX)	F (2, 259) = 53.04	P<0.0001	African CCC vs. African non-CCC	3.377	2.393	0.985 ± 0.165	52	96	****	<0.0001
				African CCC vs. European	3.377	1.734	1.644 ± 0.161	52	114	****	<0.0001
				African non-CCC vs. European	2.393	1.734	0.659 ± 0.133	96	114	****	<0.0001
2 b	log(K)	F (2, 259) = 76.21	P<0.0001	African CCC vs. African non-CCC	0.222	-0.273	0.495 ± 0.089	52	96	****	<0.0001
				African CCC vs. European	0.222	-0.813	1.035 ± 0.087	52	114	****	<0.0001
				African non-CCC vs. European	-0.273	-0.813	0.540 ± 0.072	96	114	****	<0.0001
2 d	log(CH4)	F (2, 259) = 13.11	P<0.0001	African CCC vs. African non-CCC	3.155	2.666	0.490 ± 0.124	52	96	***	0.0003
				African CCC vs. European	3.155	2.547	0.609 ± 0.120	52	114	****	<0.0001
				African non-CCC vs. European	2.666	2.547	0.119 ± 0.100	96	114	ns	0.4577
S1 a	log(pH)	F (2, 259) = 885.8	P<0.0001	African CCC vs. African non-CCC	3.994	7.069	-3.076 ± 0.095	52	96	****	<0.0001
				African CCC vs. European	3.994	7.816	-3.822 ± 0.092	52	114	****	<0.0001
				African non-CCC vs. European	7.069	7.816	-0.747 ± 0.076	96	114	****	<0.0001
S1 b	log(O2)	F (2, 259) = 87.22	P<0.0001	African CCC vs. African non-CCC	1.812	2.268	-0.456 ± 0.047	52	96	****	<0.0001
				African CCC vs. European	1.812	2.406	-0.594 ± 0.045	52	114	****	<0.0001
				African non-CCC vs. European	2.268	2.406	-0.138 ± 0.037	96	114	***	0.0008
S1 c	log(TSM)	F (2, 254) = 101.5	P<0.0001	African CCC vs. African non-CCC	0.181	1.315	-1.134 ± 0.090	52	92	****	<0.0001
				African CCC vs. European	0.181	1.340	-1.158 ± 0.087	52	113	****	<0.0001
				African non-CCC vs. European	1.315	1.340	-0.024 ± 0.073	92	113	ns	0.9414
S1 d	log(DOC)	F (2, 172) = 173.6	P<0.0001	African CCC vs. African non-CCC	1.537	0.811	0.726 ± 0.042	52	85	****	<0.0001
				African CCC vs. European	1.537	0.800	0.736 ± 0.051	52	38	****	<0.0001
				African non-CCC vs. European	0.811	0.800	0.010 ± 0.046	85	38	ns	0.9727
S1 e	log(NH4+)	F (2, 248) = 71.08	P<0.0001	African CCC vs. African non-CCC	0.046	-0.165	0.211 ± 0.136	52	85	ns	0.2676
				African CCC vs. European	0.046	1.071	-1.025 ± 0.129	52	114	****	<0.0001
				African non-CCC vs. European	-0.165	1.071	-1.236 ± 0.111	85	114	****	<0.0001
S1 f	log(NO2-)	F (2, 248) = 434.4	P<0.0001	African CCC vs. African non-CCC	-1.968	-0.992	-0.975 ± 0.095	52	85	****	<0.0001
				African CCC vs. European	-1.968	0.521	-2.488 ± 0.090	52	114	****	<0.0001
				African non-CCC vs. European	-0.992	0.521	-1.513 ± 0.077	85	114	****	<0.0001
S1 g	log(DIN)	F (2, 248) = 284.5	P<0.0001	African CCC vs. African non-CCC	0.325	0.772	-0.447 ± 0.099	52	85	****	<0.0001
				African CCC vs. European	0.325	2.269	-1.944 ± 0.094	52	114	****	<0.0001
				African non-CCC vs. European	0.772	2.269	-1.497 ± 0.080	85	114	****	<0.0001
S1 h	log(PO43-)	F (2, 199) = 14.49	P<0.0001	African CCC vs. African non-CCC	-0.420	-0.102	-0.318 ± 0.100	52	85	**	0.005
				African CCC vs. European	-0.420	0.151	-0.570 ± 0.106	52	65	****	<0.0001
				African non-CCC vs. European	-0.102	0.151	-0.253 ± 0.094	85	65	*	0.0211
S8	log(K25°C)	F (2, 259) = 24.45	P<0.0001	African CCC vs. African non-CCC	0.133	-0.246	0.379 ± 0.079	52	96	****	<0.0001
				African CCC vs. European	0.133	-0.402	0.535 ± 0.077	52	114	****	<0.0001
				African non-CCC vs. European	-0.246	-0.402	0.156 ± 0.063	96	114	*	0.0387
S15 b	log(MOX)	F (2, 506) = 61.20	P<0.0001	MOX_{inc} vs. MOX_{iso} (1)	2.595	3.340	-0.745 ± 0.127	171	167	****	<0.0001
				MOX_{inc} vs. MOX_{iso} (2)	2.595	3.989	-1.394 ± 0.126	171	171	****	<0.0001
				MOX_{iso} (1) vs. MOX_{iso} (2)	3.340	3.989	-0.649 ± 0.127	167	171	****	<0.0001

Table S4 Equations and statistics at 0.05 level of quantile linear regressions given in Figures.

Figure	Y vs X	Equation	a	b	P value	n
4	log(MOX) vs log(CH4) African CCC	Y=a+bX	-0.04981 ± 0.26130	1.08600 ± 0.08035	<0.0001	52
	log(MOX) vs log(CH4) African non-CCC	Y=a+bX	-0.37560 ± 0.20160	1.03900 ± 0.07259	<0.0001	96
	log(MOX) vs log(CH4) European	Y=a+bX	-1.55200 ± 0.19420	1.29000 ± 0.07413	<0.0001	114
	log(MOX) vs log(CH4) All	Y=a+bX	-1.13000 ± 0.14410	1.26600 ± 0.05124	<0.0001	262
5 a	log(k) vs log(catchment area) African CCC	Y=a+bX	0.93246 ± 0.33977	-0.20264 ± 0.09648	0.04078	52
	log(k) vs log(catchment area) African non-CCC	Y=a+bX	-0.98670 ± 0.14342	0.17545 ± 0.03771	0.00010	96
	log(k) vs log(catchment area) European	Y=a+bX	-1.19093 ± 0.22814	0.13802 ± 0.06648	0.04019	114
	log(k) vs log(catchment area) All	Y=a+bX	-1.07001 ± 0.11888	0.18042 ± 0.03394	<0.00001	262
6 a	log(K) vs Temp African	Y=a+bX	-2.70875 ± 0.37904	0.10244 ± 0.01539	<0.00001	148
	log(K) vs Temp European	Y=a+bX	-1.23496 ± 0.09644	0.03523 ± 0.00528	<0.00001	114
	log(K) vs Temp All	Y=a+bX	-1.43423 ± 0.08840	0.05044 ± 0.00413	<0.00001	262
6 b	log(K) vs O2 African	Y=a+bX	0.51266 ± 0.13841	-0.00351 ± 0.00059	<0.00001	148
	log(K) vs O2 European	Y=a+bX	-0.14431 ± 0.10643	-0.00231 ± 0.00044	<0.00001	114
	log(K) vs O2 All	Y=a+bX	0.52622 ± 0.12483	-0.00415 ± 0.00043	<0.00001	262
6 c	log(K) vs log(CH4) African	Y=a+bX	-0.41649 ± 0.22377	0.11710 ± 0.07034	0.09812	148
	log(K) vs log(CH4) European	Y=a+bX	-1.31114 ± 0.21038	0.20132 ± 0.06940	0.00448	114
	log(K) vs log(CH4) All	Y=a+bX	-1.14584 ± 0.17945	0.26285 ± 0.06129	0.00003	262
6 d	log(K) vs log(TSM) African	Y=a+bX	0.11357 ± 0.09667	-0.24925 ± 0.07883	0.00191	47
	log(K) vs log(TSM) European	Y=a+bX	-1.18732 ± 0.17006	0.26159 ± 0.08623	0.00301	96
	log(K) vs log(TSM) All	Y=a+bX	-0.03768 ± 0.10159	-0.32193 ± 0.06915	0.00001	113
6 e	log(K) vs log(pH) African	Y=a+bX	1.08894 ± 0.39173	-1.64494 ± 0.51265	0.00164	148
	log(K) vs log(pH) European	Y=a+bX	-3.31615 ± 1.51658	2.90790 ± 1.73305	0.09615	114
	log(K) vs log(pH) All	Y=a+bX	1.79389 ± 0.34385	-2.73665 ± 0.40502	<0.00001	262
6 f	log(K) vs log(PO43-) African	Y=a+bX	-0.20080 ± 0.06451	-0.49258 ± 0.11519	0.00004	52
	log(K) vs log(PO43-) European	Y=a+bX	-0.83201 ± 0.12794	-0.35190 ± 0.13489	0.01133	85
	log(K) vs log(PO43-) All	Y=a+bX	-0.36344 ± 0.05610	-0.53017 ± 0.09324	<0.00001	65
6 g	log(K) vs log(NH4+) African	Y=a+bX	-0.04756 ± 0.07556	-0.07357 ± 0.11155	0.51065	52
	log(K) vs log(NH4+) European	Y=a+bX	-0.90737 ± 0.12286	0.10135 ± 0.07691	0.19028	85
	log(K) vs log(NH4+) All	Y=a+bX	-0.28431 ± 0.05093	-0.25029 ± 0.04619	<0.00001	114
6 h	log(K) vs log(NO2-) African	Y=a+bX	-0.53472 ± 0.12445	-0.29813 ± 0.08249	0.00042	52
	log(K) vs log(NO2-) European	Y=a+bX	-0.89466 ± 0.08007	0.22887 ± 0.05233	0.00003	85
	log(K) vs log(NO2-) All	Y=a+bX	-0.54057 ± 0.04369	-0.28329 ± 0.03752	<0.00001	114
6 i	log(K) vs log(DIN) African	Y=a+bX	0.03703 ± 0.09354	-0.18414 ± 0.09298	0.04969	52
	log(K) vs log(DIN) European	Y=a+bX	0.50163 ± 0.50706	-0.55816 ± 0.21559	0.01090	85
	log(K) vs log(DIN) All	Y=a+bX	0.19898 ± 0.09300	-0.40309 ± 0.04634	<0.00001	114
7 a	%MOX vs log(catchment area)	Y=a+bX	-39.52238 ± 3.31011	18.22440 ± 1.09811	<0.00001	262
7 b	%MOX vs log(depth)	Y=a+bX	18.29528 ± 1.44380	44.08940 ± 2.77021	<0.00001	262
7 c	log(%MOX) vs log(k600)	Y=a+bX	2.25272 ± 0.09913	-2.18815 ± 0.20291	<0.00001	262
S3 a	log(CH4) vs log(catchement area) African CCC	Y=a+bX	4.70403 ± 0.56738	-0.43640 ± 0.14152	0.00332	52
	log(CH4) vs log(catchement area) African non-CCC	Y=a+bX	2.87036 ± 0.17141	-0.09256 ± 0.04386	0.03768	96
	log(CH4) vs log(catchement area) African	Y=a+bX	2.95544 ± 0.29199	-0.13494 ± 0.08193	0.10236	148
	log(CH4) vs log(catchement area) European	Y=a+bX	3.22818 ± 0.22869	-0.15805 ± 0.04243	0.00028	114
	log(CH4) vs log(catchement area) All	Y=a+bX	3.00667 ± 0.10255	-0.12619 ± 0.02276	<0.00001	262
S4 a	log(MOX) vs log(catchement area) African CCC	Y=a+bX	5.82227 ± 0.68862	-0.63897 ± 0.19140	0.00160	52
	log(MOX) vs log(catchement area) African non-CCC	Y=a+bX	1.70979 ± 0.30576	0.14176 ± 0.07345	0.05685	96
	log(MOX) vs log(catchement area) African	Y=a+bX	2.73207 ± 0.43446	-0.02574 ± 0.07919	0.74566	148
	log(MOX) vs log(catchement area) European	Y=a+bX	1.54283 ± 0.47657	0.04836 ± 0.12955	0.70964	114
	log(MOX) vs log(catchement area) All	Y=a+bX	1.93341 ± 0.21049	0.05695 ± 0.04861	0.24254	262
S6 a	log(K) vs inundation extent	Y=a+bX	-0.46391 ± 0.08637	0.00691 ± 0.00136	<0.00001	52
S6 b	log(K25°C) vs inundation extent	Y=a+bX	-0.41046 ± 0.07033	0.00499 ± 0.00128	0.00014	52
S7 a	d13C-CH4 vs log(K) African CCC	Y=a+bX	-32.92562 ± 0.68890	-3.14725 ± 1.39745	0.02874	52
	d13C-CH4 vs log(K) African non-CCC	Y=a+bX	-27.65375 ± 0.60738	-3.24991 ± 0.80576	0.00012	85
	d13C-CH4 vs log(K) European	Y=a+bX	-29.06662 ± 0.41988	0.17035 ± 0.33858	0.61606	96
	d13C-CH4 vs log(K) All	Y=a+bX	-29.42217 ± 0.26995	-0.86122 ± 0.35154	0.01504	233
S7 b	d13C-CH4 vs log(CH4) African CCC	Y=a+bX	-23.60560 ± 1.81161	-3.09359 ± 0.60688	<0.00001	52
	d13C-CH4 vs log(CH4) African non-CCC	Y=a+bX	-25.59346 ± 1.84255	-0.21613 ± 0.55661	0.69879	85
	d13C-CH4 vs log(CH4) European	Y=a+bX	-29.73514 ± 0.89166	0.20738 ± 0.37791	0.58447	96
	d13C-CH4 vs log(CH4) All	Y=a+bX	-27.03198 ± 0.53652	-0.89331 ± 0.28944	0.00227	233
S7 c	d13C-CH4 vs log(MOX) African CCC	Y=a+bX	-26.76237 ± 1.59425	-2.02512 ± 0.48758	0.00013	52
	d13C-CH4 vs log(MOX) African non-CCC	Y=a+bX	-23.01989 ± 1.61163	-1.25417 ± 0.58015	0.03351	85
	d13C-CH4 vs log(MOX) European	Y=a+bX	-29.44973 ± 0.33936	0.15958 ± 0.22765	0.48505	96
	d13C-CH4 vs log(MOX) All	Y=a+bX	-26.96437 ± 0.37457	-1.07833 ± 0.20281	<0.00001	233
S7 d	d13C-CH4 vs log(POC:PN) African CCC	Y=a+bX	-59.19211 ± 4.91713	25.30464 ± 4.48929	<0.00001	52
	d13C-CH4 vs log(POC:PN) African non-CCC	Y=a+bX	-31.55747 ± 6.81637	5.95275 ± 6.96996	0.39553	85
	d13C-CH4 vs log(POC:PN) European	Y=a+bX	-31.81223 ± 2.27396	2.74435 ± 2.27387	0.23021	96
	d13C-CH4 vs log(POC:PN) All	Y=a+bX	-32.62160 ± 1.83186	3.69638 ± 1.81752	0.04307	233
S9 a	log(K25°C) vs Temp African	Y=a+bX	-1.80443 ± 0.37904	0.06627 ± 0.01539	0.00003	148
	log(K25°C) vs Temp European	Y=a+bX	-0.33064 ± 0.09644	-0.00095 ± 0.00528	0.85813	114
	log(K25°C) vs Temp All	Y=a+bX	-0.52991 ± 0.08840	0.01426 ± 0.00413	0.00065	262

Table S4 (continued)

S9 b	log(K25°C) vs O2 African	Y=a+bX	0.40368 ± 0.13784	-0.00285 ± 0.00062	0.00001	148
	log(K25°C) vs O2 European	Y=a+bX	-0.23531 ± 0.13350	-0.00040 ± 0.00049	0.42215	114
	log(K25°C) vs O2 All	Y=a+bX	0.20149 ± 0.08793	-0.00198 ± 0.00034	<0.00001	262
S9 c	log(K25°C) vs log(CH4) African	Y=a+bX	-0.43518 ± 0.20700	0.10463 ± 0.07244	1.44439	148
	log(K25°C) vs log(CH4) European	Y=a+bX	-0.86032 ± 0.15176	0.19662 ± 0.05061	0.00017	114
	log(K25°C) vs log(CH4) All	Y=a+bX	-0.63981 ± 0.10691	0.14702 ± 0.03808	0.00014	262
S9 d	log(K25°C) vs log(TSM) African	Y=a+bX	0.04024 ± 0.08955	-0.19138 ± 0.07443	0.01114	47
	log(K25°C) vs log(TSM) European	Y=a+bX	-0.68941 ± 0.11289	0.23773 ± 0.06297	0.00026	96
	log(K25°C) vs log(TSM) All	Y=a+bX	-0.12729 ± 0.07381	-0.10122 ± 0.04921	0.04071	113
S9 e	log(K25°C) vs pH African	Y=a+bX	0.34918 ± 0.22535	-0.07889 ± 0.03440	0.02328	148
	log(K25°C) vs pH European	Y=a+bX	0.05029 ± 0.40026	-0.05101 ± 0.05534	0.35860	114
	log(K25°C) vs pH All	Y=a+bX	0.46549 ± 0.21380	-0.10363 ± 0.02910	0.00044	262
S9 f	log(K25°C) vs log(PO43-) African	Y=a+bX	-0.19729 ± 0.04799	-0.36259 ± 0.09175	0.00012	52
	log(K25°C) vs log(PO43-) European	Y=a+bX	-0.36252 ± 0.10290	-0.12628 ± 0.15851	0.42862	85
	log(K25°C) vs log(PO43-) All	Y=a+bX	-0.23430 ± 0.03775	-0.26692 ± 0.06580	0.00007	65
S9 g	log(K25°C) vs log(NH4+) African	Y=a+bX	-0.11997 ± 0.05770	-0.06225 ± 0.06835	0.36393	52
	log(K25°C) vs log(NH4+) European	Y=a+bX	-0.68942 ± 0.11289	0.23773 ± 0.06297	0.00026	85
	log(K25°C) vs log(NH4+) All	Y=a+bX	-0.17128 ± 0.04287	-0.08206 ± 0.03452	0.01816	114
S9 h	log(K25°C) vs log(NO2-) African	Y=a+bX	-0.38734 ± 0.11868	-0.18355 ± 0.08110	0.02522	52
	log(K25°C) vs log(NO2-) European	Y=a+bX	-0.41968 ± 0.07629	0.10412 ± 0.07761	0.18244	85
	log(K25°C) vs log(NO2-) All	Y=a+bX	-0.25933 ± 0.03273	-0.09691 ± 0.03005	0.00143	114
S9 i	log(K25°C) vs log(DIN) African	Y=a+bX	-0.00048 ± 0.09019	-0.17317 ± 0.07643	0.02507	52
	log(K25°C) vs log(DIN) European	Y=a+bX	-0.23747 ± 0.26715	-0.04586 ± 0.11656	0.69476	85
	log(K25°C) vs log(DIN) All	Y=a+bX	-0.03128 ± 0.07156	-0.13740 ± 0.03589	0.00016	114
S10	log(CH4) vs O2 African	Y=a+bX	3.8190 ± 0.1085	-0.0058 ± 0.0006	<0.0001	148
	log(CH4) vs O2 European	Y=a+bX	3.5700 ± 0.1820	-0.0038 ± 0.0006	<0.0001	114
	log(CH4) vs O2 All	Y=a+bX	3.6730 ± 0.0881	-0.0045 ± 0.0004	<0.0001	262
S12a	log(K) vs log(POC) African	Y=a+bX	-0.0358 ± 0.0520	-0.3190 ± 0.1241	0.0111	148
	log(K) vs log(POC) European	Y=a+bX	-0.9211 ± 0.0710	0.2698 ± 0.1319	0.0432	111
	log(K) vs log(POC) All	Y=a+bX	-0.3260 ± 0.0497	-0.2881 ± 0.1049	0.0065	259
S12b	log(K25°C) vs log(POC) African	Y=a+bX	-0.0740 ± 0.0471	-0.1983 ± 0.1125	0.08	148
	log(K25°C) vs log(POC) European	Y=a+bX	-0.5269 ± 0.0567	0.3308 ± 0.1053	0.0022	111
	log(K25°C) vs log(POC) All	Y=a+bX	-0.2183 ± 0.0382	-0.0616 ± 0.0807	0.4457	259
S12a	log(TSM) vs log(POC) African	Y=a+bX	0.57690 ± 0.03723	1.68400 ± 0.08882	<0.0001	148
	log(TSM) vs log(POC) European	Y=a+bX	0.89000 ± 0.03865	1.13800 ± 0.07181	<0.0001	111
	log(TSM) vs log(POC) All	Y=a+bX	0.67340 ± 0.02873	1.49400 ± 0.06062	<0.0001	259
S13a	log(K) vs log(DOC) African	Y=a+bX	-0.61574 ± 0.19994	0.50443 ± 0.16205	0.00227	51
	log(K) vs log(DOC) European	Y=a+bX	0.21311 ± 0.07556	-0.00748 ± 0.00726	0.31007	90
	log(K) vs log(DOC) All	Y=a+bX	-0.93454 ± 0.14439	0.65096 ± 0.13296	<0.00001	32
S13b	log(K) vs log(a350) African	Y=a+bX	-0.88266 ± 0.26010	0.49385 ± 0.14353	0.00077	52
	log(K) vs log(a350) European	Y=a+bX	0.30608 ± 0.08291	-0.00342 ± 0.00788	0.66661	85
	log(K) vs log(a350) All	Y=a+bX	-1.37959 ± 0.20528	0.77505 ± 0.12346	<0.00001	48
S15 a	log(MOXinc) vs log(MOXiso_-60)	Y=a+bX	1.00514 ± 0.21205	0.89630 ± 0.06866	<0.00001	171
	log(MOXinc) vs log(MOXiso_-80)	Y=a+bX	1.65340 ± 0.23859	0.87005 ± 0.07371	<0.00001	171
S16 e	Tested vs nominal MOXremoval depth=1m African	Y=a+bX	3.42651 ± 1.11687	0.52974 ± 0.04105	<0.00001	262
	Tested vs nominal MOXremoval depth=1m European	Y=a+bX	1.32646 ± 0.38461	0.46818 ± 0.03130	<0.00001	262
	Tested vs nominal MOXremoval depth=1m All	Y=a+bX	1.65413 ± 0.45937	0.54122 ± 0.03245	<0.00001	262
S16 f	Tested vs nominal MOXremoval K=0.35/d African	Y=a+bX	0.51613 ± 0.31415	0.52470 ± 0.04966	<0.00001	262
	Tested vs nominal MOXremoval K=0.35/d European	Y=a+bX	5.27977 ± 1.21702	0.86228 ± 0.09228	<0.00001	262
	Tested vs nominal MOXremoval K=0.35/d All	Y=a+bX	2.65046 ± 0.74375	0.59786 ± 0.05709	<0.00001	262
S16 g	Tested vs nominal MOXremoval k600=2.8m/d African	Y=a+bX	2.05953 ± 0.63210	0.94372 ± 0.01209	<0.00001	262
	Tested vs nominal MOXremoval k600=2.8m/d European	Y=a+bX	0.67139 ± 0.17130	0.82269 ± 0.02386	<0.00001	262
	Tested vs nominal MOXremoval k600=2.8m/d All	Y=a+bX	0.56276 ± 0.15942	0.95159 ± 0.00777	<0.00001	262
S19 a	log(K25°C) vs log(catchment area) African CCC	Y=a+bX	0.81946 ± 0.33098	-0.19984 ± 0.09365	0.03778	52
	log(K25°C) vs log(catchment area) African non-CCC	Y=a+bX	-0.68197 ± 0.14441	0.10909 ± 0.03646	0.00354	96
	log(K25°C) vs log(catchment area) European	Y=a+bX	-0.33150 ± 0.20810	-0.00399 ± 0.05614	0.94349	114
	log(K25°C) vs log(catchment area) All	Y=a+bX	-0.48346 ± 0.08701	0.06855 ± 0.02455	0.00563	262
S20	d13C-CH4 vs log(K25°C) African CCC	Y=a+bX	-33.22474 ± 0.65047	-2.64196 ± 1.43232	0.07103	52
	d13C-CH4 vs log(K25°C) African non-CCC	Y=a+bX	-27.32966 ± 0.66257	-2.82785 ± 1.00425	0.00608	85
	d13C-CH4 vs log(K25°C) European	Y=a+bX	-29.01612 ± 0.27126	0.36615 ± 0.27520	0.18626	96
	d13C-CH4 vs log(K25°C) All	Y=a+bX	-29.21824 ± 0.21868	-0.85116 ± 0.38897	0.02961	233
S21 a	log(K25°C) vs log(DOC) African	Y=a+bX	-0.58919 ± 0.16279	0.43061 ± 0.14531	0.00361	51
	log(K25°C) vs log(DOC) European	Y=a+bX	-0.64156 ± 0.399	0.26497 ± 0.51721	0.61157	90
	log(K25°C) vs log(DOC) All	Y=a+bX	-0.75251 ± 0.09556	0.52031 ± 0.11078	0.00001	32
S21 b	log(K25°C) vs log(a350) African	Y=a+bX	-0.65629 ± 0.20828	0.34032 ± 0.12388	0.00683	52
	log(K25°C) vs log(a350) European	Y=a+bX	-0.12347 ± 0.1124	-0.18285 ± 0.16687	0.27889	85
	log(K25°C) vs log(a350) All	Y=a+bX	-0.42526 ± 0.08635	0.20608 ± 0.06799	0.00279	48

Table S5 Results of unpaired two-tailed t-test (t-statistic (t), degree of freedom (DF), P value and corresponding summary) of inundation extent in the streams within (n=52) versus ouside (n=96) the Cuvette Centrale Congolaise (CCC).

Figure	Variable tested	t, DF	P value	Summary
S2	inundation extent CCC vs non-CCC	t=2.916, df=134.0	0.0042	**

Table S6 Results of Kruskal-Wallis test and Dunn's multiple comparisons test (P value, Kruskal-Wallis statistic, n, mean of ranks and mean rank difference (diff.), n1, n2, Adjusted P value and corresponding summary as shown in figures).

Figure	Variable tested	P value	Kruskal-Wallis statistic	n	Dunn's multiple comparisons test	Mean rank 1	Mean rank 2	Mean rank diff.	n1	n2	Summary	Adjusted P Value
S11 a	*K*	0.0001	17.98	48	Meuse vs. Scheldt	8.8	28.7	-19.9	11	25	***	0.0003
					Meuse vs. Tidal Scheldt	8.8	30.1	-21.3	11	12	***	0.0008
					Scheldt vs. Tidal Scheldt	28.7	30.1	-1.4	25	12	ns	>0.9999
S11 b	Particulate MOX	0.0424	6.32	29	Meuse vs. Scheldt	7.3	14.7	-7.4	3	23	ns	0.4695
					Meuse vs. Tidal Scheldt	7.3	24.7	-17.3	3	3	*	0.038
					Scheldt vs. Tidal Scheldt	14.7	24.7	-9.9	23	3	ns	0.1725
S11 c	TSM	0.0064	10.12	29	Meuse vs. Scheldt	5.0	14.7	-9.7	3	23	ns	0.1872
					Meuse vs. Tidal Scheldt	5.0	27.0	-22.0	3	3	**	0.0047
					Scheldt vs. Tidal Scheldt	14.7	27.0	-12.3	23	3	ns	0.057

Table S7 Results of paired two-tailed t-test (t-statistic (t), degree of freedom (DF), P value and corresponding summary, and number of pairs) applied to log(CH_4), log(MOX), and log(*K*) during low water and higher water in the streams draining the Congo Cuvette Centrale (Fig. S10).

Figure	Variable tested	t, DF	P value	Summary	number of pairs
S14	log(CH4)	t=3.666, df=19	0.0016	**	20
S14	log(MOX)	t=3.055, df=19	0.0065	**	20
S14	log(K)	t=0.4567, df=19	0.6531	ns	20

REFERENCES

1. M. Saunois, A. Martinez, B. Poulter, Z. Zhang, P. A. Raymond, P. Regnier, J. G. Canadell, R. B. Jackson, P. K. Patra, P. Bousquet, P. Ciais, E. J. Dlugokencky, X. Lan, G. H. Allen, D. Bastviken, D. J. Beerling, D. A. Belikov, D. R. Blake, S. Castaldi, M. Crippa, B. R. Deemer, F. Dennison, G. Etiope, N. Gedney, L. Höglund-Isaksson, M. A. Holgerson, P. O. Hopcroft, G. Hugelius, A. Ito, A. K. Jain, R. Janardanan, M. S. Johnson, T. Kleinen, P. B. Krummel, R. Lauerwald, T. Li, X. Liu, K. C. McDonald, J. R. Melton, J. Mühle, J. Müller, F. Murguia-Flores, Y. Niwa, S. Noce, S. Pan, R. J. Parker, C. Peng, M. Ramonet, W. J. Riley, G. Rocher-Ros, J. A. Rosentreter, M. Sasakawa, A. Segers, S. J. Smith, E. H. Stanley, J. Thanwerdas, H. Tian, A. Tsuruta, F. N. Tubiello, T. S. Weber, G. R. van der Werf, D. E. J. Worthy, Y. Xi, Y. Yoshida, W. Zhang, B. Zheng, Q. Zhu, Q. Zhu, Q. Zhuang, Global methane budget 2000–2020. *Earth Syst. Sci. Data* **17**, 1873–1958 (2025).

2. G. Rocher-Ros, E. H. Stanley, L. C. Loken, N. J. Casson, P. A. Raymond, S. Liu, G. Amatulli, R. A. Sponseller, Global methane emissions from rivers and streams. *Nature* **621**, 530–535 (2023).

3. M. S. Johnson, E. Matthews, J. Du, V. Genovese, D. Bastviken, Methane emission from global lakes: New spatiotemporal data and observation-driven modeling of methane dynamics indicates lower emissions. *J. Geophys. Res. Biogeosci.* **127**, e2022JG006793 (2022).

4. C. Duvert, A. V. Borges, E. Calamita, G. Rocher-Ros, A. Linkhorst, J. A. Rosentreter, S. Liu, K. Attermeyer, T. DelSontro, L. Deirmendjian, A. Dixon, C. Grasset, A. M. Herreid, L. C. Jeffrey, L. Marcon, R. M. Mwanake, J. R. Paranaíba, L. Ran, A. T. Rexroade, V. Solano, F. Ulloa-Cedamanos, J. Wang, K. M. Whitmore, L. Zhang, C. López-Lloreda, M. N. Macedo, D. Oviedo-Vargas, D. A. Riveros-Iregui, N. S. Marzolf, Hydroclimate and landscape diversity drive highly variable greenhouse gas emissions from tropical inland waters. *Nat. Water* **3**, 1303–1317 (2025).

5. F. Shelley, F. Abdullahi, J. Grey, M. Trimmer, Microbial methane cycling in the bed of a chalk river: Oxidation has the potential to match methanogenesis enhanced by warming. *Freshw. Biol.* **60**, 150–160 (2015).

6. L. Rovelli, L. A. Olde, C. M. Heppell, A. Binley, G. Yvon-Durocher, R. N. Glud, M. Trimmer, Contrasting biophysical controls on carbon dioxide and methane outgassing from streams. *J. Geophys. Res. Biogeosci.* **127**, e2021JG006328 (2022).

7. A. Bednařík, M. Blaser, A. Matoušů, P. Hekera, M. Rulík, Effect of weir impoundments on methane dynamics in a river. *Sci. Total Environ.* **584-585**, 164–174 (2017).

8. F. Shelley, J. Grey, M. Trimmer, Widespread methanotrophic primary production in lowland chalk rivers. *Proc. Biol. Sci.* **281**, 20132854 (2014).

9. P. Bodmer, J. Wilkinson, A. Lorke, Sediment properties drive spatial variability of potential methane production and oxidation in small streams. *J. Geophys. Res. Biogeosci.* **125**, e2019JG005213 (2020).

10. U. Zaiss, P. Winter, H. Kaltwasser, Microbial methane oxidation in the River Saar. *Z. Allg. Mikrobiol.* **22**, 139–148 (1982).

11. de M. A. S. Angelis, M. I. Cranton, Fate of methane in the Hudson River and estuary. *Glob. Biogeochem. Cycles* **7**, 509–523 (1993).

12. H. O. Sawakuchi, D. Bastviken, A. O. Sawakuchi, N. D. Ward, C. D. Borges, S. M. Tsai, J. E. Richey, M. V. R. Ballester, A. V. Krusche, Oxidative mitigation of aquatic methane emissions in large Amazonian rivers. *Glob. Change Biol.* **22**, 1075–1085 (2016).

13. L. Patel, R. Singh, S. C. Gowd, S. D. Thottathil, Environmental determinants of aerobic methane oxidation in a tropical river network. *Water Res.* **265**, 122257 (2024).

14. A. V. Borges, F. Darchambeau, C. R. Teodoru, T. R. Marwick, F. Tamooh, N. Geeraert, F. O. Omengo, F. Guérin, T. Lambert, C. Morana, E. Okuku, S. Bouillon, Globally significant greenhouse gas emissions from African inland waters. *Nat. Geosci.* **8**, 637–642 (2015).

15. A. V. Borges, F. Darchambeau, T. Lambert, C. Morana, G. H. Allen, E. Tambwe, A. Toengaho Sembaito, T. Mambo, J. Nlandu Wabakhangazi, J.-P. Descy, C. R. Teodoru, S. Bouillon,

Variations in dissolved greenhouse gases (CO_2, CH_4, N_2O) in the Congo River network overwhelmingly driven by fluvial-wetland connectivity. *Biogeosciences* **16**, 3801–3834 (2019).

16. K. S. Aho, P. A. Raymond, Differential response of greenhouse gas evasion to storms in forested and wetland streams. *J. Geophys. Res. Biogeosci.* **124**, 649–662 (2019).

17. T. P. A. Nijman, T. A. Davidson, S. T. J. Weideveld, J. Audet, C. Esposito, E. E. Levi, A. Ho, L. P. M. Lamers, E. Jeppesen, A. J. Veraart, Warming and eutrophication interactively drive changes in the methane-oxidizing community of shallow lakes. *ISME Commun.* **1**, 32 (2021).

18. Y. Yao, H. Tian, X. Xu, Y. Li, S. Pan, Dynamics and controls of inland water CH_4 emissions across the conterminous United States: 1860–2019. *Water Res.* **224**, 119043 (2022).

19. J. R. Blaszczak, L. E. Koenig, F. H. Mejia, L. Gómez-Gener, C. L. Dutton, A. M. Carter, N. B. Grimm, J. W. Harvey, A. M. Helton, M. J. Cohen, Extent, patterns, and drivers of hypoxia in the world's streams and rivers. *Limnol. Oceanogr. Lett.* **8**, 453–463 (2023).

20. D. J. Graham, M. F. P. Bierkens, E. R. Jones, E. H. Sutanudjaja, M. T. H. van Vliet, Climate change drives low dissolved oxygen and increased hypoxia rates in rivers worldwide. *Nat. Clim. Change* **15**, 1348–1354 (2025).

21. S. D. Thottathil, P. C. J. Reis, Y. T. Prairie, Methane oxidation kinetics in northern freshwater lakes. *Biogeochemistry* **143**, 105–116 (2019).

22. H. O. Sawakuchi, G. Martin, S. Peura, S. Bertilsson, J. Karlsson, D. Bastviken, Phosphorus regulation of methane oxidation in water from ice-covered lakes. *J. Geophys. Res. Biogeosci.* **126**, e2020JG006190 (2021).

23. G. Abril, M. V. Commarieu, F. Guérin, Enhanced methane oxidation in an estuarine turbidity maximum. *Limnol. Oceanogr.* **52**, 470–475 (2007).

24. A. V. Borges, N. Gypens, T. Bauduin, Methanogenesis pathways and methane oxidation in urban ponds. *Aquat. Sci.* **88**, 29 (2026).

25. C. Morana, S. Bouillon, , Methane paradox in tropical lakes? Sedimentary fluxes rather than pelagic production sustain methanotrophy. *Biogeosciences* **17**, 5209–5221 (2020).

26. G. Nyerges, S. Han, L. Y. Stein, Effects of ammonium and nitrite on growth and fitness of methanotrophic bacteria. *Appl. Environ. Microbiol.* **76**, 5648–5651 (2010).

27. P. Dunfield, R. Knowles, R. Dumont, T. R. Moore, Methane production and consumption in peat soils: Response to temperature and pH. *Soil Biol. Biochem.* **25**, 321–326 (1993).

28. T. Ren, J. A. Amaral, R. Knowles, Response of methane consumption by methanotrophic bacteria to oxygen. *Can. J. Microbiol.* **43**, 925–928 (1997).

29. A. Ho, F.-M. Kerckhof, C. Luke, A. Reim, S. Krause, N. Boon, P. L. E. Bodelier, Functional traits of methane-oxidizing bacteria as life strategies. *Environ. Microbiol. Rep.* **5**, 335–345 (2013).

30. S. Crevecoeur, C. Ruiz-González, Y. T. Prairie, P. A. Del Giorgio, Biogeography of methanotrophic bacteria across boreal waters. *Mol. Ecol.* **28**, 4181–4196 (2019).

31. M. Nagler, N. Praeg, G. H. Niedrist, K. Attermeyer, N. Catalán, F. Pilotto, C. G. Roberts, C. Bors, S. Fenoglio, M. Colls, S. Cauvy-Fraunié, B. Doyle, F. Romero, B. Machalett, T. Fuss, A. Bednařík, M. Klaus, P. Gilbert, D. Lamonica, A. C. Nydahl, C. R. González-Quijano, L. T. Bistarelli, L. Kenderov, E. Piano, J.-R. Mor, V. Evtimova, E. deEyto, A. Freixa, M. Rulík, J. Pegg, S. H. Ortega, L. Steinle, P. Bodmer, Abundance and biogeography of methanogenic and methanotrophic microorganisms across European streams. *J. Biogeogr.* **48**, 947–960 (2021).

32. M. Li, C. Peng, K. Zhang, L. Xu, J. Wang, Y. Yang, P. Li, Z. Liu, N. He, Headwater stream ecosystem: An important source of greenhouse gases to the atmosphere. *Water Res.* **190**, 116738 (2021).

33. M. Trimmer, S. Maanoja, A. G. Hildrew, J. L. Pretty, J. Grey, Potential carbon fixation via methane oxidation in well-oxygenated river bed gravels. *Limnol. Oceanogr.* **55**, 560–568 (2010).

34. E. Wohl, B. P. Bledsoe, R. B. Jacobson, N. L. Poff, S. L. Rathburn, D. M. Walters, A. C. Wilcox, The natural sediment regime in rivers: Broadening the foundation for ecosystem management. *Bioscience* **65**, 358–371 (2015).

35. F. Caillon, K. Besemer, P. Peduzzi, J. Schelker, Soil microbial inoculation during flood events shapes headwater stream microbial communities and diversity. *Microb. Ecol.* **82**, 591–601 (2021).

36. J. B. Gontijo, F. S. Paula, A. M. Venturini, C. A. Yoshiura, C. D. Borges, J. M. S. Moura, B. J. M. Bohannan, K. Nüsslein, J. L. Mazza Rodrigues, S. M. Tsai, Not just a methane source: Amazonian floodplain sediments harbour a high diversity of methanotrophs with different metabolic capabilities. *Mol. Ecol.* **30**, 2560–2572 (2021).

37. D. L. Kirchman, The uptake of inorganic nutrients by heterotrophic bacteria. *Microb. Ecol.* **28**, 255–271 (1994).

38. P. Heděnec, A. Alias, H. Almahasheer, C. Liu, P. S. Chee, M. Yao, X. Li, L. Vesterdal, J. Frouz, Y. Kou, K. Yue, Global assessment of soil methanotroph abundances across biomes and climatic zones: The role of climate and soil properties. *Appl. Soil Ecol.* **195**, 105243 (2024).

39. B. C. Crump, L. A. Amaral-Zettler, G. W. Kling, Microbial diversity in Arctic freshwaters is structured by inoculation of microbes from soils. *ISME J.* **6**, 1629–1639 (2012).

40. J. P. Niño-García, C. Ruiz-González, P. A. del Giorgio, Interactions between hydrology and water chemistry shape bacterioplankton biogeography across boreal freshwater networks. *ISME J.* **10**, 1755–1766 (2016).

41. T. Bambakidis, B. C. Crump, B. Yoon, E. D. Kyzivat, K. S. Aho, C. F. Leal, J. H. Fair, A. Stubbins, S. Wagner, P. A. Raymond, J. D. Hosen, Temperature, water travel time, and dissolved organic matter structure river microbial communities in a large temperate watershed. *Limnol. Oceanogr.* **69**, 1618–1635 (2024).

42. M. A. Borton, B. B. McGivern, K. R. Willi, B. J. Woodcroft, A. C. Mosier, D. M. Singleton, T. Bambakidis, A. Pelly, R. A. Daly, F. Liu, A. Freiburger, J. N. Edirisinghe, J. P. Faria, R.

Danczak, I. Leleiwi, A. E. Goldman, M. J. Wilkins, E. K. Hall, C. Pennacchio, S. Roux, E. A. Eloe-Fadrosh, S. P. Good, M. B. Sullivan, E. M. Wood-Charlson, C. S. Miller, M. R. V. Ross, C. S. Henry, B. C. Crump, J. C. Stegen, K. C. Wrighton, A functional microbiome catalogue crowdsourced from North American rivers. *Nature* **637**, 110–112 (2025).

43. M. V. Kevbrina, A. A. Okhapkina, D. S. Akhlynin, Growth of mesophilic methanotrophs at low temperatures. *Microbiology* **70**, 384–391 (2001).

44. A. T. Tveit, A. Söllinger, E. M. Rainer, A. Didriksen, A. G. Hestnes, L. Motleleng, H.-J. Hellinger, T. Rattei, M. M. Svenning, Thermal acclimation of methanotrophs from the genus *Methylobacter*. *ISME J.* **17**, 502–513 (2023).

45. N. J. Bale, W. I. C. Rijpstra, D. X. Sahonero-Canavesi, I. Y. Oshkin, S. E. Belova, S. N. Dedysh, J. S. S. Damsté, Fatty acid and hopanoid adaption to cold in the methanotroph *Methylovulum psychrotolerans*. *Front. Microbiol.* **10**, 589 (2019).

46. N. Richter, L. Villanueva, E. C. Hopmans, N. J. Bale, J. S. S. Damsté, D. Rush, Methanotroph-methylotroph lipid adaptations to changing environmental conditions. *Front. Microbiol.* **16**, 1532719 (2025).

47. N. T. Duc, P. Crill, D. Bastviken, Implications of temperature and sediment characteristics on methane formation and oxidation in lake sediments. *Biogeochemistry* **100**, 185–196 (2010).

48. B. Jiang, H. Chen, Z. Wei, J. Zhang, M. Guo, T. Yang, X. Zhou, Higher temperature sensitivity of forest soil methane oxidation in colder climates. *Nat. Commun.* **16**, 2428 (2025).

49. J. Nauw, de H. Haas, G. Rehder, A review of oceanographic and meteorological controls on the North Sea circulation and hydrodynamics with a view to the fate of North Sea methane from well site 22/4b and other seabed sources. *Mar. Pet. Geol.* **68**, 861–882 (2015).

50. S. Elliott, M. Maltrud, M. Reagan, G. Moridis, P. Cameron-Smith, Marine methane cycle simulations during early global warming. *J. Geophys. Res.* **116**, G01010 (2011).

51. Y. Chen, M. G. Dumont, N. P. McNamara, P. M. Chamberlain, L. Bodrossy, N. Stralis-Pavese, J. C. Murrell, Diversity of the active methanotrophic community in acidic peatlands as assessed by mRNA and SIP-PLFA analyses. *Environ. Microbiol.* **10**, 446–459 (2008).

52. L.-M. Pigneur, E. Falisse, K. Roland, E. Everbecq, J.-F. Deliège, J. S. Smitz, K. Van Doninck, J.-P. Descy, Impact of invasive Asian clams (*Corbicula* spp.) on a large river ecosystem. *Freshw. Biol.* **59**, 573–583 (2014).

53. G. Abril, H. Etcheber, B. Delille, M. Frankignoulle, A. V. Borges, Carbonate dissolution in the turbid and eutrophic Loire estuary. *Mar. Ecol. Prog. Ser.* **259**, 129–138 (2003).

54. M. Meybeck, Carbon, nitrogen, and phosphorus transport by world rivers. *Am. J. Sci.* **282**, 401–450 (1982).

55. P. C. J. Reis, S. D. Thottathil, Y. T. Prairie, The role of methanotrophy in the microbial carbon metabolism of temperate lakes. *Nat. Commun.* **13**, 43 (2022).

56. S. R. Carpenter, Microcosm experiments have limited relevance for community and ecosystem ecology. *Ecology* **77**, 677–680 (1996).

57. T. G. Benton, M. Solan, J. M. J. Travis, S. M. Sait, Microcosm experiments can inform global ecological problems. *Trends Ecol. Evol.* **22**, 516–521 (2007).

58. R. L. Vannote, G. W. Minshall, K. W. Cummins, J. R. Sedell, C. E. Cushing, The river continuum concept. *Can. J. Fish. Aquat. Sci.* **37**, 130–137 (1980).

59. W. J. Junk, P. B. Bayley, R. E. Sparks, The flood pulse concept in river-floodplain systems. *Can. J. Fish. Aquat. Sci.* **106**, 110–127 (1989).

60. S. Linke, B. Lehner, C. Ouellet Dallaire, J. Ariwi, G. Grill, M. Anand, P. Beames, V. Burchard-Levine, S. Maxwell, H. Moidu, F. Tan, M. Thieme, Global hydro-environmental sub-basin and river reach characteristics at high spatial resolution. *Sci. Data* **6**, 283 (2019).

61. P. A. Raymond, C. J. Zappa, D. Butman, T. L. Bott, C. Potter, P. Mulholland, A. E. Laursen, W. H. McDowell, D. Newbold, Scaling the gas transfer velocity and hydraulic geometry in streams and small rivers. *Limnol. Oceanogr. Fluids Environ.* **2**, 41–53 (2012).

62. A. V. Borges, F. Darchambeau, T. Lambert, S. Bouillon, C. Morana, S. Brouyère, V. Hakoun, A. Jurado, H.-C. Tseng, J.-P. Descy, F. A. E. Roland, Effects of agricultural land use on fluvial carbon dioxide, methane and nitrous oxide concentrations in a large European river (Meuse, Belgium). *Sci. Total Environ.* **610-611**, 342–355 (2018).

63. G. Chiriboga, A. V. Borges, Andean headwater and piedmont streams are hot spots of carbon dioxide and methane emissions in the Amazon basin. *Commun. Earth Environ.* **4**, 76 (2023).

64. R. M. Mwanake, G. M. Gettel, C. Ishimwe, E. G. Wangari, K. Butterbach-Bahl, R. Kiese, Basin-scale estimates of greenhouse gas emissions from the Mara River, Kenya: Importance of discharge, stream size, and land use/land cover. *Limnol. Oceanogr.* **67**, 1776–1793 (2022).

65. American Public Health Association (APHA), *Standard Methods for the Examination of Water and Wastewater* (American Public Health Association, 1998).

66. Standing Committee of Analysts, “Ammonia in waters: Methods for the examination of waters and associated materials” (HMSO, 1981).

67. J. Koroleff, “Determination of total phosphorus by alkaline persulphate oxidation” in *Methods of Seawater Analysis* (Verlag Chemie, 1983), pp. 136–138.

68. H. Iwata, K. Nakazawa, H. Sato, M. Itoh, Y. Miyabara, R. Hirata, Y. Takahashi, T. Tokida, R. Endo, Temporal and spatial variations in methane emissions from the littoral zone of a shallow mid-latitude lake with steady methane bubble emission areas. *Agric. For. Meteorol.* **295**, 108184 (2020).

69. R. Segers, Methane production and methane consumption: A review of processes underlying wetland methane fluxes. *Biogeochemistry* **41**, 23–51 (1998).

70. S. Yamamoto, J. B. Alcauskas, T. E. Crozier, Solubility of methane in distilled water and seawater. *J. Chem. Eng. Data* **21**, 78–80 (1976).

71. R. Wanninkhof, Relationship between wind speed and gas exchange over the ocean. *J. Geophys. Res. Oceans* **97**, 7373–7382 (1992).

72. K. Liptay, J. Chanton, P. Czepiel, B. Mosher, Use of stable isotopes to determine methane oxidation in landfill cover soils. *J. Geophys. Res. Atmos.* **103**, 8243–8250 (1998).

73. C. Morana, A. V. Borges, F. A. E. Roland, F. Darchambeau, J.-P. Descy, S. Bouillon, Methanotrophy within the water column of a large meromictic tropical lake (Lake Kivu, East Africa). *Biogeosciences* **12**, 2077–2088 (2015).

74. S. Balathandayuthabani, B. Panneer Selvam, M. Gålfalk, P. Saetre, S. Peura, U. Kautsky, L. Klemedtsson, L. Arunachalam, G. Vellingiri, D. Bastviken, Methane in two stream networks: Similar contributions from groundwater and local sediments while oxidation was a large sink controlling atmospheric emissions. *J. Geophys. Res. Biogeosci.* **129**, e2023JG007836 (2024).

75. D. Bastviken, J. Ejlertsson, L. Tranvik, Measurement of methane oxidation in lakes: A comparison of methods. *Environ. Sci. Technol.* **36**, 3354–3361 (2002)

76. R. Koenker, *Quantile Regression* (Cambridge Univ. Press, 2005).

77. R Core Team, R: A language and environment for statistical computing (2022); https://r-project.org/.

78. M. I. Bird, P. Pousai, Variations of $\delta^{13}C$ in the surface soil organic carbon pool. *Glob. Biogeochem. Cycles* **11**, 313–322 (1997).

79. A. Bagnoud, P. Pramateftaki, M. J. Bogard, T. J. Battin, H. Peter, Microbial ecology of methanotrophy in streams along a gradient of CH_4 availability. *Front. Microbiol.* **11**, 771 (2020).

80. L.-D. Shen, L. Ouyang, Y. Zhu, M. Trimmer, Active pathways of anaerobic methane oxidation across contrasting riverbeds. *ISME J.* **13**, 752–766 (2019).

81. I. A. Sanders, C. M. Heppell, J. A. Cotton, G. Wharton, A. G. Hildrew, E. J. Flowers, M. Trimmer, Emission of methane from chalk streams has potential implications for agricultural practices. *Freshw. Biol.* **52**, 1176–1186 (2007).